Physical properties of geomaterials

Vitovtova V. M [1], Shmonov V.M.[1], Zharikov A.V.[2] Distribution of the pore sizes in the continental crust: inferences from experimental data about permeability.

[1]-IEM RAS;)[2]-IGOD RAS vitovt@iem.ac.ru; shmonov@iem.ac.ru

Key words: continental crust, permeability, distribution pore size

Structural characteristics of rocks define dynamics of movement transcrust fluids, and also the contribution of surface energy to thermodynamic properties nanofluid. It defines necessity of the information about distribution of porosity, permeability, a specific surface and the sizes of a pore of rocks in an earth crust. By us are experimentally studied permeability of rocks at high pressures and temperatures. Data on permeability of samples granites, granodiorites, diorites, serpentinites, gneisses, amphibolites, marble, limestones and sandstones are presented in our monography [*Shmonov et al.,* 2002,a]. On the basis of our experimental data we have constructed a trend of permeability of continental earth crust [*Shmonov et al.,* 2002,b; *Shmonov et al.,* 2003]. Paleopermeability established on an isotope exchange [*Ingebritsen and Manning,* 1999] or to flow in metasomatic and metamorphic processes [*Manning and Ingebritsen,* 1999] it will well be coordinated with our trend. Our experimental data about permeability of rocks have allowed to receive representation about distribution of a pore in the sizes within earth crust.

Permeability measurements are executed by a steady-state method gas (argon) of a filtration [*Shmonov et al.,* 2002,a]. At a gas filtration through porous media its speed depends on a parity of mean free path length of molecules of gas and the pore size. Klinkenberg [*Klinkenberg*, 1941] has found that

$$k_g = k_w (1 + b/p), \quad (1)$$

where k_g – gas permeability, k_w – water permeability, p – average pressure of filtered gas, and b – a constant for given pair «gas – porous media». Thus the method allows to define on a gas stream simultaneously a) values of permeability of the sample for the condensed fluid, k_w, b) permeability of the sample for gas, k_g, at various pressure of a filtration and c) constant, b, characterizing structure of pore spaces of rocks. The equation (1)

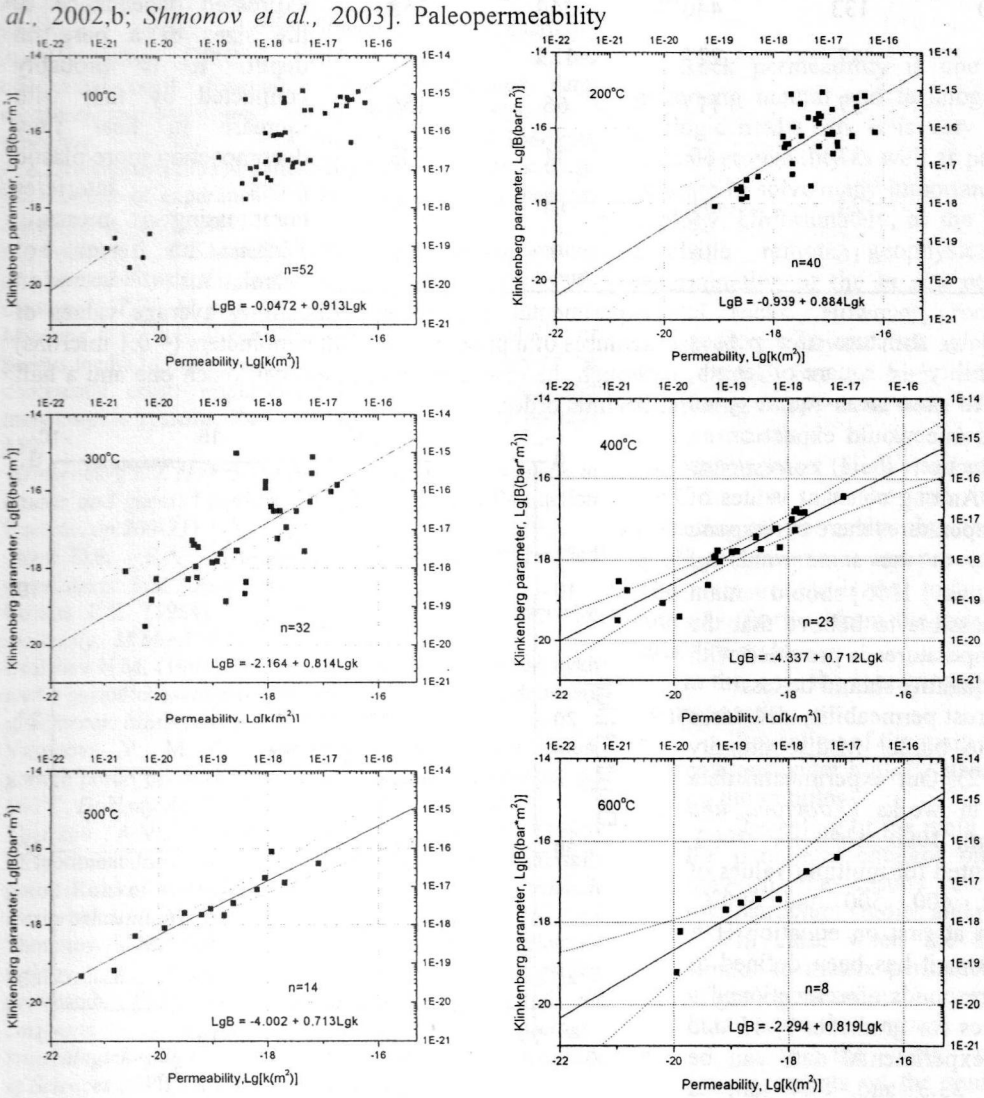

a), b)

c),d)

e),f)

Fig.1 . Dependence of parameter of Klinkenberg on permeability at various temperatures. On each schedule a) n designates quantity of experimental points, b) the equation of linear regress for a continuous line is resulted and c) the dotted line gives the top and bottom borders of 99 % of a confidential interval

transformed to a kind $k_g = k_w + B/p$ gives value of parameter of Klinkenberg in the form of $B = k_w b$ allowing to calculate effective radius of capillaries of the cylindrical form on the equation from [*Scott and Dullien,* 1962] in a kind

$$r = 4/3\ \pi\tilde{\upsilon}\mu\ (k_w/B) \qquad (2)$$

where $\tilde{\upsilon}$ – average thermal speed of movement of molecules, μ – dynamic viscosity of argon, k_w – permeability, and B – parameter of Klinkenberg. As a result of processing of a primary material values of parameter of Klinkenberg, B, for various temperatures have been defined. Their values depending on permeability are presented on fig. 1. On the equation (2) effective radiuses of a pore for model of rocks with a series of parallel cylindrical capillaries of identical radius have been calculated. Results of calculations are resulted in tabl. 1.

Earlier by us [*Shmonov et al.,* 2002,b] it has been shown that dependence k=f (H) can be presented the sedate equation $\log k = a + bH^c$. For k-H at low heat flow the equation looks like a curve log k =-12.56 – 2.703H0.2682; at average heat flow log k =-12.55 – 3.124H0.2447 and log k =-12.45 – 4.330H0.1360 - at high heat flow. On these equations for the above-stated depths values permeability have been calculated.

At a following stage according to the equations on schedules fig. 1 for values of permeability parameters of Klinkenberg, B. And on the equation (2) radiuses of a pore have been defined.

The result of data processing is shown on fig. 3 a, b and c. On schedules are shown limiting values of radiuses of a pore calculated according to a range of 99 % of a confidential interval of values of parameter of Klinkenberg and permeability (fig. 1). At low heat flow reduction of radius of a pore with depth from 179÷827 nanometer at level of 11.1 km to 36÷139 nanometer at level of 44.4 km is observed. At average and high heat flow there is no obviously expressed dependence of the sizes of a pore on depth. It is probably connected by that with increase in heat flow decompaction more plastic rocks interferes compressing pressure. Within an error of calculations on experimental data about permeability average values of radiuses of a pore is about 100 nanometers (~ 0.1 microns) though the disorder on occasion can reach one and a half decimal order.

Table №1. Values of effective pore radius, r (nanometer), in rocks with various permeability, k, at temperatures 100 ÷ 600°C.

k, m^2	100°C	200°C	300°C	400°C	500°C	600°C
1×10^{-16}	38	130	205	854	482	543
1×10^{-17}	31	100	133	440	249	358
1×10^{-18}	25	76	87	227	129	236
1×10^{-19}	21	58	57	117	66	156
1×10^{-20}	17	45	37	60	34	103
1×10^{-21}	14	34	24	31	18	68
1×10^{-22}	11	26	16	16	9	45

Permeability, k, is defined by structure of a porous material. Dimension of permeability – a square of length, [L^2] that is «a rough measure root-mean-square pore diameter» [*Collins*, 1964]. As one would expect on an isotherm to permeability reduction there corresponds reduction of radius of a pores. Among constant values of permeability to higher value temperatures there correspond the big sizes of a pore. But at the same value of permeability «openancy» [*Dmitriev*, 1995] should remain a constant. In this case it is possible to believe that the same permeability at higher temperatures is provided with a pores more the size, but their quantity should be less.

In the conditions of earth crust permeability decreases from a surface of the earth to border M-discontinuity under the power law [2] (fig. 2). Our experimental data about permeability of rocks in works [*Vitovtova and Shmonov*, 1982; *Zharikov et al.*, 1990; *Shmonov*, 2000; *Zharikov et al.*, 2003] are presented for multiple values of temperatures: 100, 200, 300, 400, 500 and 600°C. Therefore at trend construction at first on equation H = T/gradT, where H - depth in km, it has been defined to what depths in earth crust corresponds aforementioned a number of multiple temperatures for gradients 9, 15 and 26°C/km. At gradT=9oC/km experimental data can be used for depths 11.1, 22.2, 33.3 and 44.4 km; at gradT=15°C/km - a number of depths will be values 6.7, 13.3, 20.0, 26.7, 33.3, and 40.0 km and for gradT=26°C/км - 3.8, 7.7, 11.5, 15.4, 19.2 and 23.1 km.

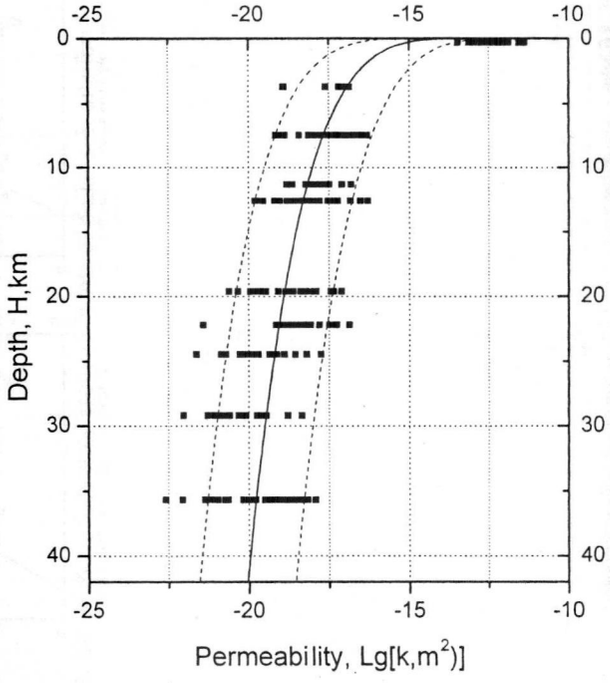

Fig.2. A permeability trend of continental earth crust constructed on our experimental data.

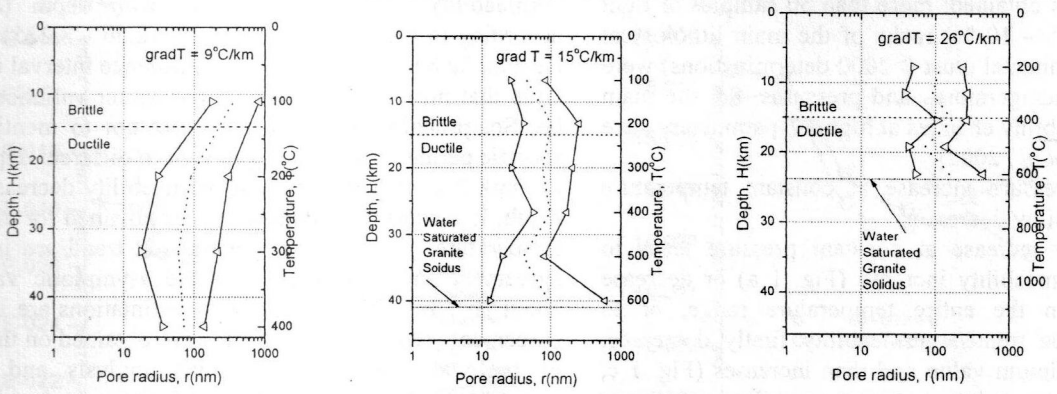

Fig.3. Trend of effective radius of a time of breeds for a cut continental crust at various thermogradients.

Researches are lead at financical support of the Russian Federal Property Fund support (the grant 11-05-00778), to Programs 4 Russian Academies of Sciences (the Direction №1) and Programs №8 DSE the Russian Academy of Sciences.

References

1. Shmonov V.M, V.M.Vitovtova, A.V.Zharikov (2002,a) *Fluidnaya pronitsaemost porod zemnoi kory, M: Nauchnyi Mir*, 216 p.
2. Shmonov V.M., V.M.Vitovtova, A.V.Zharikov, A.A.Grafchikov (2002,b) Fluid permeability of the continental crust: Estimation from experimental data, *Geochemistry International, Vol. 40, Suppl. 1*, S3-S13.
3. Shmonov V.M., V.M.Vitovtova, A.V.Zharikov, A.A.Grafchikov (2003) Permeability of the continental crust: implications of experimental data. *Journal of Geochemical Exploration, 78-79*, p.697-699.
4. Ingebritsen S.E., C.E.Manning (1999) Geological implications of permeability-depth curve for the continental crust, *Geology.V.27. No.12.* pp.1107-1110.
5. Manning C.E., S.E. Ingebritsen (1999) The permeability of porous media to liquids and gases, Amer Permeability of the continental crust: implications of geothermal data and metamorphic systems, Rev. *Geophysics, V.37. No1* pp.127-150.
6. *Klinkenberg L.J. (1941) The permeability of porous media to liquids and gases.* Petrolium Inst. Drilling and Production Practice. *pp.200-211.*
7. Scott D.S. , F.A.L. Dullien (1962) The flow of rarefied gases, *Amer. Inst. Chem. Eng. J., v.8, №3,* pp.293-297.
8. Collins R.E. (1964) *Techenie Zhidkostei cherez poristye materialy, M.Mir*,350 p.
9. Dmitriev N.M. (1995) Prosvetnost i pronitsaemost poristykh sred s periodicheskoi mikrostrukturoi, *Izv. Russian Academy of Sciences. MLG. №1.* p.79-85.
10. Vitovtova V. M, V.M.Shmonov (1982) Pronitsaemost gornyh porod pri davleniah do 2000 kg/cm^2 i temperatur do 600°C, *Doklady AS USSR, v.266. №5.* pp.1244-1248.
11. Zharikov A.V., V.A.Vitovtova, V.M.Shmonov (1990) Eksperimentalnoe issledovanie pronizaemosti Arheiskih porod Kolskoi sverhglubokoi skvazhiny , *Geologia rudnyh mestorozhdenii. N6.* p.79-88.
12. Shmonov V.M. (2000) Pronitsaemost porod i plotnost fluidov v vysokotemperaturnykh geokhimicheskikh protsessah. Eksperimentalnoe issledovanie, *Avtoref. na coiskanie uchenoi stepeni doktora geologo-mineralogicheskih nauk . M: GEOKHI the Russian Academy of Sciences of V.I.Vernadsky*, 48p.
13. Zharikov A.V., V.M.Vitovtova, V.M.Shmonov, A.A.Grafchikov (2003) Permeability of the rocks from the Kola superdeep borehole at high temperature and pressure: implication to fluid dynamics in the continental crust, Tectonophysics, 370, pp.177-191.

Zharikov [1,2] A.V., Shmonov [2] V.M., Vitovtova [2] V.M. Permeability, pore structure and dynamics of natural and technogeneous fluids in crystalline rocks (experimental data)

[1] *IGEM*, [2] *IEM RAS* vil@igem.ru fax: +7(499)9511587, ph.: +7(499)2308440)

Keywords: *permeability, porosity, pressure, temperature, Earth crust*

Rock permeability is one of the main parameters governing natural and technogeneous fluid dynamics in geologic media. So, it is very important to estimate the recent permeability as well as paleo-permeability of rocks, in order to solve many important problems of geology and ecology. Unfortunately, at the present time there are no available remote geophysical methods for direct determination of the *in situ* permeability of deep-seated crustal rocks. However, rock permeability can be measured on relevant rock samples. These studies can be also carried out at high temperatures and pressures simulating *in situ* conditions of deep zones of continental crust, near-field of the depositories of high level radioactive waste (HLW) and paleogeothermal systems, as well. In this case the data interpretation - a proper offsetting of the results obtained on the small samples on geological structures and processes – is greatly important. The main trouble is that today there is no any universal rule of offsetting from the sample scale to the geological structure scale.

In this case the following manner of investigations can be proposed:

- Revealing of the main trends of rock permeability changes under high *PT* using the results of the studies on the samples.
- Revealing of the main causes and mechanisms of the parameter changes on the basis of correlation between the results obtained and the data of microstructure studies and numerical simulations.
- In case, when the bulk permeability can be similar to matrix permeability, numerical estimation of geological media *in situ* can be made using the data obtained on the samples.
- Using the data of physical experiment (measurements on the samples) as the input data in numerical one (simulating of fluid flows in geological media).

A thematic team lead by V.M. Shmonov has been performing the permeability studies in IEM RAS during the last 20 years. After all an unprecedented experimental

data collection is obtained: more than 50 samples of tight low porous (0.05 – 10 %) rocks of the main lithological types of the continental crust (>2000 determinations) were studied at high temperatures and pressures. So, the main trends of permeability changes at high *PT*-parameters were found [*Smonov et al.,* 2002].

Effective pressure increase at constant temperature leads to permeability decrease.

Temperature increase at constant pressure leads to monotonous permeability increase (Fig. 1 a) or decrease (Fig. 1b) within the entire temperature range, or to inversions on the trends: permeability firstly decreases, reaching its minimum value and than increases (Fig. 1 c, d). It should be noted that the permeability trends are complicated by abrupt threshold transitions.

Correlation of the data obtained with the results of microstructure studies under optical and electronic microscopes and with the results of numerical simulation shows that such *PT*-trends pattern in crystalline rocks is caused by their pore structure changes: first of all, by microcracking changes.

Behavior of microcracks of different shape is different when heating. Amount, apertures and interconnectivity of microcracks with high aspect ratio increase with temperature rise, with low aspect ratio, in contrary, - decrease. Under conditions of simultaneous high pressure and temperature action these processes run concurrently, as a result, inversions on the temperature trends may occur.

The main factor governing rock permeability is a degree of interconnectivity of fluid conductive clusters (pores and microcracks). Minor changes in microcracks amounts, lengths or apertures may lead to dramatic permeability changes. So, permeability temperature and pressure trends are frequently complicated by threshold transitions.

A presence of microcrack systems oriented in line with rock structure elements (for example along to foliation or fluidization etc.) is also an important factor. Such systems present strong fluid conducting clusters.

A generalized trend of the rock permeability of the continental crust on depth (Fig. 2) was obtained as result of experimental data processing. It was found that rock permeability (k, m^2) decreases with depth (h, км) according to the power law: $lgk = -12.56 - 3.225h^{0.223}$. A field in the boundaries of 90 % confidence interval is quite wide that means how intensive parameter variations may be. So, probably, it is more correct not to mention the specific permeability values relevant to different depth, but to mark the main tendency of permeability decrease with depth. It is significant that all curves obtained for different temperature gradients and generalized trend are in good agreement and approximate to the asymptotic value of about 10^{-20} m^2. Such permeability estimations are in good agreement with that ones which were obtained on the basis of regional ground water flows analysis and active metamorphic systems studies [*Manning u Ingebritsen,* 1999], as well. It is also significant that rocks with permeability values more than 10^{-18} m^2 – minimal value when hydrothermal systems can operate - by D. Norton (1979) – may occur down to 10-13 km of depth in accordance with our data.

The main aims of the experimental study of filtration properties carried out on the samples collected from the sites of probable underground HLW disposal: metavolcanits from the area of PA Mayak and granitoids from the area of Krasnoyarsk Mining and Chemical Combine, were to test matrix permeability of the rocks from the near-field of a HLW depository, to estimate minimal thickness of massive blocks of such rocks, providing safe HLW disposal, and to forecast possible parameter changes due to heating as a result of HLW heat generation.

Specific character of PA Mayak consists of the fact that a HLW depository for more than 2000 t of solidified wastes with total activity about $3 \cdot 10^8$ Ci has to be located in a sanitary-protective zone (SPZ) of the enterprise. Two sites, which sizes are enough for location of HLW well-depositories, are found in the SPZ. The data on effective porosity and permeability obtained on the most representative samples collected from the boreholes drilled at these sites shows that metavolcanits located outside the disjunctive zones are solid and have low porosity (mean value - 0.26 %) and permeability (mean value - $1.92 \cdot 10^{-19}$ m^2).

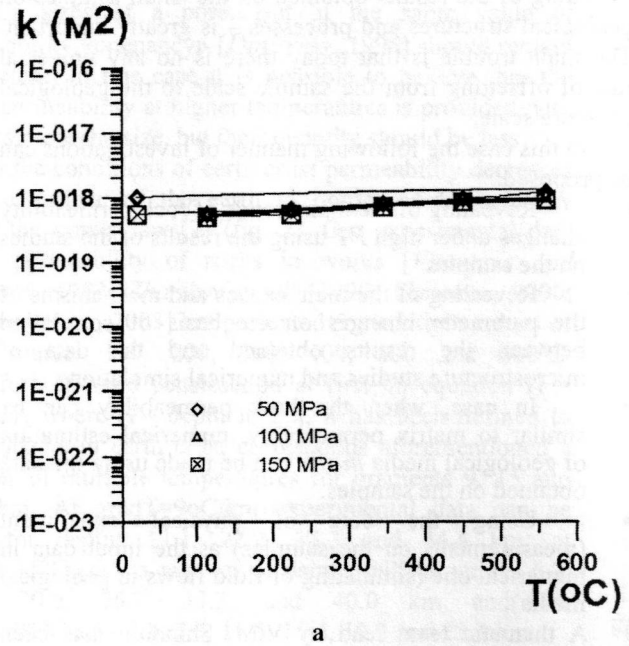

a

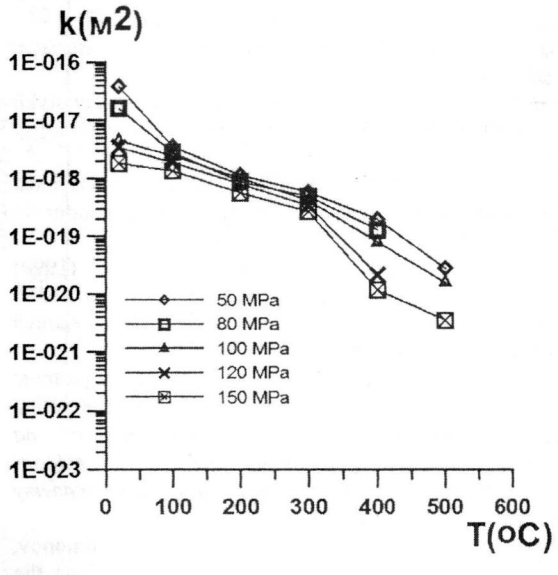

b

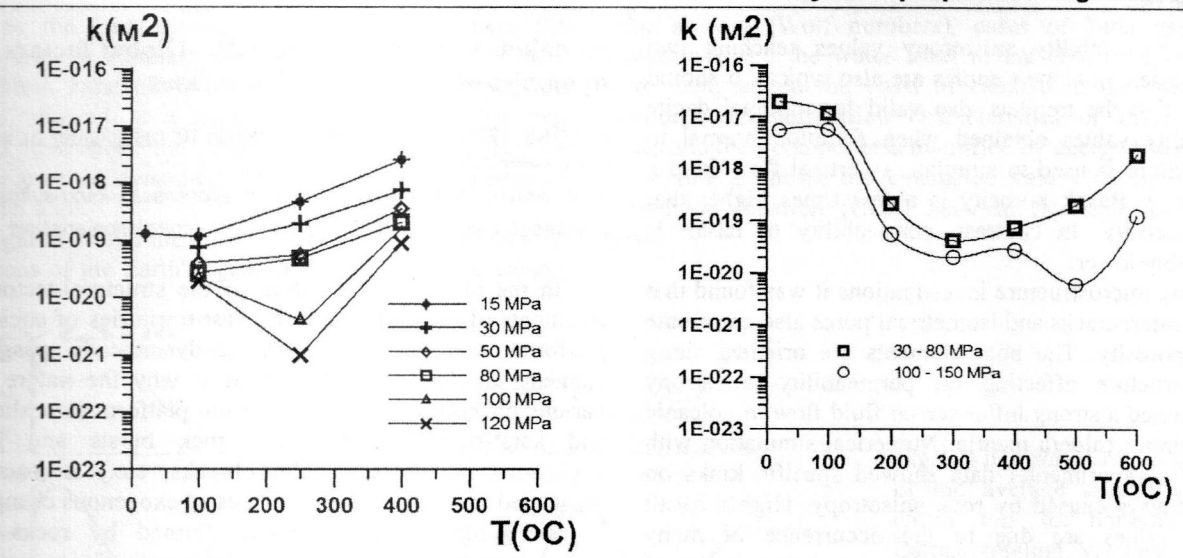

c d

Fig. 1. Permeability vs temperature, P_{eff}=const.
a – marble, sam. 1, b – granodiorite, sam. 82066, c –granite, sam. 2., d - amphibolite, sam. 43639.

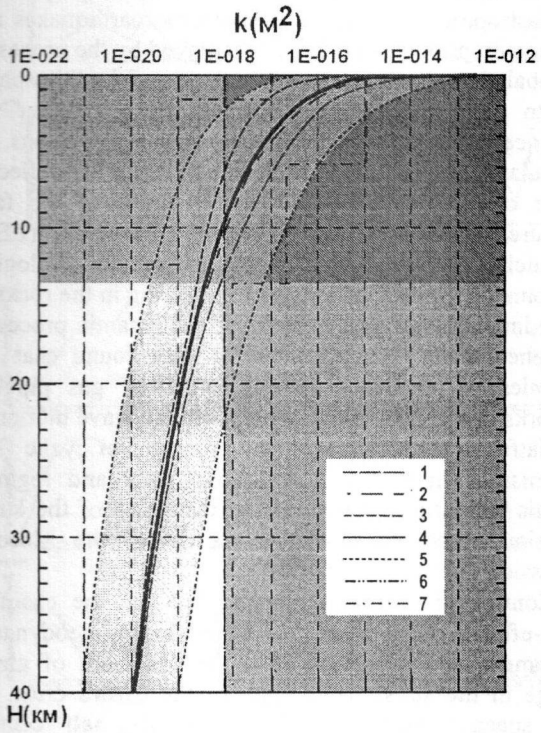

1. trend for temperature gradient of 9°C/км,
2. trend for temperature gradient of 15°C/км
3. trend for temperature gradient of 26°C/км
4. generalized trend,
5. limits of 90 % confidence interval,
6. permeability of 10^{-18} m^2 – according to D. Norton (1979)minimal value when hydrothermal systems can operate,
7. permeability according geophysical data.

Fig. 2. Generalized trend of the rock permeability of the continental crust on depth

The results of effective porosity and permeability measurements on the main lithological types of rocks collected from the core samples of the boreholes drilled in the area of the Krasnoyarsk MCC, where HLW depositories also can be located, show that mean porosity values is 0.44 % and mean permeability values is $1.30 \cdot 10^{-18}$ m^2.

Thus, low porosity values are typical for metavolcanits and granitoids, as well. Mean parameter values are close. At the same time mean permeability value for granitoids is one decimal order higher than for metavolcanits. The difference is caused by different structure of rock pore shape. The microcracks are widely propagated in granitoids which, according V.I. Starostin (1988), belong to rocks of fragile low-solid (weak) petrophysical type in contrast with metavolcanits, which are rocks of viscous solid type. However, permeability values of granitoids and metavolcanits are low enough for safe HLW depositories location and in case when they will be placed in the massive blocks of adequate thicknesses.

In order to estimate the enough thickness of the massive blocks necessary for a HLW disposal numerical simulation of radionuclide transport by thermal convective groundwater flow was carried out. On the basis of ^{90}Sr concentration the safe depth of HLW location was found as a function of rock permeability. The data of permeability determinations on the rock samples were used as input data for the model.

In order to reconstruct a functioning of paleo-hydrothermal ore-forming system an experimental study of filtration properties of main types of Streltsovskoe ore-field was carried out. It was found that contrast difference in filtration properties of rocks is caused by character of their pore structure. It is significant that as in case of granitoids and metavolcanits mentioned above there is also no direct relationship between porosity and permeability of the rocks.

It was found that ore-bearing dacite has maximal permeability and porosity values. For the rock the

maximal permeability anisotropy values reaching two decimal orders in some samples are also typical. It should be noted that the trend is also valid for minimal dacite permeability values obtained when filtration normal to fluidal texture is used to simulate a vertical flow from a deep source. Basalt porosity is a few times higher that granite porosity. In contrast, permeability of basalt is considerably lower.

During microstructure investigations it was found that in dacite microcracks and isometrical pores also contribute in total porosity. The both elements are oriented along fluidal structure effecting on permeability anisotropy which exerted a strong influence on fluid flow in volcanic rocks forming caldera mantle. Numerical simulation with use of the experimental data showed specific kinks on fluid pathways caused by rock anisotropy. Higher basalt porosity values are due to the occurrence of many isometrical pores in the rock. However, the results of sample inspection using scanning electron microscope showed that about a half of pores in basalt are dead-end. So, there is no fluid flow in a half of pore rock volume and, as a result, permeability of basalt is low. Intersecting microcracks forming interconnecting clusters contribute to granite porosity. As a result, permeability of granite is higher than that one of basalt.

During the permeability investigations at high temperatures and pressures corresponding to the conditions of ancient hydrothermal system in Streltsovskaya caldera it was found that pressure increase lead to monotonous permeability decrease. In contrast, temperature increase lead to rise of permeability in all the studied samples. It is significant that the ratio between initial permeability values kept at all *PT*: granite permeability is comparable to dacite one measured normal to fluidization. Dacite permeability along fluidization is considerably higher.

Conclusion. An experimental study of the main types of crystalline rocks at high PT-parameters corresponding to deep zones of continental crust and near-field of HLW repository *in situ* and paleo-hydrothermal systems was carried out.

It was found that rock permeability and PT-trend pattern is caused by their pore structure changes: first of all, by microcracking parameters.

Use of the physical experiment results as input data for numerical one allowed to determine safe depth of HLW well-repositories and fluid pathways pattern in hydrothermal ore-forming system of Streltsovskoye ore field.

The work is supported by RFBR (*grant 11-05-00778*), Presidium of the RAS (*Program 4*) and Earth Sciences Division of the RAS (*Program 8*).

References

1. Shmonov V.M., V.M. Vitovtova, A.V. Zharikov (2002), *Fluid permeability of the rocks from the Earth crust*, Nauchniy Mir, Moscow.
2. Manning C.E., S.E. Ingebritsen (1999), Permeability of the continental crust: implications of geothermal data and metamorphic systems, *Rev. Geophysics.*, 37, № 1, pp. 127-150.
3. Norton D. (1979), Transport phenomena in hydrothermal system: the redistribution of chemical components around cooling magmas, *Bull.Mineral.*, 102, № 5/6. pp. 689-716.
4. Starostine V.I. (1988), *Paleotectonical conditions and mechanisms of formation of ore deposits architecture*, Nedra, Moscow.

Rudakov V.P, Tsyplakov V.V. Global factors in dynamics of petrophysical processes

EPI RAS 123995 Moscow, B.Gruzinskaja 10; rudak@mail.ru; ph.: (499) 254-90-06

***Key words**: global geodeformation processes; karst-suffosion processes, fluid dynamic regime, spectral –correlation analysis*

In the classical description of the structural-tectonic fragments of the earth crust the vast territories of ancient platforms are represented as geodynamically passive elements of the lithosphere. That is why the nature of various phenomena occurring on the platform (landslides and karst-suffosion processes, rock bursts and gas explosions in mines, pipeline breaks, etc.) is usually associated solely with the processes of exogenous changes in the geological environment, formed by rocks of sedimentary cover [1]. However, the results of many years investigations of the geodeformation regimes of the geodynamically (seismically) active and platform regions allowed experimentally establish [2] that in the preparation of catastrophic geodynamic phenomena (earthquakes and volcanic eruptions) prominent role played by the processes of global change of the stress-strain state of the lithosphere due to the processes of self-organization under the influence of the Earth velocity rotation variations. In particular, it was shown that these processes are reflected in the changes of fluid dynamic regimes of the fault structures of the East European Platform (EEP), influencing the processes of the exogenous geological environment transformation, and, appearing in the rocks of the sedimentary cover by the local geodynamic processes and phenomena. For example, it was found that the dynamics of accidents on the routes of gas pipeline networks of the EEP is connected with the wave motion of the platform, as well as with the processes of cyclic fluid transmission in the fault transcontinental and regional tectonic formations that form the dynamics of the karst-suffosion processes in the territories of the Moscow depression [3].

Continuing to investigate the links in the chain of cause-effect dependence of the local geodynamic phenomena and processes from the processes of global change in the stress-strain state of the earth's crust, we made spectral and correlation analysis of a half century (49 years) time series of mean annual cases of the karst gap formation in Dzerzhinsk, Nizhny Novgorod region in comparison with the variations of the water level in the Oka River, which flows in the area, variations in the Earth's rotation and the change in solar activity. It allowed to trace the development of karst-suffosion processes influenced by changes in fluid dynamic regimes in the region controlled by variations in the stress-strain state of the earth's crust in the region associated with variations in the Earth's rotation and changes in solar activity, controlling the climate changes on the Earth as a whole, and in each particular region of the planet.

Note that the problem of assessing the influence of solar-terrestrial relationships in the processes of the terrestrial atmosphere, hydrosphere, and even biosphere, after A.L. Chizhevsky concerned by many researchers [4] but geological and geophysical aspects of this problem are practically not affected. Especially not enough investigated the processes that control in the platform conditions the development of the exogenous processes,

such as the karst-suffosion. And in this respect the opportunity to examine long-term observations, of the" Dzerzhinsk karst observatory" of the Nizhny Novgorod region allowed, as it seems to us, to take another step toward assessing the extent of planetary processes influence on the dynamics of the geodynamic processes of the local scale.

Figure 1 shows the original time series of mean annual variations of the Earth's rotation velocity (relative value), solar activity (Wolf numbers), cases of karst gaps in Dzerzhinsk and the water level in the Oka river, which were analyzed on the basis of calculation the spectral-temporal and correlation characteristics of these time series and their components identified by energy filtering.

Figure 2 shows the calculated values of the cross-correlation function (CCF) between the analyzed time series.

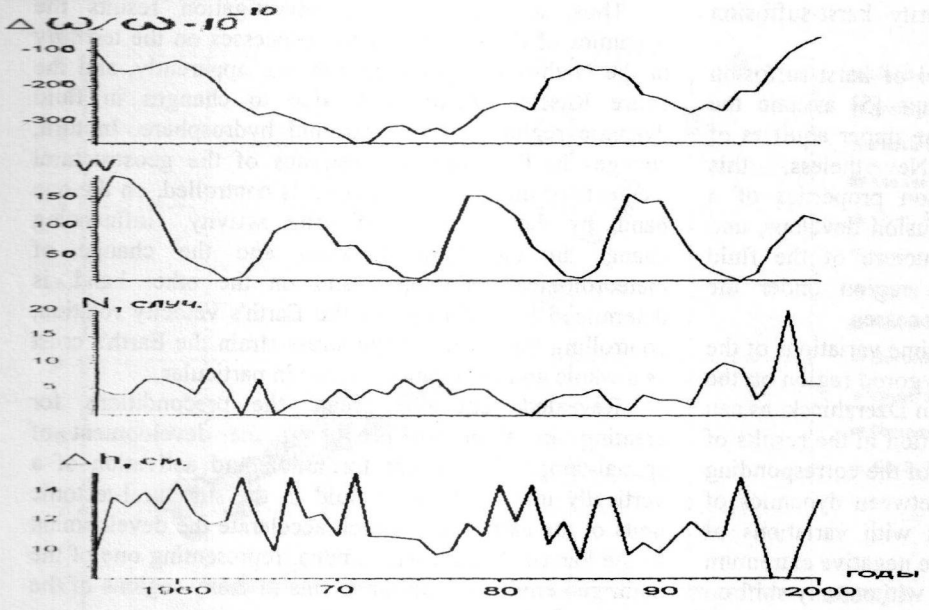

Fig.1. Time series of variations of the average annual values (from top to bottom): the Earth's rotation velocity, solar activity index; karst gaps in Dzerzhinsk, water level variations in the river Oka.

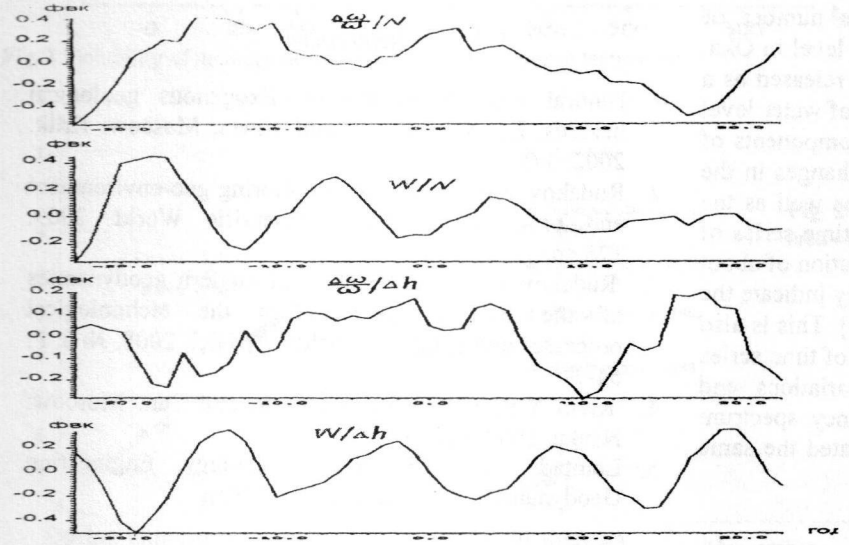

Fig.2. Graphs of the cross-correlation between the time series (top to bottom): variations in the Earth's rotation and the number of karst gaps in Dzerzhinsk, variations in solar activity and the number of karst gaps in Dzerzhinsk, variations in Earth rotation velocity and variations of water level in the river Oka, variations in solar activity and water level variations in Oka river.

As can be seen from Figure 2a, the characteristic of CCF between variations in the Earth's rotation and the number of karst gaps in Dzerzhinsk, indicate of a weak (K = 0.25) but significant (P= 0,9) direct correlation, as well as the correlation with a shift 2 years and 17 years. In this case, the spectrum allocated CCF peak with a period of 22 years, typical for a spectrum of variations in solar activity.

At the same time, from Fig. 2b follows that, despite the absence between the time series of solar activity variations and the number of karst gaps in Dzerzhinsk (2b) direct significant correlation, the form, of resembling a damped sinusoid with a period of 11 years is testimony to the presence of a significant correlation in retrospect. In this case, the correlation coefficient with a shift in the past 17 years is significant K = 0.5 (P= 0.9). In the spectrum of the CCF of these parameters are distinguished peaks with a period of 11 and 5 years, which are also characteristic for the spectra of the time series of precipitation falling in the region.

The influence of global factors on the variation of water level in Oka, associated with the hydrodynamic regimen of the region, manifested as follows.

According to the cross-correlation function between the variations of Earth rotation and variations in water level in the Oka (Fig. 2c) there is no direct significant correlation. However, with a lag of 10 years there has been significant (P = 0,9) negative correlation (R =-0.3) between these parameters and the spectrum of CCF stand out peaks with a period of 11 years and 22 years.

Between the time series of solar activity variations and water level variations in Oka (Fig.2g) direct significant correlation is also absent, however, the function has the

form of almost regular sinusoid with a period of 11 years, indicating the relationship of changes in water level in Oka with variations in solar activity. In the spectrum of CCF stands clear peak with a period of 11 years.

Proceeding from the results of mathematical analysis of time series of seemingly unrelated parameters, we attempt to assess the influence and role of global factors (variations in the Earth's rotation and changes in solar activity) in the chain of cause-effect relations of the formation and development of local geodynamic processes and phenomena to what are primarily karst-suffosion processes in the Russian platform.

Note that the conventional model of karst-suffosion processes and formation of karst gaps [5] assume the aggressive participation in them of the upper aquifers of the underground hydrosphere. Nevertheless, this participation confined to the filtration properties of a specific rock complex, in which suffusion develops, and virtually ignored the space-time structure of the fluid dynamic regimes formation in the region under the influence of global geodeformation processes.

Influence of the fluid dynamic regime variations of the geostructural complex of Nizhniy Novgorod region on the dynamics of the karst gaps formation in Dzerzhinsk, as can be seen, have found an indirect reflection in the results of the interrelation and spectral analysis of the corresponding time series. The direct connection between dynamics of karst formation gaps and variations with variations of water level in the river Oka clear in the negative extremum in the curve of interrelation functions without any shift on the horizontal axis relative to the zero coordinates. Latter shows almost simultaneous increase in the number of failures in response to the lowering of water level in Oka. At the same time, the periodic components, released as a result of interrelation of time series analysis of water level variations in Oka, in comparison with the components of time series of solar activity variations and changes in the Earth's rotation for 11 years and 22 years, as well as the periodicity, standing out in the spectrum of time series of the karst gaps and water level in the Oka duration of about 2 and 4 years and 8, 11, and 22 years, directly indicate the relation with the processes of global scale [4]. This is also confirmed by the results of spectral analysis of time series of monthly averages of solar activity variations and changes in the Earth's rotation, the frequency spectrum sliding correlation functions are fairly allocated the same frequency lasting 2 and 4 years, 8, 11 and 22 years, as well as components with a period of 1 year.

Nature of the trend (regional) component of the time series of karst failures, selected by the energy filter, similar to the nature of the trend component of the change in the Earth's velocity variations is an additional argument in favor of approval of the connection of local geodynamic phenomena, to what is the periodic activation of karst-suffusion processes in the Nizhny Novgorod region, with the processes of global scale.

Thus, according to the investigation results the dynamics of the karst-suffosion processes on the territory of the Nizhny Novgorod region (as, apparently, and the entire Russian platform) is due to changes in fluid dynamic regimes of underground hydrosphere. In turn, changes in fluid dynamic regimes of the geostructural elements of the Russian platform is controlled, on the one hand, by the variations of solar activity influencing change in the Earth rotation and the change of meteorological parameters and on the other hand, is determined by variations in the Earth's velocity rotation, controlling the nature of the stress-strain the Earth's crust as a whole and on a regional scale in particular.

Revealed regularity create the preconditions for creating an algorithm predicting the development of spatial-temporal structure formation and activation of a vertically upward flow of fluid in the structural-tectonic units of the earth crust, which accelerate the development of the karst-suffosion phenomena, representing one of the main geo-environmental problems in many regions of the Russian platform.

References

1. Natural Hazards in Russia. Exogenous geological hazards. Ed. V.I. Osipov and others, Moscow: Kruk. 2002. 345.
2. Rudakov V.P. Emanation monitoring geo-environment and processes. Moscow: Scientific World. 2009. 176 pp.
3. Rudakov V.P. Manifestation of modern geodynamics of the Russian platform in the technological processes and emanation fields. / ANRI. 2008. № 2. P. 64-71.
4. Rivin Y.R. Cycles of the Earth and Sun. Moscow: Nauka. 1989. 165pp.
5. Lomtadze V.D. Engineering geology. Engineering Geodynamics. L.: Nedra. 1977. 479pp

Experimental geoecology

Alekhin Y.V., Zagrtdenov N.R., Mukhamadiyarova R.V, Smirnova A.S.

Experimental study of metallic mercury solubility in water

Geol.dep. MSU alekhin@geol.msu.ru fax.: +7 495 939 4808, ph.:+7 495 939 4962

Key words: *metallic mercury solubility; mercury solubility in water; Henry's coefficient for steams of mercury*

Solubilities of elementary mercury in water in the range of temperatures 120-500^0 C are devoted the experimental works executed in IEM of the Russian Academy of Sciences [Sorokin, 1973; Sorokin et al., 1978; Sorokin et al., 1988]. The great number of publications suffices for an interval 20-120^0 C along a line of pressure of sated steam of water at a seeming coordination and unity of temperature dependence of solubility are in the obvious contradiction with the reliable high-temperature data (fig. 1).

Unusual nonlinearity of dependence lg m – 1/T for simple reaction Hg^0_{liquid} - Hg^0_{aq} at $\Delta C_p = 0$ forces to assume change of the dominating form in a solution in the field of low temperatures. We had been suggested the version about complete dominance of form Hg^0_{aq}

(dissolved) at high temperatures when solubility of elementary mercury is high also prevalence of the oxidized forms of mercury at the low.

Extrapolation of this version in area of low temperatures (fig. 2) had been received the value of solubility Hg^0 appropriating at temperature 20^0 C to concentration 1,99 ppb. Other values of extrapolation are resulted in table 1.

Table 1. The values of concentration calculated on extrapolation of the literary data

t, ^{0}C	1000/T	-lg m	C $_{Hg(0)}$, ppb
20	3,411	8,004	1,99
25	3,354	7,830	2,97
40	3,193	7,343	9,10
60	3,002	6,763	34,65
80	2,831	6,248	113,45

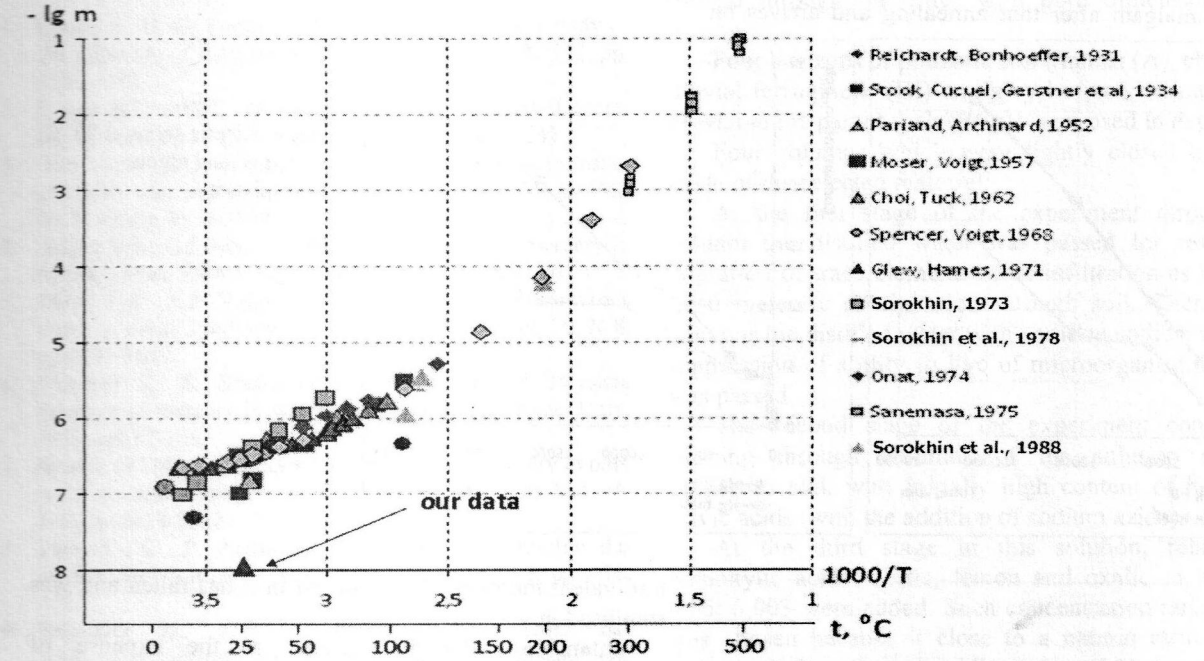

Fig. 1. Solubility of mercury in water as function of inverse temperature

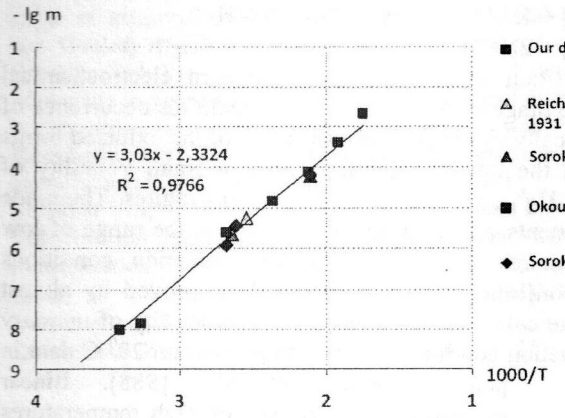

Fig. 2. Extrapolation of the high-temperature data in area of low temperatures and position of our data

During experiment a small amount of metal mercury has been placed in three round-bottomed three-litre flasks with 2,5 litres of twice distilled water. Gases barbotage and sampling were carried out through glass tubes of different length in apertures of bottlenecks. Bottlenecks and all joints have been hermetically sealed by a parafilm. The first flask is left equilibrium with atmospheric air, through two others under pressure argon throughout 15 minutes was passed. In the third flask has initially been added sodium borohydride as a reducer. Scheme of experiment is presented in figure 3.

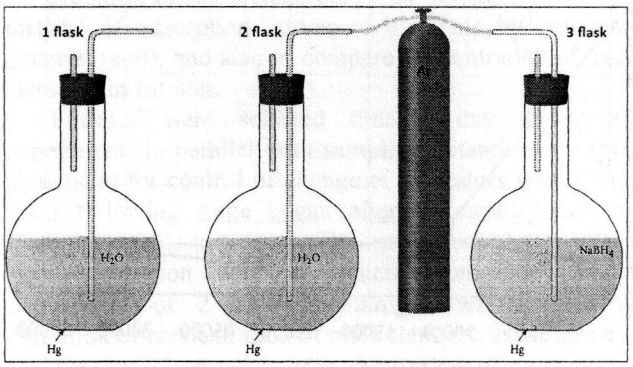

Fig. 3. Scheme of experiment:1st flask: oxygen atmosphere;2nd flask: argon atmosphere;3rd flask: argon atmosphere + $NaBH_4$

Samples in volume of 25 ml were selected during experiment some times by means of a 50 ml syringe. At first experience was spent at 20^0 C. Then the flask №3 has

been placed in drying box and sated at temperature 33^0 C. Under this data kinetic series have been constructed (fig. 4, 5).

Mercury definition on atomic absorber UCM-1MC was spent by a method of cold steam by means of analytical block PAR-3M. The analysis principle is based on discrete measurement of concentration of steams of elementary mercury with preliminary accumulation of this mercury on a collector presented by a double helix sorbent with a gold covering. Mercury collects on a gold substrate, forming an amalgam after that annealing and arrives on the detector which represents atomic absorption photometer with stabilised nonelectrode mercury lamp, length of a wave of radiation: 254 nanometers. Thus, the device registers the contents of elementary mercury. In the beginning samples were put directly, without any preparation, so such way defined quantity null-valent mercury. In parallel aliquots of samples solutions $NaBH_4$ that restored all other forms to null valency before definition of total contents of mercury were brought.

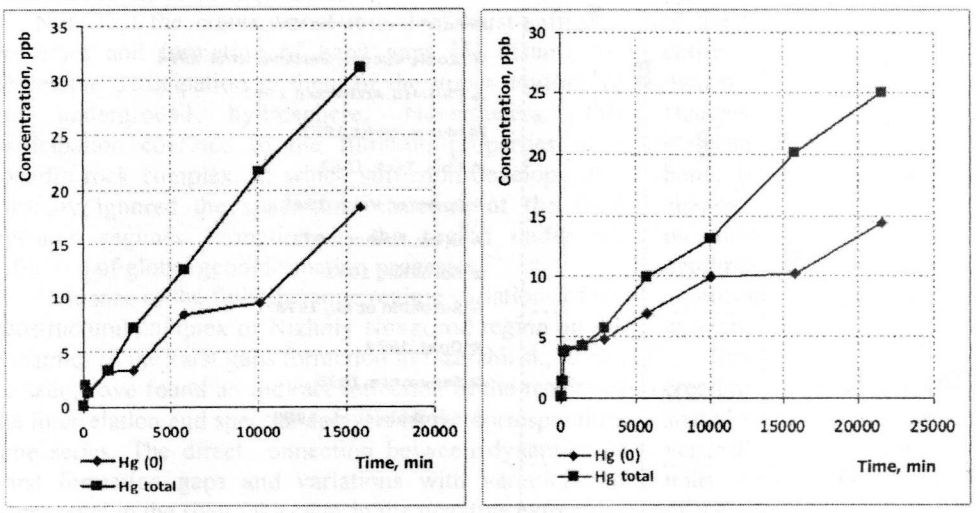

Fig. 4. Kinetic series at 20 ^{0}C at oxygen and argon atmospheres

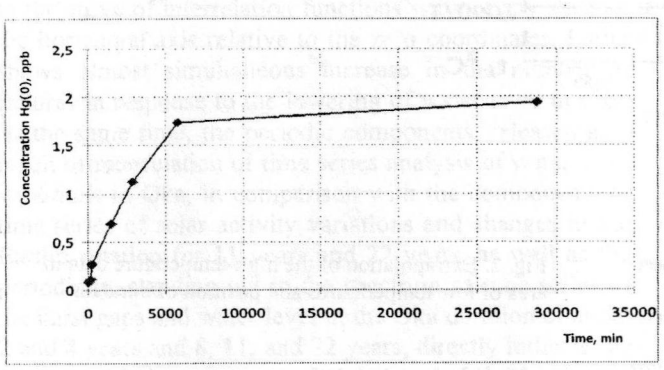

Fig. 5. The kinetic series in strongly reducing conditions at 20 ^{0}C, which is formed by hydrogen generation on reaction $NaBH_4 + 4H_2O \leftarrow\!\!\rightarrow H_3BO_3+NaOH+4H_2\uparrow$

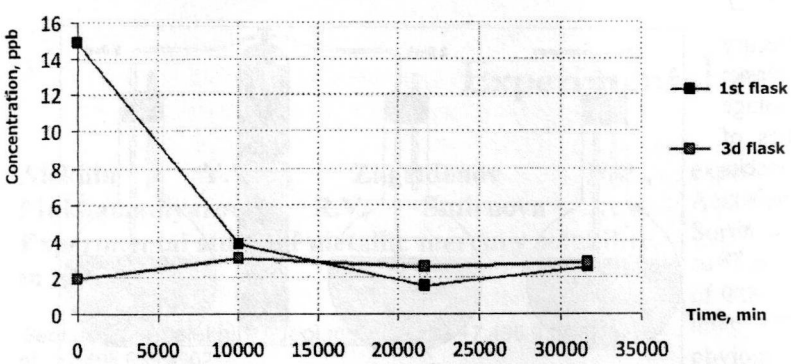

Fig. 6. The approach to balance "from below" and "from above" at 33 ^{0}C in reducing conditions

At 33^0 C in a flask with oxygen atmosphere has been brought sodium borohydride and, apparently on fig. 6, null-valent mercury concentration in it has fallen and was stabilised in value of 2,75 ppb.

Intensive reduction realised at the expense of hydrogen, which evidently formed during decomposition reaction sodium borohydride $NaBH_4$ in water:

$NaBH_4 + 4H_2O \leftarrow\!\!\rightarrow H_3BO_3+NaOH+4H_2\uparrow$

$NaBH_4 + 2NaOH + H_2O \leftarrow\!\!\rightarrow Na_3B0_3 + 4H_2\uparrow$

Position of mercury in a standard electrochemical voltage range of metals isn't an obstacle for occurrence of analytically significant concentration of the oxidized forms against the lowest solubility Hg^0_{aq} at small volatility of steams Hg^0_{liquid} in the field of low temperatures. The made experiments on solubility of mercury in the range of low temperatures in various oxidation-reduction conditions have confirmed this assumption. It is proved by almost absolute coincidence of our data on solubility of mercury in reduction conditions with extrapolated on 20^0 C data in paper [Sorokin et al., 1988]. Linear extrapolation from area of high temperatures for Hg^0_{aq} gives quantity of solubility 1,99 ppb. We experimentally receive value 1,95 ppb. This value on one and a half order more low, than total solubility in oxidising conditions.

Conclusions

1) version about domination of form Hg^0_{aq} is experimentally confirmed at high temperatures and the constant of reaction $Hg^0_{liq} - Hg^0_{aq}$ (lg K = lg m = - 8,01) is found at full prevalence of the oxidised forms of mercury in the field of low temperatures, that allows to calculate Henry's coefficients for steams of mercury from the data on fugacity.
2) The quantity of the oxidised forms of

mercury in time continuously grows in oxygen atmosphere that speaks about constant oxidation of mercury by water.

3) Values of solubility of 1,95 ppb are experimentally received at 20^0 C that on one and a half order more low, than total solubility in oxidising conditions, and 2,75 ppb at 33^0 C.

RFFR 11-05-93107-CNRS-a

References

1. Choi S.S., D. G. Tuck (1962). A neutron-activation study of the solubility of mercury in water. J. Chem. Soc. N 797, pp. 4080-4088.
2. Clever H.L. (1987). Mercury in liquids, compressed gases, molten salts, and other elements. Pergamon Press, 245 p.
3. Glew D.N., D.A. Hames (1971). Aqueous nonelectrolite solutions. Mercury solubility in water. Canad. J. Chem. Vol. 49, N 19, pp. 3114-3118.
4. Kuntz R.R., G.J. Mains (1964). The solubility of mercury in hydrocarbons. J. Phys. Chem. Vol. 68, N 2, pp.408-410.
5. Moser H.C., A.F. Voight (1957). Dismutation of mercurous dimer in dilute solutions. J. Amer. Chem. Soc. Vol. 79, N 8, pp.1837-1841.
6. Okouchi S., S. Sasaki (1983). Chemical and Physical behavior of mercury in water. Rept. Colll. Eng. Hosei Univ. N 22, pp. 57-106.
7. Onat E. (1974). Solubility studies of metallic mercury in pure water at various temperatures. J. Inorg. Nucl. Chem. Vol. 36, N 9, pp. 2029-2032.
8. Pariand J.C., P. Archinard (1952). Sur la solubilite des metaux dans lean. Bull. Soc. Chim. France. F. 5/6, pp. 454-456.
9. Reichardt H., K.F. Bohoeffer (1931). Uber das Absorptionsspectrum von gelostem Quecksilber. Ztsch. Phys. Bd. 67. H. 11/12, ss. 780-789.
10. Sorokhin V. I. (1973). Solubility of mercury in water in the range of temperatures 300-500 ^{0}C and pressure 500-1000 atm. Doklady AS USSR. V. 213, №4, pp. 852-855 (in Russ.).
11. Sorokhin V. I, Yu..V.Alekhin, T.P. Dadze (1978). Solubility of mercury in systems Hg-H_2O, HgS - (Cl)-H_2O and forms of its existence in sulphide forming thermal waters of Kamchatka and island Kunashir. Sketches physical and chemical petrology. Issue. 8, pp. 133-149 (in Russ.).
12. Sorokhin V. I, V.A.Pokrovsky, T.P. Dadze (1988). Physical and chemical conditions of formation surmjano-mercury mineralization. 144 p. (in Russ.).
13. Stook A., F. Cucuel, F. Gerstner et al. (1934). Uber Verdampfung, Loslichkeit und Oxidation des metallischen Quecksilber. Ztschr. Anorg. Und allg. Chem. Bd. 217. H.3, s.241.

Drozdova O.Y.[1], Alekhin Y.V.[2], Ilina S.M.[2], Lapitskiy S.A.[2], Sokolova M.N.[2] Results migration mobility investigation of microelements in the soil horizons under the influence of humus and carboxylic acids

[1] Soil. Dep. MSU; [2] Geol Ddep. MSU alekhin@geol.msu.ru.
fax:(495) 939 48 08, ph.: 4959394962

Formation of regular soil profiles podzols of boreal zone is defined by extracting features of humic and carboxylic acids formed during the biodegradation of plant litter. The structure features of soil profiles associated with variable, but high rates of downward filtering of these aggressive acids in landscapes with seasonal humidity. We experimentally simulated these conditions for studying a wide range of mobility of trace elements in soil horizons [Alekhin and Kostyukova, 2002].

Experimental methods receptions at carrying out of these experiences were similar to what are used at chromatographic differentiation into columns with processing of results by a method of concentration curves [Alekhin and Lakshtanov, 2008; Lakshtanov and Alekhin, 2005].

Objects and method Soil and soil water samples were collected in Meshcherskaya lowland. Soil water was filtered through the filter with pore dimension of 0.2 micron.

Four horizons of podzolic soil (humus (A), eluvial (E), illuvial ferruginous (Bf) and gley horizon transition from illuvial to the parent rock (BCg)) were used in experiment.

Four columns which were tightly closed have been made of the selected material.

At the first stage of the experiment through each column the distilled water was passed for research of migration of trace elements at its infiltration as analog of fresh meteoric precipitation through soil. Then through columns the distilled water with addition sodium azide (for suppression of ability to live of microorganisms of soils) was passed.

The second stage of the experiment consisted in filtering through columns of the solution close on properties soil, with initially high content of humic and fulvic acids (with the addition of sodium azide).

At the third stage in this solution, related soil, carboxylic acids: acetic, lemon and oxalic in a ratio 1: 0,05: 0,003 were added. Such concentration ratio of acids was chosen because it close to a natural ratio in water extracts from soils and acidity (pH = 4,2) the solution is comparable to natural size [Hees et.al., 1996]. Addition of these acids in filtrant allowed to make active process of migration of elements of soil layers, remaining within the limits of experiment approach to natural process.

At the fourth stage of the experiment polyelement standard ICP-MS-68B Solution A (High-Purity Standards) was added to a solution with humic and carboxylic acids. The standard solution contains elements (Al, As, Ba, Be, Bi, B, Cd, Ca, Ce, Cs, Cr, Co, Cu, Dy, Er, Eu, Gd, Ga, Ho, In, Fe, La, Pb, Li, Lu, Mg, Mn, Nd, Ni, P, K, Pr, Re, Rb, Sm, Sc, Se, Na, Sr, Tb, Tl, Th, Tm, U, V, Yb, Y, Zn) with concentration 100,0 ± 0,5 mg/l. The standard was dissolved so that initial concentrations of all elements in a solution were 1 mg/l (pH = 3,5).

Addition of microelements given the chance to study method of adsorption curves of elements by columnar material (soil), and also to compare concentration of trace elements in filtrates.

Filtrates were selected time a day during all experiment. In parallel with sampling potentiometry (pH, pNa, pCa) for control of change of indicators were spent. Each following stage began after an establishment in system of stable indicators. The mass spectrometer of the high permission with is inductive-connected plasma ELEMENT of 2 Thermo Finnigan was applied to definition of concentration of trace elements in filtrates.

Results of research of a desorption of elements at various modes of filtering Activity of a desorption of trace elements was defined by the coefficient of delay calculated on the equation: $R_1 = 1 - C_{filtrate} / C_{initial\ solution}$, where $C_{filtrate}$ is concentration of element in the filtrate, $C_{initial\ solution}$ is concentration of element in filtrante (initial solution).

Abstracts

For the first column (humus horizon) rows of microcells on increase in migratory activity have the following sequences: at a filtration of the distilled water: Eu< Er< Dy< Sm< Gd< Pr< Cd< La< Nd< Ce< Pb< Ti< Cu< Sr< Ba< Zn< Fe< K. At a filtration of natural solutions (soil water): Sr (0,94)< Ba (0,27)< Eu (-5,32)< Ti (-5,66)< Cd (-6,72)< Er (- 8,15)< Dy (-11,71)< Gd (-18,37)< Nd (-29,51)< Pb (-37,59)< La (-40,33)< Pr (-41, 13)< Ce (-59,98)< Sm (-69,75)< Fe (-107,40)< Cu (-244,08)< K (-1,8 * 104)< Zn (-2, 7 * 1012). At a filtration of natural solutions with carboxylic acids: Sr (-0,2)< Ba (-1,22)< Cd (-10,31)< Eu (-12,54)< Ti (-26,21)< Er (-36,06)< La (-37,94)< Nd (-41,36)< Gd (-46,10)< Pr (-49,09)< Dy (-49,23)< Sm (-53 , 37)< Ce (-55,83)< Cu (-255,66)< Pb (-258,51)< Fe (-656,10)< Zn (-4 * 104)< K (-3 * 107). Addition carboxylic acids increases the transfer of trace elements (except Zn), but mobility rows essentially don't differ from rows transport by fulvic acid drainage water.

The material of the second column (eluvial horizon) differs from the first considerably the smaller maintenance of humus, therefore rows of migratory mobility slightly different, but all basic laws remain the same: at a filtration of the distilled water: Eu< Er< Dy< Gd< Sm< Pr< La< Nd< Cd< Ce< Pb< Ti< Cu< Sr< Ba< K< Fe< Zn. At a filtration of natural solutions: Sr (0.37)< Ba (-0.58)< Ti (-2.10)< Er (-3.29) < Dy (-4.31)< Eu (-4.46)< Gd (-6.36)< Cd (-9.3)< Nd (-11.47)< Pr (-14.10)< Pb (-16.7)< La (-16.85)< Sm (-22.23), Ce (-22.23)< Fe (-42.51)< Cu (-5683.58)< K (-18279.29)< Zn (-9.9 * 1011). At a filtration of natural solutions with carboxylic acids: Sr (-0.15)< Ba (-0.68)< Cd (-3.49)< Er (-3.76)< Eu (-3.96)< Dy (-9.18)< Gd (-14.69)< Ti (-15,28)< Nd (-18.30)< Sm (-18,44)< Pr (-27,34)< La (-29,17)< Ce (-37,34) < Cu (- 104,25)< Pb (-109,93)< Fe (-186,93)< Zn (-52242,14)< K (-4.1 * 106).

For the third column following numbers of migratory mobility were received: at a filtration of the distilled water: Pr< La< Ce< Nd< Sm< Gd< Eu< Dy< Er< Ti< Cd< Pb< Sr< Ba< Cu< Fe< K< Zn. At a filtration of natural solutions: Sr (-0,02)< Er (-1,37)< Ti (-1,91)< Ba (-2,30)< Nd (-9,45)< La (-10, 27)< Fe (-10,45)< Ce (-11,39)< Pr (-15,44)< Gd (-58,16)< Eu (-81,62)< Cd (-91,12)< Pb (-96,28)< Dy (-131,96)< Sm (-162,03)< Cu (-1195,10)< K (-15249,37)< Zn (-4,3 * 1011). Comparing with the previous columns, it is possible to notice that values of coefficients of delay Gd, Eu, Cd, Dy and Sm have decreased that shows increase in their migratory mobility. Reduction of their migratory activity is visible on values of coefficients of delay Cu and Fe. The coefficient of delay Sr became negative, it shouldn't be adsorbed. At a filtration of natural solutions with carboxylic acids: Sr (-0,47)< Ba (-4,25)< Ti (-32,21)< Ce (-1443,22)< Nd (-1694,37)< Cd (-1768,45)< La (-1988,63)< Fe (-2014,10)< Cu (-2201,85)< Pb (-3633,88)< Dy (-6688,51)< Gd (- 7080,42)< Eu (-7567,98)< Er (-7709,76)< Pr (-8005,51)< Sm (-8791,10) < Zn (-151862,87)< K (-6, 5 * 107). In comparison with the previous regime the sequence changed in copper position and if to compare to other columns, - that it is necessary to note cardinal change in the ratio of the coefficients of delay in group of the rare earth elements. But the main difference from other columns and the previous regimes is considerable changes of coefficients of delay for the majority of elements. It speaks about intensification of carrying out of elements at addition carboxylic acids for illuvial horizon of podsolic soils.

For the fourth column at a filtration of the distilled water the received row of migratory activity looks as follows: Sr< Cd< Ba< La< Ce< Pr< Nd< Sm< Eu< Gd< Dy< Er< Pb< Ti< Fe< Cu< Zn< K. At a filtration of natural solutions: Sr (-0,02)< Ba (-0,54)< Ti (-0,57)< Cd (-6,66)< Fe (-6,84)< Nd (-10,67)< Pb (-15,05)< Eu (-16,87)< La (-18,33)< Gd (-23,24)< Dy (-25,01)< Ce (-25,95)< Pr (-46,30)< Er (-50,97) < Sm (-81,10)< Cu (-4824,24)< K (-8139,56)< Zn (-3.5 * 1012), for this column it differs from previous in high coefficient of delay of iron. At a filtration of natural waters with addition of carboxylic acids iron moving by the end of row of migratory mobility after all number of the rare earth elements also is marked: Sr (-0,20)< Ba (-0,99)< Cd (-6,74)< Ti (-23,44)< Eu (-58,740)< Er (-74,77)< Fe (-136,89)< Dy (-161,01)< Gd (-248,92)< Nd (-308,45)< Sm (-335,53)< La (-338,43)< Pr (-409,48)< Pb (-410,30)< Ce (-545,80)< Cu (-1564,75)< Zn (-149511,07)< K (-4.4 * 107).

Results of experiments show that actively migration of trace elements occurred in illuvial horizon that is natural as trace elements contain in it in the greatest quantity. If to compare various regimes for the majority of considered trace elements (excepting iron, potassium, zinc) the adsorptions occurred most actively in the infiltration of the soil solution with carboxylic acids.

Table 1. Integrated factors of a delay of elements

Soil horizon	Cd	Sr	Ba	Pb	Cu	Fe	Zn	K
A	0,7	0,9	0,9	1	1	-17,5	-1,6	-0,1
E	0,3	0,4	0,4	0,7	0,5	-2,9	-0,8	-0,04
Bf	0,2	0,3	0,3	0,7	0,5	-7,1	-3,7	-0,05
BCg	0,2	0,2	0,2	0,5	0,3	-0,6	-1,4	0

Table 2. Integrated factors of a delay of elements

Soil horizon	La	Ce	Pr	Nd	Sm	Eu	Gd	Dy	Er
A	1	1	1	1	1	1	1	1	1
E	0,8	0,6	0,5	0,4	0,4	0,4	0,4	0,4	0,4
Bf	0,7	0,5	0,4	0,4	0,3	0,3	0,4	0,3	0,2
BCg	0,8	0,7	0,6	0,6	0,5	0,5	0,6	0,5	0,4

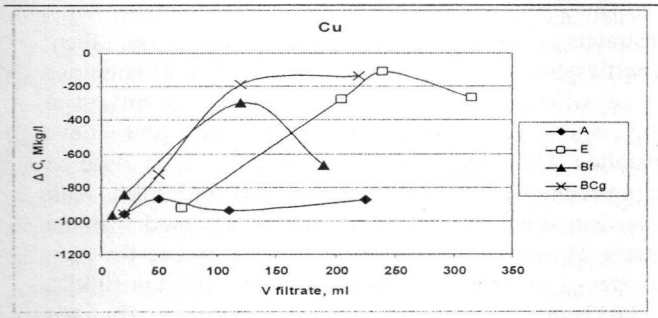

Fig. 1. Adsorption-desorption curves of Cu

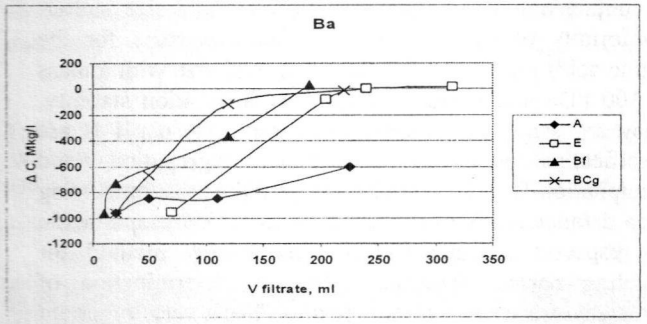

Fig 2. Adsorption-desorption curves of Ba

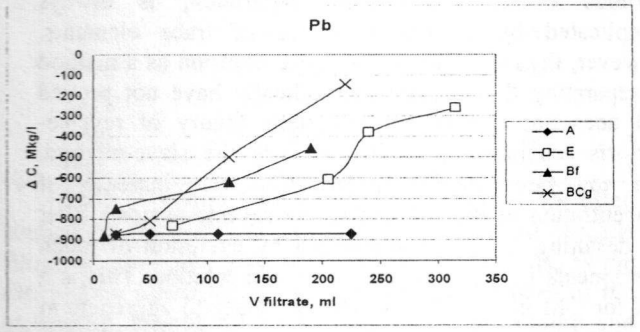

Fig 3. Adsorption-desorption curves of Pb

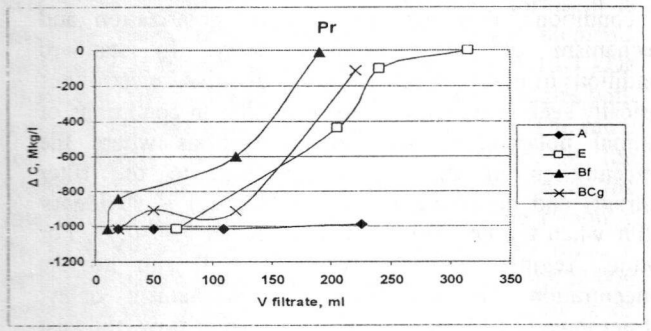

Fig 4. Adsorption-desorption curves of Pr

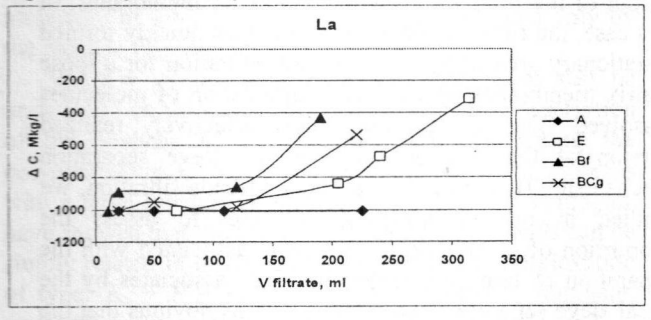

Fig 5. Adsorption-desorption curves of La

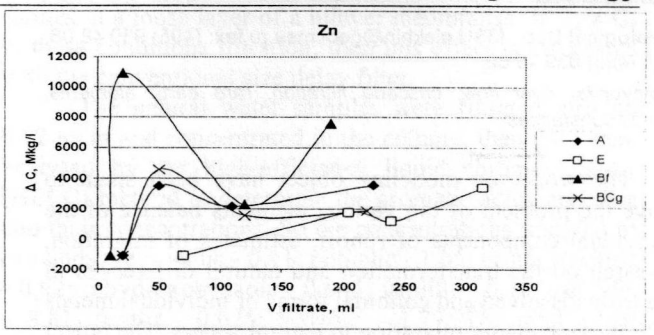

Fig 6. Adsorption-desorption curves of Zn

Results of research of elements adsorption The characteristic of intensity of realization of process of adsorption is the indicator of integrated coefficient of delay:

$R_2 = 1 - (\sum(C_{filtrate} * V_{filtrate})/(C_{initial\ solution} * \sum V_{filtrate}))$, where $C_{filtrate}$ is concentration of element in the filtrate, $V_{filtrate}$ is the volume of filtrate taken, $C_{initial\ solution}$ is concentration of element in filtrante (initial solution). The integral coefficient of delay are presented in Tables 1 and 2.

On the calculated integrated coefficients of delay it is visible that all considered elements most actively sorbed in humus horizon (especially rare earth elements).

Adsorption of bivalent metals (Cu, Sr, Cd, Pb, Ba) is shown more poorly in BCg horizon (table 1 and fig. 1-3); adsorption of rare-earth elements is shown in the minimum degree in illuvial and eluvial horizons (table 2 and fig. 4,5).

As a result of an ionic exchange and extraction from soils, against adsorption of most trace elements, the desorption for Fe, Zn and K (table 1 and fig. 6) continues.

Grants of RFFR 11-05-00464-a, 11-05-00638-a

References

1. Alekhin Yu.V., E.E. Kostyukova (2002). Membrane transport in geochemical systems, Matertaly the Scientific Conference for Basic Research in Geology, Geochemistry, Geophysics at the turn of XX and XXI centuries. V. 2, pp.31-33 (in Russ.).
2. Lakshtanov L.Z., Yu.V. Alekhin (2005). The main mechanisms of directed evolution of pore solutions. (Modern state of the art filtration effect). The collection of articles entitled "Geology at the turn of the XXI Century, V. 2, pp.279-296 (in Russ.).
3. Alekhin Yu.V., L.Z. Lakshtanov (2008). Filtration effect in the works of VA Zharikov and his staff. (Rocks as geological membranes - the complicated history of a scientific concept). I Readings them. VA Zharikov. Chernogolovka, OIHF, pp.12-34 (in Russ.).
4. Hees P. v., A.-M. T Andersson., U. S. Lundström (1996). Separation of organic low molecular weight aluminium complexes in soil solution by liquid chromatography. Chemosphere, Vol.33, N 10, pp. 1951-1966 Results migration mobility investigation of microelements in the soil horizons under the influence of humus and carboxylic acids

Ilina S.M., Alekhin Yu.V., Lapitsky S.A., Sokolova M.N. Behaviour of chromatographic separation of Rare Earth elements on dynamic membranes that formated in the process of ultrafiltration

Abstracts

Geological Dep., MSU alekhin@geol.msu.ru fax: (495) 939 48 08, ph.: (495) 939 49 62

Keywords: *river flow, cascade filtration, rare earth elements, humic substances*

The works on modeling object have been spent to solve the problem of the various elements balance of the individual components of runoff, estimates of migration, research on the transformation and natural differences in the truly dissolved and colloidal forms of individual metals with organic matter migration in natural waters. The object is a classic watershed with soil sampling and soil extracts, samples of bog and river water with an analysis of the composition and distribution of dissolved organic matter (DOM) and trace elements in the components supply and runoff. There was a sampling of large volumes (40 - 80 liters) with consistent use of methods of stepwise cascade filtration and ultrafiltration to divide these groups on various types of filters and to study molecular weight distribution of OM. Objects of study are the small rivers of Russia (North Karelia and Vladimir region). Composition of isolated fractions of filtrates and sediments were analyzed sequentially and separately by different methods. All filtrates and dialysate were analyzed for a wide range of elements by ICP-MS, the DOM - using three methods: catalytic combustion; spectrophotometrically in the range of 400-590 nm (differential spectra of DOM) and chromatographic HPLC method. Using the method of cascade (series) filter allows us to obtain analytical information about correlations of organic content and other elements in a series of Using the method of cascade (sequential) filter allows us to obtain analytical information about correlations of organic content and other elements in a series of sequential filtrates. In the latter case it is sufficient to effectively apply the method of «elimination curves», when a series of sequential filtrates compared themselves to reduce the concentration of trace elements and their values are normalized to the total, and also changes the number of macro components - the complexing compounds and potential of sorbents. Fresh and ultrafresh river water of boreal zone with the usual predominance of bog nutrition, and small rivers of the taiga boreal forest area was generally dominated among macro-components of OM humic nature complexes and iron hydroxide sols, and a relatively small amount of suspended clay particles. For the separation of such mixtures on size fractions, so that the last filtrate is contained only «truly» dissolved forms, requires a combination of filtration, ultrafiltration and hyperfiltration. The overall cascade consecutive filters, technologically and chemically different nature, usually not more than 5-7 denominations. But the basic principle procedures are the branches coarse, so sedimentation volatile fraction more 0,2-0,4 microns (filtering), the separation of humic and fulvic acids by ultrafiltration and the separation of narrow molecular fractions of dissolved OM in the range of molecular weights of 1-100 kDa by methods hyperfiltration. Hyperfiltration in the standard version is already an example of reverse-osmosis filtration and is widely used for desalination of water. But on the basic physico-chemical mechanism of separation of solution components is different enough from the processes of filtration and ultrafiltration. The last two processes on the mechanism of separation is a process analogous to the usual sieve separation, in which principal are steric constraints - the ratio of particle sizes and then. Hyperfiltration of natural waters, especially OM solutions with a wide range of molecular masses, is always a combination of reverse-osmosis process and sieve separation. The nomenclature «kilodaltons» filter based on the molecular density of spherical protein molecules. With some degree of conditionality can be assumed that the passage of molecules of 100 kDa correspond to the pore diameter of 68 Angstroms (0.0068 micron) for the 10 kDa - 0.0037 micron, 1 kDa - 0.0017 microns. The last membranes (1 kDa) are very similar to the declared limit of 10 - 20 Angstroms, after which the filtrate was assumed to contain only the solute free ultracolloidal size matter. Conformity of the border is obvious, because for the humic acids molecules formally colloidal size with a mass of 100 kDa and a more satisfied sedimentation stability. They are «truly dissolved», while changes in pH is not specifically provoked by their aggregation and precipitation. The 1 - 100 kDa range is the most interesting for a detailed study of the natural humic OM properties in all respects. Cascade filtration as a new method for isolating narrow fractions OM and determination of associated trace element composition has a very important advantage over methods of studying the molecular weight distribution adopted in the chemistry of soils. For example, methods of chromatographic separation, is always complicated by adsorption losses of trace elements. However, the use of filters for hyperfiltration as a method of separating the factions methodically have not proved and does not rely on electrokinetic theory of reverse-osmosis separation, formally inherits the sieve-method. The ion concentration polarization (an increase of concentration of the solution to the reverse-osmosis filter for desalting) is not accompanied by excretion of much components in the sediment and sedimentation. This is a fact for OM in the filter, when the ability to aggregate in concentration and the shift of adsorption equilibrium. Therefore, the use of bilayer membrane hyperfiltration to study the molecular weight distribution requires a number of conditions, reducing concentration polarization and mechanism of reverse-osmosis delay. In standard conditions of desalting ratio of delay dissolved electrolytes typically seek to maximize. For this filter in conditions of optimal polarization, so under conditions where the concentration of dissolved electrolytes to the filter (filtrant) and demineralized water (filtrate) is stationary differ when the coefficient of delay reach 0,97-0,99. For optimal regime realizing, when R = 0 and no the concentration and reverse-osmosis mechanism delay, filtrant must not stirred, filtered in a current flow (the vast potential of the flow) and have retarding layer on the output of the filter for bilayer asymmetric membranes. In this case, the filter substrate gruboporistoy quickly formed a stationary area of high filtrant concentration for a loose matrix membranes prevents the aggregation of molecules dissolved OM. In this case most effectively realized version of the division only on the sieve separation mechanism. This special area under cascade filtration, we studied in our experiments, in order to assess the proportion of reverse-delay and delay associated with the separation of large molecules and their associates by the usual sieve separation mechanism. It was obvious that the integral coefficient of seeming delay, R_{Σ}, is the sum of these two effects. For information about the true molecular weight distribution (MWD) is necessary to reduce reverse-

osmosis desalinization. There is significant capillary backpressure in bilayer membranes, where the radius of the substrate pores, r_1 = 0,11 micron, and in starving layer r_2 = 0,0014 micron. In according with the law of Laplace, $\Delta p = 2\sigma (1/r_2 - 1/r_1)$ for membranes of 10, 1 kDa, it is close to 3 atm. When the reverse-osmosis desalination has to overcome the capillary backpressure, filtering at high differential of applied pressure. If the filter through an inverted bilayer membrane, the direction of the applied pressure coincides with the direction of the capillary pressure and effective filtering possible even at low applied pressures about 0,1-0,5 bar. If we filter mode the minimum concentration polarization (without mixing the initial solution), then go to a regime with $R \rightarrow 0$. The stationary of high concentration area, when $C_1 = C_2$, formes in a loose layer of a bilayer membranes. If $C_1 \neq C_2$ in these conditions filtration, then this effect is associated with the conventional size delay filter.

The natural water samples were filtrated through 0,22 mcm and concentrated in the column, then they were analysed by the high-efficiency liquid chromatography (HELC) method to determine the aromatic acids presence and their concentrations. So the concentrations (mcg/L) of the acids are - gallic - 0,11; phthalic - 1,05; protocatechuic - 0,62; p-hydroxobenzoic - 0,045; vanillic - 0,18; salicylic – 3,83; ferulic - 0,025; benzoic – 1,79. The total molar concentration of these acids as well as cinnamylic, oxalic, acetic, hydroxy tricarballylic and vinic acids is less then the molar concentration of the low-molecular fulvic acids.

Table 1. Dissolved organic matter (DOC), nitrogen, macro-anions concentrations and the weight-average molecular weight (WAMW) values for the samples of the river Senga (Seng), the lake Ignatkovo (Ignat) – Vladimir Meshchyora; the stream Vostochniy (OR), the river Palojoki (KAR), the bog «ZPBL» –North Karelia.

sample	DOC mg/L	N mg/L	C/N	Cl^- mg/L	SO_4^{2-} mg/L	NO_3^- mg/L	WAMW
Seng-1	23,81	1,47	16	3,71	46,10	0,10	970
Seng-2	25,39	1,11	23	4,40	40,90	0,24	960
Ign	12,40	0,58	21	-	-	-	920
OR-9	51,15	0,49	104	1,10	0,76	0,003	1260
OR-6	19,26	0,33	58	0,52	1,10	0,01	1020
OR-1	16,20	0,34	48	0,40	0,85	0,05	1010
OR-8	4,27	0,18	24	0,76	2,44	-	960
KAR-1	10,84	0,42	26	0,83	2,40	0,17	910
ZPBL-1	38,99	0,54	72	0,70	1,54	0,002	1080

MWD of humic OM in aqueous solutions are often studied by the methods of chromatography and cascade filtration separation with the construction of terns, as the distribution functions of the diameters and masses of the molecules. Spectra of molecular weights of humic and fulvic acids in river waters and soils are sufficiently wide, continuous (0,5 - 500 kDa), bad reproducible. The main part of the complexes is the truly dissolved forms. It is therefore there aren't any noticeable trace elements elimination in the fulvate complexes forms up to 10-1 kDa filters. Our HPLC analysis showed that the molecules with a mass 1 kDa are dominated (Fig. 1, Table. 1). The mole (not weight!) concentrations of OM present in the formulas for the constants of complexation. So in the interval 0,2 mcm-10 kDa (0,0028 mcm) while retaining the DOC mass concentration at the level of 5,2 mg/L 8 molecules with a mass 5200000 corresponds to 4,400,000 molecules with a mass of 10 kDa. Thus, the fulvic acids molar concentrations are responsible for the main transport of trace elements, but not adsorption on the large molecules of OM. So their MWD can be studied only by the cascade filtration method.

WAMW of the large molecular aggregates can be understood on the basis of the thermodynamic description of the analysis of their relative stability during the polymerization. On the example of the organic complexes with a large number of associated molecules I. Prigogine have showed that the solubility of these compounds can be simply related to the reactions of sequential complexation of type: $A_n + F = A_{n+1}$, where F - monomer fragment, under the assumption that for $>> 1$ $K_n \approx K_{n+1} \approx K_{n+2} \approx K_{n+3}$, etc. This realistic assumption is equivalent to saying that for large cluster polymers the free energies of joining of the elementary fragment in a consecutive series of associates are almost indistinguishable. We developed this approach to the properties of more complex real forms of transfer - clusters of humic acids that sedimentation stability, i.e., they have Stokes diameters up to 0,2-0,4 mcm (filtrates of the conventionally dissolved forms are not capable for the fast aggregation). At a density of humic acids 1,6 g/cm3 the associates of this size have large molecular weights ($4,03*10^6$ and $32,28*10^6$ kDa, respectively), and actually observed (often dominated by mass) in the filtrates of bog waters and streams of the primary hydrographic network. Our calculations of the constants of humic acid sequential polymerization made from the condition that the kinetic stability of the largest associations determined by the proximity of energy addition of the monomer fragment to the energy of thermal vibrations of RT (600 cal/mol at 25°C). Calculation of association constants is made in the coordinates $\lg K_n$ – 1/n for the interval of values of n 1 - 8000000 (maximum diameter of 0,2 mcm at a mass of fulvic monomer 500 Da), when at $1/n \rightarrow 0$ lim RT $\lg K_n \rightarrow 600$ cal/mol and $\lg K_n \rightarrow 0,44$ (Fig. 2). Using of the results of cascade filtration and HPLC allows to specify diffraction patterns on the relative amounts of the dominant first associates (monomers, dimers, trimers) and to agree their association constants, which, may not exceed ($\lg K_n$) values of 5,5. Small binding energy predetermine stochasticity exposure mass fraction of large aggregates fluctuations of the hydrodynamic conditions and temperature at the absolute dominance of the mole (not weight!) amounts in solution of fulvic acids with a mass of 500-1500 Da.

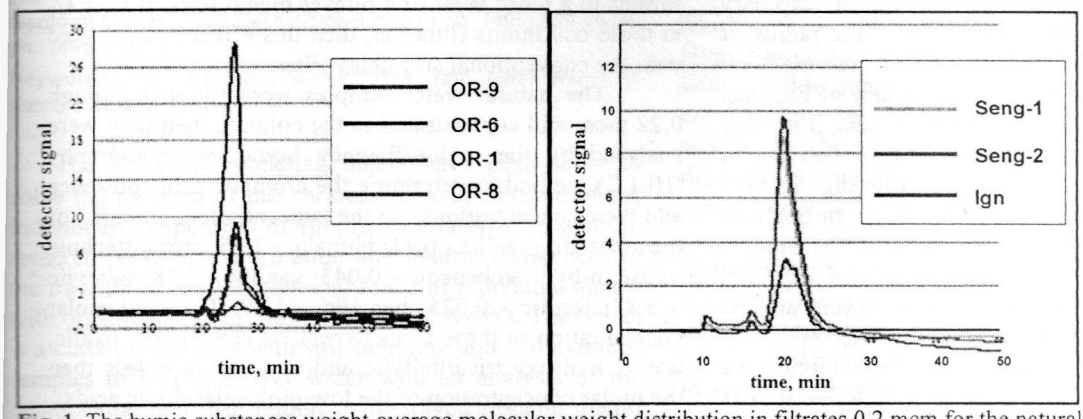

Fig. 1. The humic substances weight-average molecular weight distribution in filtrates 0,2 mcm for the natural water samples of the North Karelia (left) and Vladimir Meshchyora (right), measured by the high-efficiency liquid chromatography (HELC) method

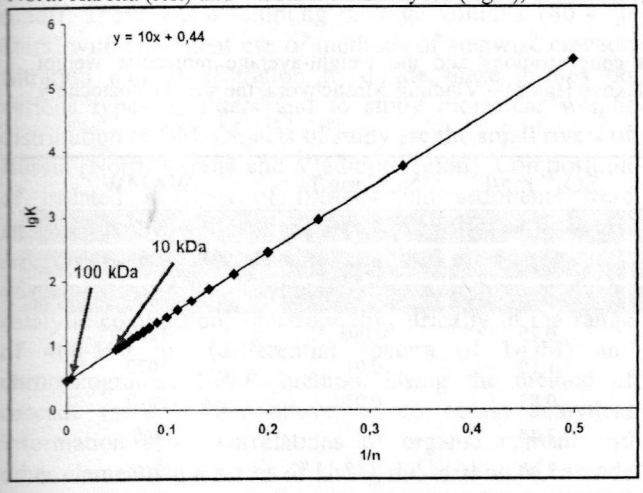

Fig. 2. The dependence of the humic cluster association constant (lgK) for the sequential reactions of addition for the 500 kDa-weight unit (for illustration purposes the means of the constants were dissembled for the molecular weights range 10-100 kDa)

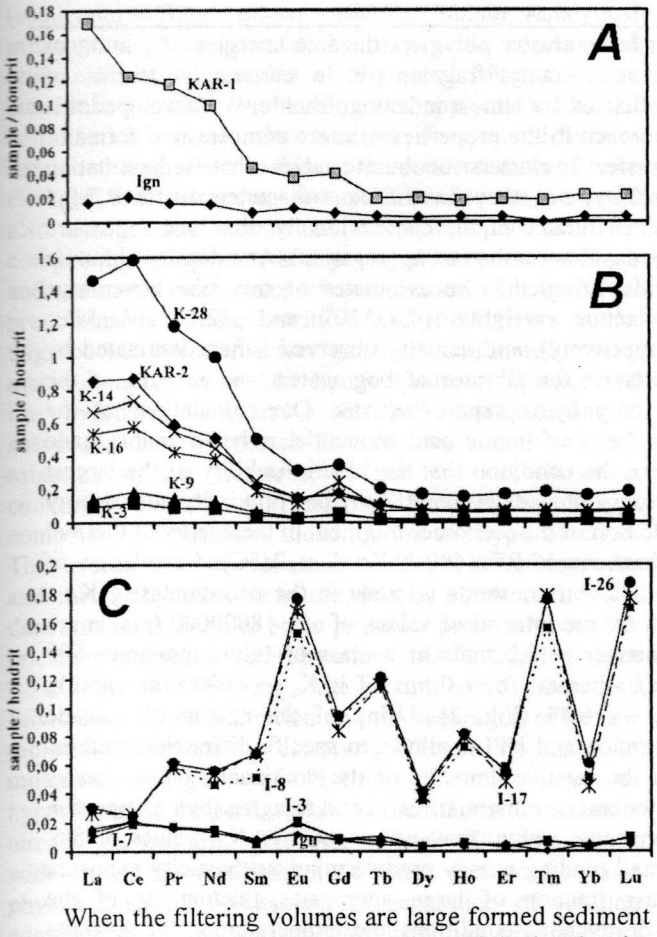

Fig. 3.
(A) REE normalized patters for the natural water samples of the North Karelia (KAR-1) and Vladimir Meshchyora (Ign);
(B) REE normalized patters distortion in the sequential samples of the reverse osmosis filtration mode;
(C) REE normalized patters distortion in the sequential samples of the filtration mode of the chromatographic fractionation on the formed sediment.

When the filtering volumes are large formed sediment layer can itself act as an adsorption-precipitation barrier with chromatographic separation of components in this layer. The most demonstrative example of this behavior of sediment are experiments with reverse osmosis (Fig. 3, *B*) and inverted membrane (Fig. 3, *C*). There is a progressive separation of REE in series of successive portions of the filtrate. All REE patterns of the filtrates and the initial solutions (Fig. 3, *A*) were normalized to their individual global prevalence for its smoothing in the samples of continental waters. But we see (Fig. 3, *B*) that in the first samples of filtrates the concentration of light REE is significantly lower than in the initial solutions due to the reverse-delay. In the case of inverted membrane (Fig. 3, *B*) the content and the patterns of REE are approximate to the initial ones in the first portions of filtrate. However, in both cases by the filtering there is a general increase of REE concentrations in sequential filtrates. By the end of experiments, we see increasing of the concentrations by 2-10 times and REE patterns complete smoothing. On the background of a general increase of the concentrations the solutions are progressively enriched in odd REEs but even REEs are delayed adsorptionaly due to the ion exchange of macrocomponents within the membrane. This significant accumulation of the odd REEs in the last filtrate completely turn the usual pattern - in these solutions odd elements with lower global prevalence are dominated. This experimental fact is analogous in the different REE

patterns of the initial solutions of two regions. That repetition of these elements adsorption-desorption in the long history of forming flyuvio-glacial sediments and soils of Meshchyora lowland is reflected in the smoothing of the REE patterns with the removal of lighter elements and adsorptional retention of heavy ones. For both regions the rocks of Fennoscandia are the initial substrate, but the processes of transformation of the REE patterns are far from complete in the North Karelia, which is also reflected in higher concentrations of REE in the waters of this region.

References

1. Ilina S. M., Y. V. Alekhin, S. A. Lapitsky (2010). Results of complex physical-chemical studies of metal-organic forms of heavy metal migration in the continental waters of contrasting climatic environments. Abstracts of the XVI Russian meeting of the experimental mineralogy, Chernogolovka, pp. 247-248 (in Russ.).
2. Ilina S. M., Y. V. Alekhin, S. A. Lapitsky (2010). The study of the natural organic complexes by the methods of cascade filtration and perturbation of the stationary state. Abstracts of «Lomonosov Readings - 2010». http://geo.web.ru/db/msg.html?mid=1183766&uri=12.html (in Russ.).
3. Ilina S. M., Y. V. Alekhin, S. A. Lapitsky, M. V. Sitnikova (2010). The results of the trace elements and organic matter joint migration studying in the river flow of the boreal zone. Vestnik MGU, Series «Geology», MSU, № 6, pp. 49 – 55 (in Russ.).
4. Alekhin Y. V., S. M. Ilina, S. A. Lapitsky, O. S. Pokrovsky (2011). The eexperience of the comparative analysis of individual components of the small rivers flow of the boreal zone and the middle zone of Russia. Bulletin MOIP, geological section, MSU, vol.1, pp. 58-81 (in Russ.).
5. Prigogine I., R. Defay (1966). Chemical Thermodynamics. 510 p. (in Russ.)
6. Migdisov Art. A., A. E. Williams-Jones, L. Z. Lakshtanov, Yu. V. Alekhin (2002). Estimates of the second dissociation constant of H_2S from the sulfidation of crystalline sulfur. Geochim. et Cosmochim. Acta. Vol. 66, №10, pp. 1713-1725.

Grants RFBR №№ 11-05-00464-a 11-05-00638-a, 11-05-93111-НЦНИЛ_а

Korobova E.M., Danilova V.N., Khushvakhtova S.D., Beryozkin V.Yu. Geochemical differentiation of iodine and selenium in landscapes: first results on example of the Bryansk region

GEOKHI RAN

Key words: iodine, selenium, landscape geochemistry, drinking water, soils, forage grasses, Bryansk region

Introduction A study of iodine and selenium in landscapes of the Bryansk region was started to estimate contribution of the natural background of these elements essential for thyroid gland (Arthur et al., 1999; Ermakov, 2004), to spatial distribution of thyroid diseases after contamination of the area by the Chernobyl radioiodine isotopes.

The Bryansk region is noted for a variety of the soil-forming rocks and soils (Prosyannikov, 2002), a pronounced deficiency of iodine in local diets (Proshin, Doroshchenko, 2005) which contributed to the risk of thyroid cancer in the region contaminated due to the Chernobyl accident (Shakhtarin et al., 2003). At the same time an increase of the thyroid cancer in areas with different radiogenic load is comparable that could be a result of different reaction to radioiodine impact due to variation of stable iodine and selenium background.

The main objective of experimental work presented in this paper was to evaluate natural variation of selenium and iodine concentration in the components of the local food chain noted for I and Se sink (the soils) and transfer (drinking waters, plants).

Study region and methods Selection of the test sites and sampling. Landscapes and soils of the Bryansk region are characterized by different geochemical features. Figure 1 presents a schematic map of landscapes different in soil and vegetation cover and in the dominating pH-Eh types of water migration according to Perelman (1975).

Landscape groups: 1, 2 – watersheds in areas of fluvio- and limnoglacial sands and sandy loams sand coniferous and mixed woodlands on podzolic and soddy-podzolic soils and agricultural lands; 3, 4 - watersheds in areas of covering and loess-like loams, primary oak and secondary birch and poplar forests on grey forest soils and agricultural lands; 5, 6 – ancient terraces and draining hollows in areas of: 5 – sandy and loamy deposits underlain by carbonate sedimentary rocks covered by oak forests and secondary broad- and small-leaf forests on light grey and grey forest soils including cultivated lands; 6 – sandy and loamy sand ancient alluvial, lacustrine, fluvioglacial deposits covered by pine and pine-spruce forests on soddy-podzolic soils and agricultural lands; 7,8 – modern flood plains and river terraces in areas of: 7 – reworked sandy limno-glacial deposits with domination of marshy meadows and peat bogs including meliorated areas used for grazing and haying; 8 – modern and ancient alluvial deposits of various texture, meadows and marshes used for grazing and haying; 9 – out-of-scale small areas of broad-leaf forests and meadows on soddy carbonate soils on outcrops of marls and limestone; 10 – out-of scale areas of marshy woodlands and meadows on soddy-gley, humus-gley soils located on watersheds and terraces.

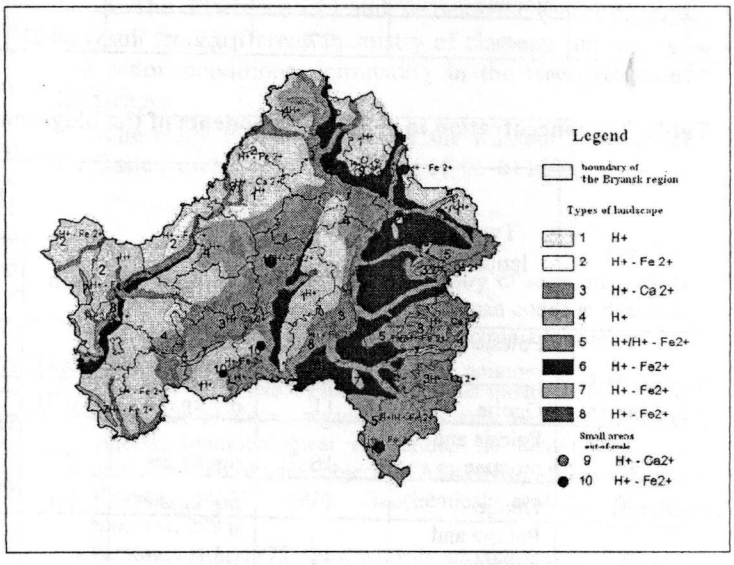

Fig. 1. A schematic map of geochemical landscapes Обзорная of the Bryansk region (created by Korobova E. and Beryozkin V. on the basis of thematic maps of the Bryansk oblast' and the corresponding sheet of the State soil map, scale 1: 1000 000)

Classes of water migration (after Perelman, 1975): H^+ - acid; H^+ - Fe^{2+} - acid gley; H^+-Ca^{2+} - transitional to calcium (weakly alkaline); Ca^{2+}- Fe^{2+} - calcium-gley (locally).

The two most geochemically different landscape types situated in areas of fluvioglacial and moraine sandy and loamy sand sediments with mainly H^+; H^+ - Fe^{2+} classes of the soil water migration (polesje and moraine landscapes) and the areas of covering and loess-like loamy deposits the presumably H^+-Ca^{2+}, Ca^{2+}- Fe^{2+} soil water migration class (opolje landscapes) were selected for location of the test sites. To provide spatial proximity of the geochemical and medical date sampling was also carried out close to (pasture areas) or within (private farms) the settlements with statistical data on thyroid gland diseases and iodine renal excretion (Proshin, Doroshchenko, 2005). In 2010 ten settlements (30 private farms) were examined. At the pastures the soils were sampled with the help of an auger to the depth of 20-30 cm with the further core slicing in increments of 5-10 cm. Plants were cut over the soil sampling area of 30x30 cm (50x50 cm in case of rare cover or damaged by cattle). Soil samples were stored in plastic bags. Plants were air-dried. Water samples were kept in a freezer isolated from air.

Laboratory analysis. Soil samples were analyzed for iodine without drying, the results were recalculated for the air dry basis to compare with the published data. Plants were milled using grain mill and ZM200 (Retsch, Germany). Iodine determination in water samples was performed without pre-concentration. Iodine was determined with the help of kinetic rodanide-nitrite method (Proskuryakova, Nikitina, 1976) using photometer KFK-3-01 (Russia). Iodine detection limit in solution was within 1-4 mg/ml, reproducibility varied from 7- to 20%. Se was determined in air-dry soil and plant samples by spectrofluorimeter (Ermakov, 1987). Se detection limit equaled 1 ng/ml, reproducibility (according to plant standards) was up to 7%.

Results and their discussion Se supply of drinking waters varied within two orders (0,02-4,4 μg/l) and corresponded to the general level characteristic for the natural waters (<1 μg/l, Plants et al., 2004). Se concentration in the upper humus horizons of the areas used for pasturing (0-5 cm, n=20) varied from the deficiency (0,07 mg/kg) to the relative normal level (0,95 mg/kg). However in plant samples (n=29) the Se content did not exceed deficiency level for forages (0,02-0,1 mg/kg dw) (Table 1).

Table 1. Se concentration in source components of the biogeochemical food chain in different landscapes

Object	Type of landscape	Number of samples	Parameters of Se concentration						
			units	min	max	mean	std*	Ge.	Me
Topsoil (0-5 cm, pastures)	Polesje and moraine	14	mg/kg dw	0,070	0,950	0,301	0,215	0,250	0,239
	Opolje	6	mg/kg dw	0,110	0,510	0,261	0,154	0,227	0,213
Grasses (pastures)	Polesje and moraine	15	mg/kg dw	0,021	0,079	0,044	0,018	0,041	0,038
	Opolje	14	mg/kg dw	0,024	0,100	0,056	0,026	0,050	0,060
Drinking water	Polesje and moraine	8	μg/l	0,02	0,40	0,14	0,15	0,07	0,06
	Opolje	17	μg/l	0,02	4,40	0,81	1,05	0,41	0,40

*standard deviation

Table 2. I concentration in source components of the biogeochemical food chain in different landscapes

Object	Type of landscape	Number of samples	Parameters of I concentration						
			units	min	max	mean	std*	Ge.	Me
Topsoil (0-5 cm, pastures)	Polesje and moraine	11	mg/kg dw	0,37	15,8	2,09	4,57	0,89	0,75
	Opolje	11	mg/kg dw	0,77	15,5	3,21	4,49	1,84	1,32
Grasses (pastures)	Polesje and moraine	16	mg/kg dw	0,08	0,72	0,33	0,23	0,25	0,25
	Opolje	14	mg/kg dw	0,18	0,63	0,38	0,16	0,35	0,36
Drinking water	Polesje and moraine	14	μg/l	1,28	25,1	10,2	6,1	8,33	9,20
	Opolje	21	μg/l	0,70	23,5	5,95	5,64	4,06	3,65

*standard deviation

The upper horizons of the grey forest soils developed in oplje landscapes and those of the soddy-podzolic soils collected in pasture areas of polesje and moraine landscape did not practically differ in Se content. Its mean value for the first group of samples was even lower than for the second. Nevertheless the content of Se in forage grasses

sampled in opolje landscapes was pronouncedly higher as compared to those of the polesje and moraine areas (0,038 and 0,60 1 mg/kg correspondingly). This indicates that in areas used for pasturing in polesje and moraine areas Se may be less available to the plants. This was likely to result from water logging which was widespread within these areas and probably contributed to Se fixation in soils. In weakly alkaline oxygenic conditions typical for the opolje soils Se is known to be more mobile which could contribute to its availability to plants. Probably for the same reason drinking waters (mainly tap water) collected in the opolje settlements were characterized by a higher Se content as compared to those located within the polesje and moraine landscapes (0,06 и 0,4 μg/l, median values). Negative correlation between Se concentration in topsoil (0-5 cm) and grasses of the wet meadows also witnessed the low Se transfer to plants in water-logged conditions (Figure 2).

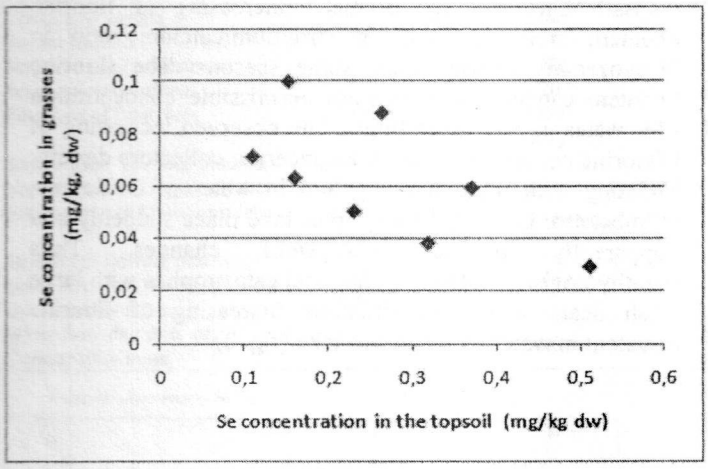

Fig. 2. Relation between Se content in the upper soil horizon of wet meadows used for pasturing and the grasses growing above.

Unlike Se the minimum and mean estimates of I concentration in the same samples was considerably higher in soils and plants of the opolje landscapes as compared to those of the polesje and moraine. This proved a higher iodine status of the former landscapes (Table 2). Mean I concentration in the upper soil horizons of the polesje and moraine landscapes equaled to 2,1 mg/kg dw that corresponds to the lower threshold concentration established for soils (<2-Kovalsky, 1974) In the opolje topsoils the mean I content exceeded this threshold (3,21 mg/kg dw). Maximum I values were characteristic for topsoil layers of wet meadows located in subordinated landscapes (up to 15 mg/kg). I concentration in plants of the pastures varied from 0,08 to 0,72 mg/kg (Table 2).

Similar to I in topsoil the amount of I in forage grasses collected in the opolje landscapes was higher than in the polesje and moraine areas (Table 2) but exceeded the lower threshold of the optimal interval for cattle rations (< 0,07 mg/kg dw, Kovalsky, 1974) in all the regions. The reason for this needs further investigation.

Analysis of I and Se transfer to plants for the topsoil (transfer coefficients, TC, weight basis) proved that on the average I uptake by plants is relatively higher than Se (0,55±0,06, n=22 and 0,22±0,05, n=16 respectively). When the type of landscape was considered, it appeared that Se uptake by plants at the test plots located in the polesje and moraine landscapes was lower than I (TC_{Se} 0,29±0,09 and TC_I=0,72±0,14, n=6). At four test plots situated in opolje landscapes Se uptake by plants was in two cases higher in one case –equal and in one –lower than that of I that lead to a slightly higher median of TC_{Se} value as compared to TC_I (0,44 and 0.38 correspondingly). Obtained results showed different behavior of Se and I in soils and their transfer to grasses in similar landscape geochemical conditions.

Iodine concentration in drinking water collected in areas of polesje and moraine landscapes was generally higher than in the opolje landscapes. This may result from a higher mobilization of I in the iodide form in the reduced environments typical for the former group of landscapes. In opolje areas I may be fixed in soils and sediments on carbonate oxidizing barrier.

Therefore the difference in I and Se behavior was likely to reflect different chemistry of elements, as well as pH and redox conditions dominating in the two groups of landscapes. Further studies are necessary to verify the observed tendencies.

Conclusion

1. First experimental data to characterize I and Se behavior in geochemically different landscapes were obtained.

2. Iodine and selenium concentration and distribution in topsoil, grasses and drinking water appeared to be different within areas of landscapes formed on fluvioglacial and moraine deposits (polesje and moraine) and on the covering loess-like loams (opolje).

3. Forage grasses of the opolje landscapes were proved to contain a higher amount of I and Se as compared to those of the polesje and moraine. However topsoil and drinking water in particular collected in the former landscape type had lower Se content as opposed to I which concentration was higher in these objects within the polesje and moraine group of landscapes.

4. Selenium uptake by plants appeared to be relatively lower as compared to iodine uptake particularly in areas of the polesje and moraine landscapes.

5. The difference in I and Se behavior was suggested to result from different chemistry of elements and the pH and redox conditions dominating in the two groups of landscapes.

The study was supported by the Russian Foundation for Basic Research Работы (grant 10-05-01148).

References

1. Ermakov V.V., 2004. Biogeochemistry of selenium and its importance in prophylactics of the human endemic diseases. Vestnik Otdeleniya Nauk o Zemle. Electronic Journal 1, 22, , 16 p.
2. Ermakov V.V., 1987. Fluorimetric determination of selenium in animal produce, organs, tissues and the environmental objects. Methodological regulations for determination of pesticides in biological objects. VASKHNIL, Moscow, 8-18.
3. Kovalsky V.V., 1974. Geochemical ecology. Nauka, Moscow, 299 p.
4. Perelman A.I., 1975. Geochemistry of landscapes. Vysshaya Shkola, Moscow, 342 p.
5. Proskuryakova G.F., Nikitina O.N., 1976. Accelerated variant of the kinetic rodanide-nitrite technique for determination of micro-quantities of iodine in biological objects. Agrokhimiya 7, 140-143.

6. Prosyannikov E.V., 2002. Patterns of development of natural and anthropogenically transformed ecosystems of the Bryansk region suffered from the global accident at the Chernobyl NPP. Scientific and educational publication. Electronic issue supported by RFBR (CD-ROM).
7. Proshin A.D., Doroshchenko V.N., 2005. Iodine deficiency among population of the Bryansk region. Ladomir, Bryansk, 164 p.
8. Arthur John R., Geoffrey J. Beckett and Julie H. Mitchell, 1999. The interactions between selenium and iodine deficiencies in man and animals. Nutrition Research Reviews, 12, 55-73.
9. Plant J.A., D.G. Kinniburgh, P.L. Smedly, F.M. Fordyce and B.A. Klinck, 2005. Arsenic and Selenium. In: H.D. Holland & K.K. Turekian (Eds), Environmental Geochemistry, Treatise on Geochemistry 9, 17-66.
10. Shakhtarin V.V., Tsyb A.F., Stepanenko V.F., Orlov M.Y., Kopecky A.J., and S. Davis, 2003. Iodine deficiency, radiation dose, and the risk of thyroid cancer among children and adolescents in the Bryansk region of Russia following the Chernobyl power station accident. International Journal of Epidemiology 32, 584-591

Kotelnikov A.R., Akhmedjanova G.M., Kovalskii A.M., Suk N.I. Composition of the surface waters of Lovozerskiy district (Murmansk region)

Institute of Experimental Mineralogy of Russian Academy of Sciences, Russia, Chernogolovka, e-mail: kotelnik@iem.ac.ru

Key words: surface water, geochemical investigation, ecology.

During the field seasons 2006-2010 in July and August there were sampled surface water from natural and engineering collectors of Lovozerskiy district of Murmansk region. Analyses of water samples were carried out using methods ICM-AES, ICP-MS, photocolorimetry and potentiometry. Some elements (Cl, F) and parameters (T, pH) were measured directly during the field trip. The results of particular investigation of parameters of natural and engineering waters in different collectors in various seasons.

As is seen from results of investigation the composition of water of Lovozerskiy district (Umbozero, Lovozero and Seydozero) practically similar to composition of largest lake of Murmansk region – Imandra lake (Devjatkin, 2008). On the content of chlorine, sulfur, sodium, potassium, aluminium, copper, zink, this natural collectors correlate well with the longitude scheme of pollution (apparently concerned with transportation of elements by aerosol from the Northern basin of Atlantic: the content of this elements decrease from the west to the east (fig. 1).

Seydozero lake by its composition of rare-earth elements correlatewith rocks of Lovozerskiy alkaline massif. One can see dramatic increasing of fluorine content and decreasing of strontium/calcium ratio in Lovozerskiy district lakes some seasons. The fluorine content can exceed maximum permissible concentration for water in 3 ot more times. The observed increasing of fluorine content in water of engineering collectors directly relating with mine working and in water of Seidozero, Umbozero, Lovozero water areas take place suddenly and apparently produce ecosystem changes. Thus ichthyologists relate environmental catastrophes with large fish death with such dramatic increasing of fluorine content in water of Seidozero lake (fig. 2).

Table 1. The compositions of lake waters of Murmansk region (data of 2008 year testing). The containing of elements represented in mg/l.

Parameter	Imandra lake, mountain Belaya	Umbozero lake, southern part	Lovozero lake, Yulinskaya salma	Seydozero lake, western part	Seydozero lake, eastern part	Baykal lake, 1000 m depth	Ladojskoe lake	Max. permiss. concent. in water, mg/l
pH	7.34	7.1	6.18	6.28	6.56	-	-	-
S	7.16	1.27	0.66	0.58	0.95	1.6	0.8	500
Cl	4.50	1.80	0.30	1.14	0.96	15.0	7.0	100
F	<0.25	<0.25	1.9(?)	1.60	0.43	-	-	1.5
Na	13.3	5.8	4.3	5.2	4.7	6.1*	8.6*	200
Mg	1.00	0.40	0.53	0.06	0.07	4.2	1.9	50
Al	0.087	0.025	0.01	0.02	0.21	-	-	0.2
P	0.004	0.002	<0.05	<0.05	<0.05	-	-	3.5
K	2.8	1.4	0.8	0.4	0.3	-	-	?
Ca	4.0	1.7	1.43	0.28	0.26	15.2	7.1	?
Fe	0.05	0.008	0.05	0.01	0.05	-	-	0.3
Sr	0.063	0.065	0.035	0.029	0.021	-	-	7
Zn	0.003	0.001	0.005	0.049	0.004	-	-	1
Cu	0.008	0.001	0.0015	0.002	0.001	-	-	?
Ni	0.015	0.001	-	-	-	-	-	0.02
Cr	0.0002	0.0002	0.002	0.001	0.004	-	-	0.05
Cd	0.00015	0.0001	0.00002	0.0002	0.00002	-	-	0.001
Co	0.0001	0.0002	-	-	-	-	-	0.1
Li	-	-	0.0005	0.0004	0.0003	-	-	0.03
Zr	-	-	0.00031	0.0001	0.00007	-	-	?
Nb	-	-	0.000013	0.000008	0.000004	-	-	0.01
Mo	-	-	0.001	0.003	0.002	-	-	0.25
Hg	-	-	<0.00003	<0.00003	<0.00003	-	-	0.0005

Parameter	Imandra lake, mountain Belaya	Umbozero lake, southern part	Lovozero lake, Yulinskaya salma	Seydozero lake, western part	Seydozero lake, eastern part	Baykal lake, 1000 m depth	Ladojskoe lake	Max. permiss. concent. in water, mg/l
Tl	-	-	0.000001	0.000003	0.000001	-	-	0.0001
Pb	-	-	0.00051	0.00032	0.00069	-	-	0.1
Tl	-	-	0.000001	0.000003	0.000001	-	-	0.0001
U	-	-	0.000025	0.000014	0.000017	-	-	0.1
Na/K	4.75	4.14	5.37	13.0	15.7	-	-	-
Ca/Sr	63.5	26.2	40.8	9.65	12.4	-	-	-
(Na+K)/(Ca+Mg)	3.22	3.43	2.60	16.5	15.2	0.314	0.956	-
East longitude	33.16	34.5	35.2	34.8	34.9	-	-	-

Table 2. Results of analysis of water samples collected during a field trip 2010 year. The compositions of lake waters of Murmansk region (data of 2008 year testing). (Results for samples collected in 2009 year are presented within brackets).

	pH	Cl, mg/l	F, mg/l	Al, mg/l	SiO_2, mg/l	K, mg/l	Na, mg/l	Ca, mg/l	Mg, mg/l
Vostochniy stream	6.15	4.8	0.02	0.40	5.17	0.01	2.93	1.0	0.01
Stream Raslaka	7.70	6.7	0.06	1.50	10.58	0.61	4.0	1.0	0.013
Sergevan river headstream	7.63	11.6	3.60	2.41	10.57	1.25	26.11	1.0	0.02
Sergevan river inflow	6.75	4.2	2.20	0.94	5.16	1.55	21.12	2.5	0.56
Filter bed of Ilma mine	9.10 (6.89)	14.3 (2.9)	139.0 (6.7)	10.08	70.49	11.80	712.5	2.0	0.03
Stream from Vavnbed mountain	6.1	2.1	0.03	1.17	9.35	0.71	4.08	1.6	0.25
Nothern part of Lovozero lake	6.5	1.1	0.33	0.84	0.13	0.98	5.84	2.0	0.58
Nothern part of Umbozero lake	6.53 (6.26)	1.6 (6.0)	0.20 (2.9)	0.44	2.40	2.1	8.0	3.0	0.49
Stream fall flowing into Umbozero from day drift of Umbozerskiy mine	6.75 (6.87)	2.96 (6.7)	3.8 (4.3)	2.24	9.78	2.62	37.5	4.0	2.24
Water from day drift of Umbozerskiy mine	9.61	5.52	36.0	1.56	21.98	3.02	159.1	1.5	0.01

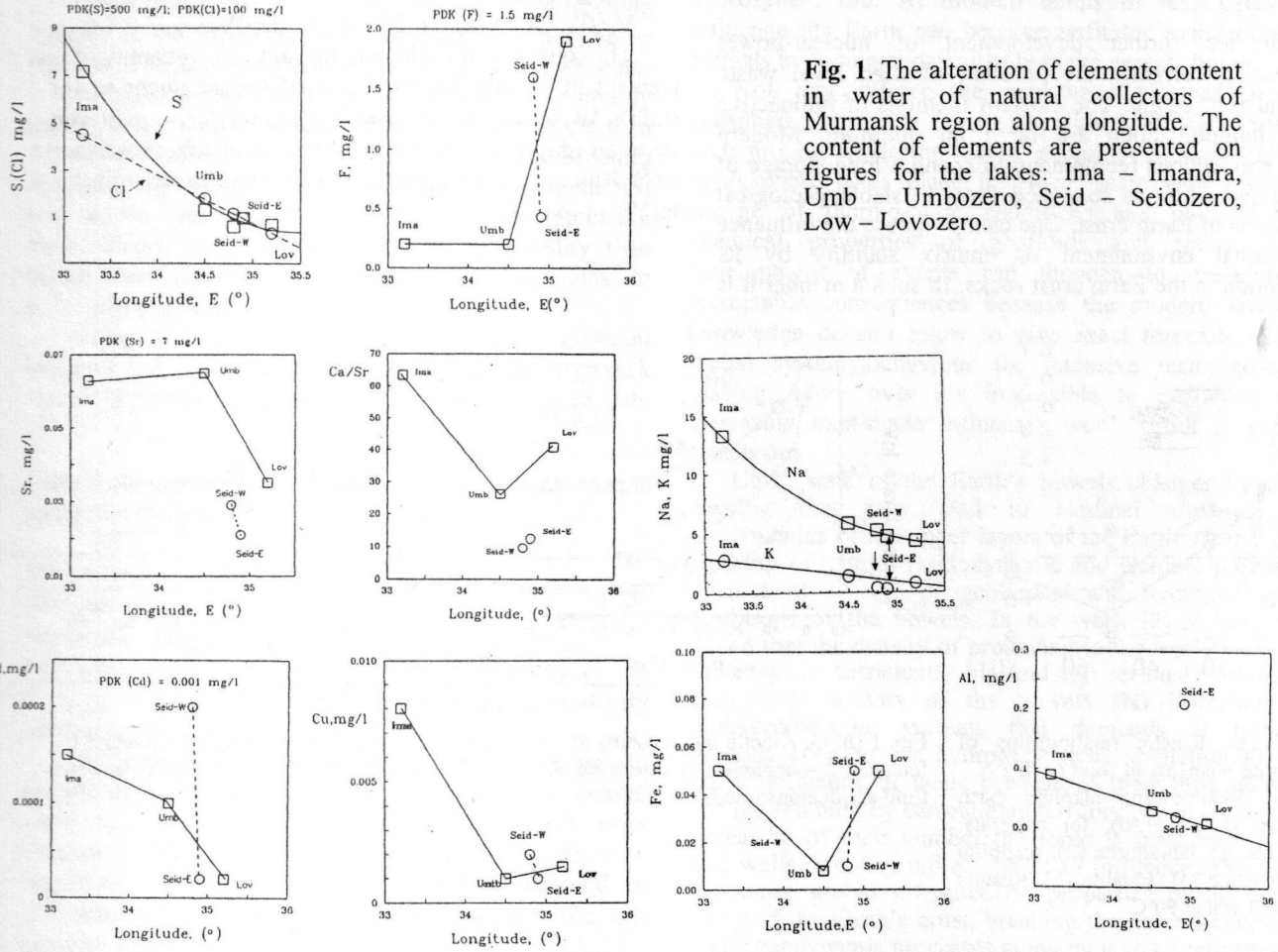

Fig. 1. The alteration of elements content in water of natural collectors of Murmansk region along longitude. The content of elements are presented on figures for the lakes: Ima – Imandra, Umb – Umbozero, Seid – Seidozero, Low – Lovozero.

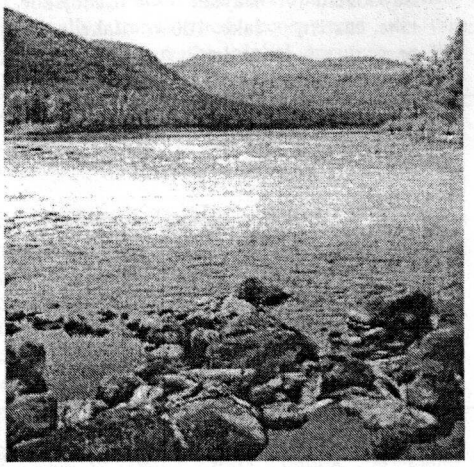

Fig. 2. Environmental catastrophe on Seidozero lake (2006 year). Large fish death scientists relate with mycosis of fish which is causes by dramatic increasing of fluorine content in water.

Kotelnikov A.R., Akhmedjanova G.M., Suvorova V.A. The experimental study of leaching rates of elements (Na, K, Al, Si) from framework aluminosilicates

Institute of experimental mineralogy of Russian Academy of Sciences, Russia, Chernogolovka, e-mail: kotelnik@iem.ac.ru

Key words: radioactive waste, mineral matrix materials, leach rates, exogenous process rates.

For the further development of nuclear-power engineering currently the problem of high level waste disposal is strategic. The existent methods of radioactive waste immobilization are far from optimum. Modern IAEA conceptions recommend to spend a long storage of radioactive waste in solidified form in stable geological formations of Earth crust. One cannot ignore the influence of external environment on matrix stability by its distribution in the Earth crust rocks. In such a manner it is necessary to investigate the stability of mineral matrix materials in the system mineral matrix – fluid - host rock. Moreover values of leach rates of different minerals of rock able to give an information on intencity of exogenous geologic processes and time of location of rock in present conditions.

The investigation of leach rates of Na, K, Al, Si in framework alumosilicates: alkaline feldspar, nefeline and sodalite at 90°C and at 20°C presented in this work.

The experiment on of leachability of samples at 90°C is based on test IAEA MCC-1. The dimensions of samples for testing were 4-5×10×10 mm. Surfaces of sample tables were polished on fine pouncing paper and then on diamond paste (20 mkm). After polishing, cleaning and drying samples were weighing on analytic balance and their geometrical proportions were measured. Geometrical square of samples surface were up to 10 cm^2, weight up to 4 g. Leachability runs were carried out in teflon autoclaves with volume of 80 ml. Pressuretight closed autoclaves were located in thermostatically controlled chamber; water level in chamber was always rise above level in autoclaves. The temperature was automatically kept at 90±1°C. Series of experiments was carried out with duration of 1, 7, 14 and twice of 28 days. The experiments at 20°C were carried out using the same technique, but the duration in this case was up to 520 days.

After every run period fluid was acidified with chlorine hydride and analysed by AAS and ICP methods. Sample and autoclave were carefully flushed out by triply distillate water and filled out by new portion of water.

For any element the leaching rate was estimated using following equation:

$V_i=(l)_i \cdot W / [(c)_i \cdot \tau \cdot s]$ [g/(m^2·day)],

$(l)_i$ - quantity of i- element in fluid, $(c)_i$ - quantity of i-element in sample (in same unit of measurement as for fluid), W – weight of sample (gramm), τ - total run duration (days), s - Geometrical square of sample surface (m^2). Run results are presented on diagram in coordinates $lg(V_i)$ - τ (days).

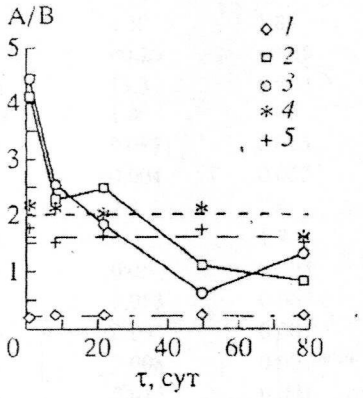

Fig. 1 (a). Kinetic relationships of enleaching elements in fluid (A/B), A – sum of alkaline and alkaline earth elements; B – (Si+Al); for minerals: orthoclase (1), labradorite (2), scapolite (3), nepheline (4), sodalite (5). Results of MCC-1 test at 90°C.

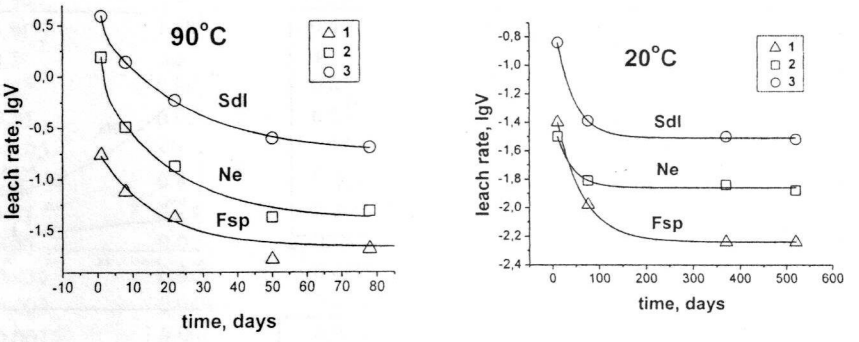

Fig. 1 (b, c). Kinetic relationships of leaching rates of elements from natural minerals: 1 – feldspar, 2 – nepheline, 3 – sodalite. Results of MCC-1 test at 90°C and at 20°C in water fluid are demonstrated.

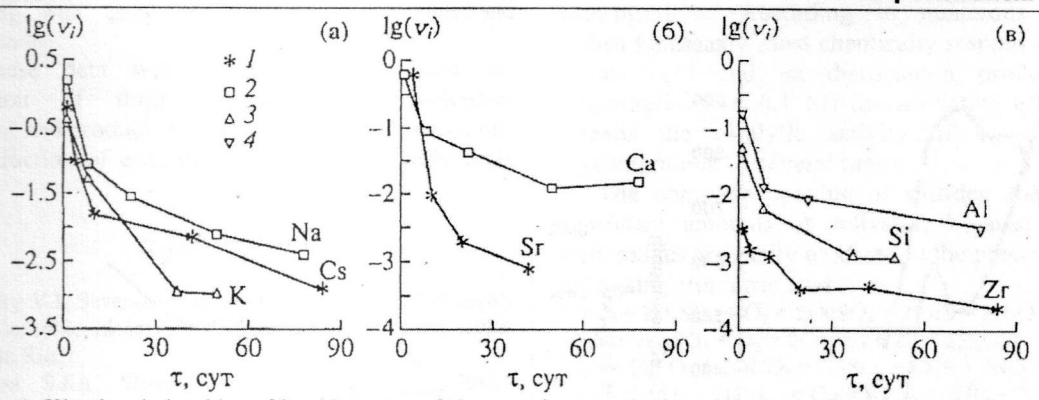

Fig. 2 (a, b, c). Kinetic relationships of leaching rates of elements from synthetic matrix materials and natural minerals. 1 – Synroc-C, 2 – labradorite, 3 – sanidine, 4 – orthoclase.

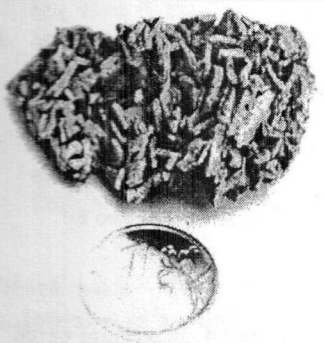

Fig. 3. Nephelinic syenite collected in coastal zone of Seydozero lake (Murmansk region). Crystals of feldspar and relicts of nepheline grains are in a good light on the leached surface.

It was shown that stability of minerals during leaching increase in the following chain: sodalite → nepheline → feldspar. The process of interaction of minerals with water is complicated: the leaching of feldspar is primarily incongruous, rates of enleaching of Na, K are greater then Al, Si. But after some time leaching process becomes close to congruous (fig. 1). As a result of investigation it was shown that matrix materials based on framework alumosilicates are exceed in leachability stability than borosilicate glasses and close by leaching rates to polymineral matrices Synroc (fig. 2).

Using the difference in leaching rates for different minerals the equations for estimation of water – rock sample interaction time (for 20°C) were concluded (tab. 1).

Table 1. Equations for estimation of water – rock sample interaction time (for 20°C)

Mineral pair	Equation
Feldspar - nepheline	$T\ (years) = 952.4 \cdot h_{leach}$ [1)]
Nepheline - sodalite	$T\ (years) = 344.8 \cdot h_{leach}$
Feldspar - sodalite	$T\ (years) = 253.2 \cdot h_{leach}$

[1)]- h_{leach} – depth of leaching of one mineral relatively another mineral (mm).

On basis of this equations leaching rates of minerals in sample of nephelinic syenite (fig. 3), collected in coastal zone of Seydozero lake (Murmansk region) were estimated. The average values h_{leach} (for feldspar – nepheline pair) give 5±2 mm, which correspond to minimum water – rock sample interaction time for this samples about 5000 years.

Maghidov S.Kh. Study of anthropogeneous changing of underground geohydrosphere for estimation and prediction of geoecological danger

(IG DSC RAS

In the forties of the last century V.I. Vernadsky have written about origin of a new geological phenomenon, where "the Man had become the largest geological force" [1]. From that time the scales of human activity have grown many times that creates conditions for ecological catastrophes both regional and global level.

Electrical and magnet background of the planet increased by orders, geochemical background of the atmosphere on some components and substances changed several times; unfavorable changes take place in hydrosphere too. At modern temps of technogeneous influence the Earth can become unfit for living of high animals including a man already in the nearest future.

Not less danger the man-made changes in the geosphere represent. Owing to wide scale recovery of underground fluids the forced evolution of underground hydrosphere takes place in global scale with essential change of thermo-baric conditions and physical and chemical properties of geofluids and rocks. Such development of events can threaten to cause non-predictable consequences because the modern level of knowledge doesn't allow to give exact forecasts of the global system behaviour for intensive technogeneous loading. More over it's impossible to guarantee that increasing man-made influences won't result in global cataclysms.

Close state of the Earth's bowels changes by their opening that may lead to cardinal alteration of geodynamics of the upper layers of the Earth's crust with breaking of natural fluidodynamic and tectonic processes because of change of geological and hydrogeological conditions of the bowels. In the work [2] it has been shown that the density of producing in the world oil wells nowadays is sufficiently big and can seriously influence geotectonic activity of the bowels and behaviour of geohydrodynamic systems that demands of reliable methods creation for hydrogeological prediction [3]. If earlier influence of wells because of their little number was limited only by surrounding territory, when significant increasing of their number the force is spreading to the next wells, creating united sphere of influence. This field can cause global influence on properties of the upper layers of the Earth's crust, breaking the natural course of cyclic geodynamic processes going on with transference of great masses and energies.

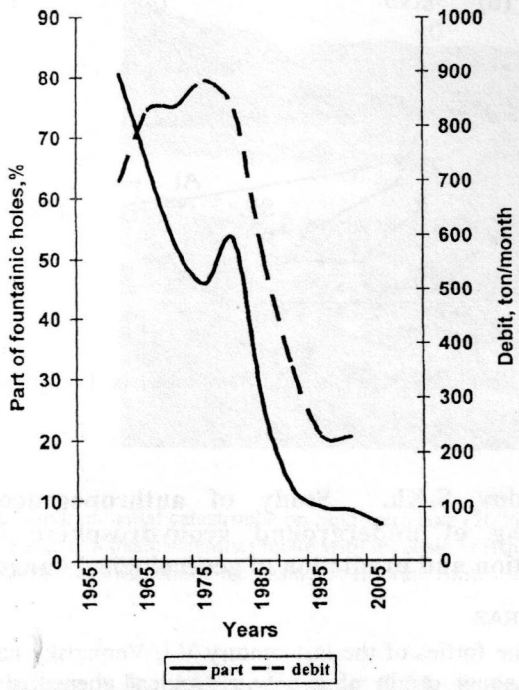

Fig.1. Discharge of oil wells of RF and compressibility potential of formation

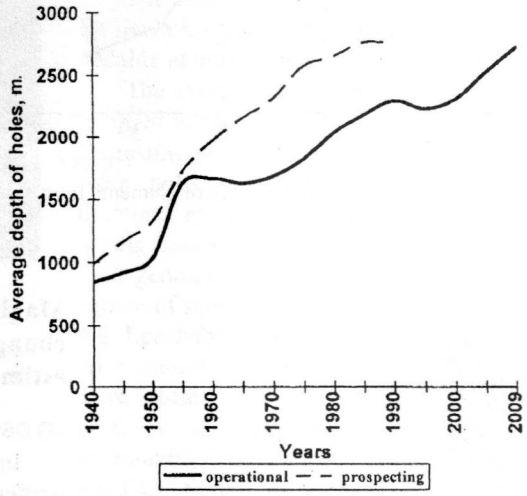

Fig.2. Average depth of wells in RF compketed by drilling

Natural elastic and plastic system owing to defluidization turns into *hard and brittle* system, which hindering the natural course of geodynamic processes promote accumulation of strong strains that can cause super power tectonic earthquakes (STE) [2,4,5]. In the work [5] a possibility had been proved of super strong earthquake origin with magnitude 9 and more in the nearest future. The forecast came true during 10 years and at the beginning of XXI century two STE took place. Increasing scales of influence on geosystem will result in global change of upper strata properties of the Earth's crust that potentially can result in origin of hyperstrong earthquake with magnitude 10 and more, which will bring irreplaceable losses [5].

Because of heat losses and intensive defluidization, reduction of geothermal gradient takes place and also parameters of baric field in the upper crust, undergone to technogeneous force. Some data, illustrating scales of technogeneous influence on natural geohydrosystem, are given in Fig. 1 and 2. As parameters for illustration of stratal pressure changes in the bowels the discharge of oil wells and a quote of flowing oil wells from the total their number have been used. In Fig. 1 we can see that for a half of the century the both parameters have been decreased significantly that testifies to essential alterations in underground geohydrosphere. This, in its turn, leads to alteration of thermodynamic and physico-chemical properties (strength, elastic and plastic ones, filtration and so on).

In Fig.2 data of average depths of oil wells are given, which testify to scales of thechnogeneous influence on geosphere in the largest region of the world – Russian Federation -, the depth of development wells here exceeds already 2500 m.

In some areas of the RF this parameter is significantly higher. So, in Daghestan the middle depth of development oil wells two decades ago was more than 4 km. Nowadays in the world a lot of deep and super deep wells are drilled and every year a quote of them increased. Maximum depth of wells exceeds already 12 km.

For prediction the further man-made alterations of geological environment and prevention of ecological catastrophes of global nature it will demand to carry out investigations of several types: in vitro, in situ, as well analog and computer modeling.

List of geological objects and their properties requiring in urgent laboratory investigation (in vitro)

Compounds: fluids (HC, H_2O, CO_2, N_2, H_2 , He and so on), silicates, oxides, combinations of Al , Fe .

Measurement ranges: t = 20-600 °C; p = 1-3500 bar.

Thermodynamic properties

Molar volume (V), entropy (S), heat of formation (ΔH), free energy (ΔE).

Physical and chemical properties

Temperature of melting t_m, temperature of boiling t_b, permeability, solubility in liquid fluids.

Chemical interactions of fluids and rocks, decomposing and synthesis of fluids, depolymerization of non-organic polymers.

Physical and mechanical properties

Elastic and plastic properties of rocks under strain and stress in different time scales.

Nature investigations, hydrogeological and geothermal monitoring (in situ).

Hydrogeological monitoring

Regimen observations for natural fluido-dynamic processes and influence of anthropogeneous component on them.

Thermo-baric monitoring

Continuous observation for thermal conditions and study of geothermal gradient dynamics in time.

Systematic monitoring of baric field and investigation of exhaustion of elastic energy because of artificial exposing the Earth's bowels.

Geochemical investigations by express-methods

Determination pH, content of hydrocarbon dioxide, ions of Fe, Mg ets.

Analog and computer modeling

Analog formation

Processes modeling with using of alternate physical ground.

Mathematical simulation

Modeling with using of mathematical apparatus and computer technic.

All these data will need in further time for normalization of limiting loading on geological environment and producing of necessary recommendations for risk reduction of ecological cataclysms of man-made nature.

References

1. Vernadsky V.I. Several words about noosphere // Vernadsky V.I. Philosophic ideas of the naturalist. M.: Nauka, 1988. P.509. (In Rus.).
2. Maghidov S.Kh. Wide-scale geochemical and fluido-dynamic "experiment" and its possible consequences in the nearest prospect // Vestnik Otdelenija Nauk o Zemle RAN, 2009. № 1(27). (In Rus.).
3. Konikov D.F., Patten E.P. Hydrogeological forecasting // M.: Mir, 1988. P. 271-334. (In Rus.).
4. Maghidov S.Kh. On possibility of super strong tectonic earthquake // Proceedings of the Conference on results of geographical investigations in Daghestan. Makhachkala, 1994. P.20-22. (In Rus.).
5. Maghidov S.Kh. On possibility of super strong tectonic earthquakes display // Geodynamic and seismic activity of Eastern Caucasus. Makhachkala, 2002. P. 86-88. (In Rus.).

Markovich T.I., Razvorotneva L.I. Udokan sulphide ore oxidativ leaching with acting oxygen compounds of nitrogen in the cryogenic conditions

Institute of Geology and Mineralogy SB RAS, 630090 Novosibirsk, Koptyug ave.,3 mark@uiggm.nsc.ru fax: (383)333-27-92; tel.: (383)333-31-12

Key words: Sulfides, oxidation, sulfuric acid leaching, catalysis, nitric oxides, nitrous acid

Sulfide mining wastes, as well as the natural geochemical anomalies, represent an uncontrolled sources of heavy metals into the environment. As a result of a complex multifactorial process of chemical and biochemical weathering of ore minerals in these landscapes there is a formation of aggressive sulfuric acid solution (upto pH <1) promoting the mobilization of Fe, Cu, Zn and other elements [1]. During the last decade a large number of works cover the development of geotechnical methods of migratory flows management in the fields of waste storing on the basis of experimental studies of the interaction of sulfide minerals with the components of the environment [2].

It is known that the processes of chemical weathering with atmospheric oxygen are limited by the activation phase O_2 (E^o = + 1.23 B) and noticeably accelerated in the presence of catalysts, whose role in the oxidative horizon of sulphide dumps along with ions, Fe^{3+}, Cu^+ is acted by nitrogen oxycompounds coming from atmosphere in the form of acid deposition (dry and wet) [3].

From the point of view of thermodynamics, nitric oxides and products of their interaction with water have higher oxidation potential (E^o = + 0.85 ÷ + 1.77 B) than univalent copper ions (E^o = 0.15 B) and ferric (E^o = + 0.77 B).

The mechanism of catalysis is extremely complex and currently do not have details. During oxidation in the system there is a number of nitrogen compounds (NO, N_2O_3, NO_2, N_2O_4, HNO_2, NO_2^-, HNO_3, NO_3^-, NO^+, NO_2^+ etc.) with different catalytic activity and varying concentrations. According to numerous experimental studies kinetically most chemically responsive form is the nitrous acid and its dissociation products. At low concentrations (< 0.1 M) the activating effect of HNO_2 exceeds the catalytic activity of all other nitrogen oxycompounds by several times.

The complete opening of sulfides does not require significant amounts of activator, because the escaping nitric oxides are easily oxidized in the presence of oxygen, and again form nitric acid.

$2Cu_2S + 2H_2SO_4 + O_2 = 2CuSO_4 + 2CuS + 2H_2O$ (1)

$2CuS + 2H_2SO_4 + O_2 = 2CuSO_4 + 2S + 2H_2O$ (2)

$Cu_2S + H_2SO_4 + 2HNO_2 = CuSO_4 + CuS + 2NO + 2H_2O$ (3)

$CuS + H_2SO_4 + 2HNO_2 = CuSO_4 + S + 2NO + 2H_2O$ (4)

$2NO + O_2 = 2NO_2$ (5)

$2NO_2 + H_2O = HNO_3 + HNO_2$ (6)

$2NO_2 = N_2O_4$ (7)

$N_2O_4 + H_2O = HNO_3 + HNO_2$ (8)

$NO + NO_2 = N_2O_3$ (9)

$N_2O_3 + H_2O = 2HNO_2$ (10)

Activating effect of HNO_2 intensifies with its concentration increase and is limited by HNO_2 disproportionation in the range of positive temperatures and low pH values. Currently, it is experimentally determined that in cryogenic conditions nitrous acid stability increases many times, even in strongly acidic environment [4].

Simulation of cryogenic weathering was realized on the patterns of Udokan sulphide ore (fraction - 0.2÷+0.063 mm) of the following chemical and mineralogical composition: (Cu – 20,50 %; Fe_2O_3 – 12,96 %; FeO – 9,87 %; $S_{overall}$ – 6,89 %; $S_{sulphite}$- 0,14 %; Ag – 199,33 g/t), (chalcosine - 13,87 %; magnetite - 6,89 %; quartz + feldspar - 38,84 %; limonite - 0,43 %; brochantite, ilmenite and chalcopyrite < 0,1 %). Leaching of ore by the sulphuric solutions (0.5 M) was carried out in closed polyethylene containers (500 ml) at - 20 and + 20 °C. The initial ratio of solid and liquid phases (S: L) is 1:5 (5 g of ore: 25 ml of solution). Nitrous acid (0.1 M) was obtained directly in the reaction pulp according to the exchange reaction: $2NaNO_2 + H_2SO_4 = 2HNO_2 + Na_2SO_4$, by adding a calculated amount of $NaNO_2$ solution (0.25ml 2 M) in the reaction vessel. The leaching periods were 2, 24 and 144 hours. Solutions after complete thawing and filtering were analyzed for copper content by atomic absorption (determination mistake with the account of dilution does not exceed 6%).

Preliminary investigations showed that the acid opening of Udokan ore in a wide range of pH values from 0.39 (0.5 M H_2SO_4) upto 3.01, (0.0005 M H_2SO_4) both in cryogenic conditions and at positive temperatures consisted of two stages: the initial oxidative leaching (according to eq. 1-4) and secondary mineralization (precipitation of soluble hydrosulfate).

The choice of sulfuric acid concentration (0.5 M) in these series of experiments has been determined by the following circumstances:

- opening of the ore by concentrated solutions of H_2SO_4 is limited by oxygen content in the closed system and does not go beyond the first stage, that allows us to investigate the activating effect of nitrous acid directly on the oxidation process without imposing the stage of brochantite loss.

- in cryogenic conditions environment acidity does not depend on the initial content of H_2SO_4 in the solution and it is determined by the preset temperature. According to

the diagram of system of H_2SO_4 – H_2O - T thermostating at – 20 °C of model solutions containing 0.5 M H_2SO_4 + 0.1M HNO_2 and 0.0005 M H_2SO_4 + 0.0001M HNO_2 - close to natural waters (pH 3, the content of NO_2^- -in the mist 1-5 · 10^{-4} M, in the rain 0.02-2 · 10^{-5} M) leads to equalization of values upto 2.9 M H_2SO_4 + 0.58 M HNO_2.

- freezing of more acid solutions allows leaching at lower S:L values, that is, with a larger amount of unfrozen liquid phase. This circumstance can reduce the diffusion constraints and enhance the mass transfer processes.

The experimental results of the sulfuric acid leaching of Udokan sulfide ores (including the addition of $NaNO_2$) at different temperatures are presented in Table 1.

According to the introduced results there is the positive dynamics in the process of copper extraction into the solution under all experimental conditions. Obviously even at subzero temperatures after complete freezing of the reaction mixture (20 - 50 minutes from the start of the experiment), the concentration of copper continues to rise.

Cooling of the system from 20 to 0 C° increases the solubility of oxygen from 6.94 to 10.19 ml per 1000 ml of water. According to the stechiometry of 1-2 equations with the full consumption of oxygen dissolved in the liquid phase at the beginning of the experiment, the copper content in the solution reaches approximately only 0.058 and 0.040 g/l (that is much lower than the values listed in the table). This fact indicates that O_2 molecules diffuse from the free volume of the reactor to the surface of sulfide not only at room temperature, but also in cryogenic conditions.

Table 1. Changing the copper concentration in solution* during leaching of Udokan ore

Acid concentration, M		Concentration Cu^{2+}, g/l			$k = C_{Cu}(-20\ °C)/ C_{Cu}(+20\ °C)$		
		Experiment duration, hours			Experiment duration, hours		
H_2SO_4	HNO_2	2	24	144	2	24	144
0.5	0.1	4.10 3.52	6.32 4.92	7.56 7.56	1.16	1.28	1.00
0.5	-	1.44 1.48	1.55 1.82	1.64 2.77	0.97	0.85	0.59

* - values were averaged over the three parallels; in the numerator - the concentration of copper at T = - 20 C° in the denominator - the concentration of copper at T = + 20 C°

Probably, in this case the volume of unfrozen liquid phase located in the intergranular space of polycrystalline ice is of significant importance.

Oxidation of copper sulfides is much faster with nitrous acid and proceeds with almost equal intensity on the entire range of parameters. Activating action of HNO_2 is more pronounced during freezing. Extraction of copper from the solid phase increases by 2.7 times at room temperature and 4.7 times in cryogenic conditions.

References

1. D.K. Nordstrom Chemical modeling of acid mine waters in the Western United States// Meeting Proceedings USGS Water Resources Investigations Report N91-4034. 1991. P.534-538.
2. Yu.V.Alekhin, S.M.Ilina, S.A.Lapitskii "Vestnik Otdeleniya nauk o Zemle RAN" №1(24)'2006, ISSN 1819-6586, URL:http://www.scgis.ru/russian/cp1251/h_dgggms/1-2006/informbul-1_2006/geoecol-3.pdf.
3. A.B.Ptitsyn, V.A.Abramova, T.I.Markovich, E.S. Epova Geohimiya kreogennyh zon okisleniya, Nauka, Sib. otdelenie, Novosibirsk, 2009.
4. N.Takenaka, A. Ueda, Y. Maeda Nature. №358. 1992. P.736

Martynov K.V.[1], Budantseva N.A.[1], Tananaev I.G.[1], Kovalsky A.M.[2], Kotelnikov A.R.[2] Experimental study of modifying component agency on devitrification of Na_2O-Al_2O_3-P_2O_5 glasses under elevated temperatures

[1]- IPCE RAS; [2]- IEM RAS mark0s@mail.ru; fax: (495) 335 20 30; ph.: (495) 335 20 30

Keywords: radioactive waste, aluminophosphate glasses, immobilization of radio nuclides

The immobilization of radio nuclides containing in a high level liquid radioactive waste (HLW) into aluminophosphate glasses is the basic solidification technology of the most dangerous to the nature and human person nuclear fuel cycle waste in our country. Behavior of glasses as metastable phase under the influence of various factors represents direct practical interest for the radiochemical industry. One of processes which considerably changes properties of glass matrixes is their crystallization. Influence of the elevated temperature, as crystallization (devitrification) factor on glasses and dependence of this process on presence in glasses Si and Fe is investigated in the present study.

Samples for research and experimental procedure

It is a little exemplary of transparent modeling glasses having a smooth surface and conchoidal fracture prepared by CZL FGUP PO "Mayak" have been selected for experiments. Chemical compounds of glasses have been studied by electron microprobe analysis (EMPA) on a scanning electron microscope (SEM) Tescan Vega II XMU combining with X-ray energy dispersive spectrometer INCAx-sight. Glasses differ on color (fig. 1) depending on presence of impurity (tab.1). Base glass (C-0) has no impurity and on figurative compound coincides with average procedural compound of glassing HLW by FGUP PO "Mayak" (fig.2). Other glasses have additives of various components and there compounds are richer with aluminum. Slices of glasses in weight 0.2 g subjected to heating on air at temperatures 420°C (44 hours), 470°C (39 hours), 530°C (12 hours), 640°C (4 hours) and 690°C (4 hours).

Table 1. Average procedural compound of glassed HLW by FGUP PO "Mayak" and compounds of samples by EMPA results in mol.%. Symbols of phases correspond to the same on fig. 2.

Sample, phase	Charac-teristic	Na_2O	Al_2O_3	SiO_2	P_2O_5	CaO	Fe_2O_3	NiO
Glassed HLW by FGUP PO "Mayak"		40(5)	17(4)	-	38(2)	3(2)	1(1)	1(1)
C-0, glass (■)	Starting	43.2(6)	17.7(3)	-	39.1(4)	-	-	-
C-0, NAP+ glass (□)	530°C (12 hours)	42(1)	18(2)	-	40(2)	-	-	-
C-3, glass (▲)	Starting	38.1(2)	20.5(1)	1.3(2)	37.3(4)	1.0(2)	1.8(2)	-
C-3, glass (Δ^1)	530°C (12 hours)	38.7(5)	19(1)	1.7(3)	36.5(7)	2(1)	2.2(5)	-
C-3, NAP (Δ^2)	530°C (12 hours)	36(2)	22(1)	2.4(8)	38(1)	0.6(3)	1.0(4)	-
C-4, glass (♦)	Starting	34.1(3)	20.2(4)	9.1(2)	34.8(4)	-	0.8(1)	0.9(3)
C-4, glass (◊)	530°C (12 hours)	32.9(7)	20.4(5)	9.3(2)	35.6(5)	-	0.8(1)	1.0(1)
C-5, glass (●)	Starting	41.0(4)	20.6(2)	-	34.7(6)	-	3.6(2)	-
C-5, glass (o^1)	640°C (4 hours)	40(1)	20.7(2)	-	33.5(4)	-	6.0(8)	-
C-5, NAP (o^2)	640°C (4 hours)	40.7(6)	19.7(3)	-	38(1)	-	1.9(5)	-
C-5, NFP (o^3)	640°C (4 hours)	32(1)	-	-	35.3(8)	-	33(1)	-

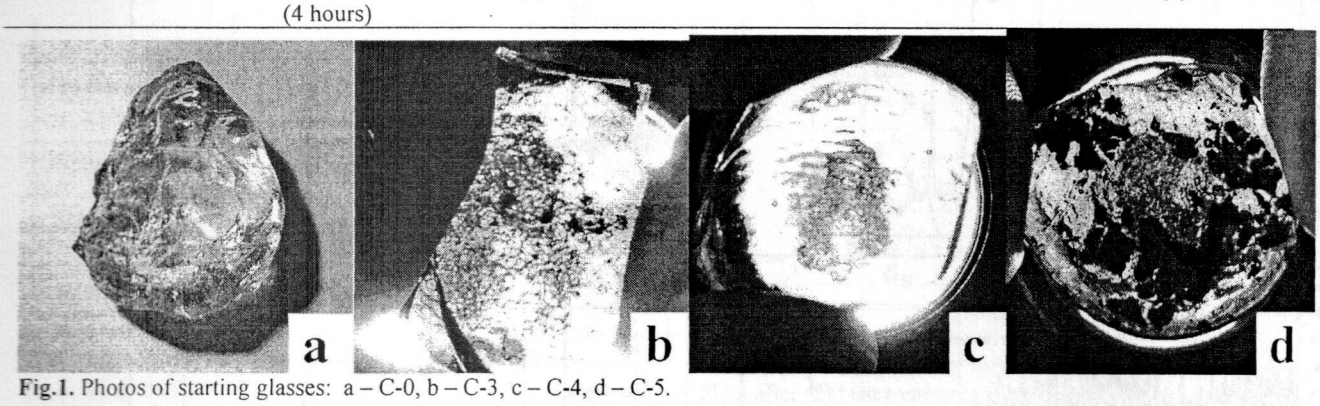

Fig.1. Photos of starting glasses: a – C-0, b – C-3, c – C-4, d – C-5.

Experimental results On visual supervision over products of experiments melting and crystallization processes occurred differently depending on compound of glasses. Glass C-4 containing SiO_2, melted at 530°C, but didn't crystallize. In samples C-0 (base compound) and C-3 (the small containing of impurity) crystallization occurred from melt, formed at 470°C. In glass C-5 enriched with iron, at first there was a crystallization in a solid condition, and partial melting occurred at the further rise in temperature to 690°C.

After heat treatment the glasses have been investigated by X-ray powder diffraction (XRPD) method, EMPA and infrared (IR) spectroscopy. XRPD pattern of sample C-4 after heat treatment (fig.4c) has confirmed the assumption about absence of crystallization. Also it is not revealed some heterogeneity of phase and chemical compound of this sample by EPMA (tab.1). Other picture was observed after heat treatment of glasses C-0 and C-3 (fig.4a,b). On both XRPD patterns there are reflections of the phase identified as sodium aluminophosphate (NAP) having compound $Na_3Al_2(PO_4)_3$ (database PCPDFWIN v.2.02, card 31-1265). For sample C-0 compound of this phase coincides with the glass one, that doesn't allow to observe phase heterogeneity by SEM backscattered electron detector. We have another matter for sample C-3 (fig.3a) in which microimpurity are distributed irregularly between glass (light) and a crystal phase (dark) (tab.1), and structure of the sample generated at devitrification is reveal. The most expressed effect of phase compound change is found out in sample C-5, in which after heat treatment without melting two crystal phases (fig.4d) were formed: Fe-NAP - $Na_{3.3}Al_{1.6}Fe_{0.1}P_{3.1}O_{12}$ (dark gray on fig.3b) and NFP - $Na_{2.6}Fe_{2.4}P_{3.1}O_{12}$ (white), and the glass (light gray) has remained also. All phases had contrast compounds (tab.1).

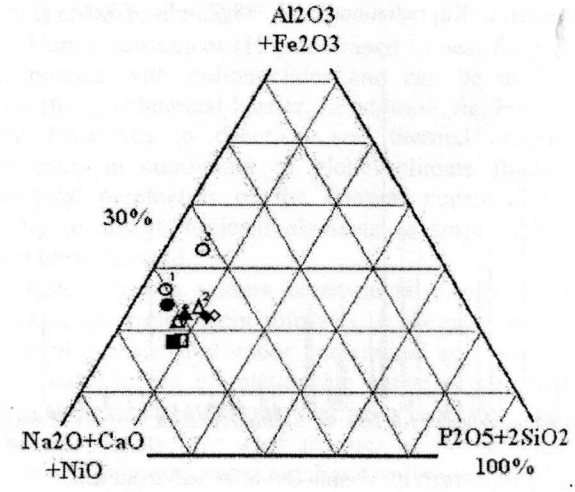

Fig.2. Chemical compounds of samples by EMPA results in mol.%. Symbols see tab.1.

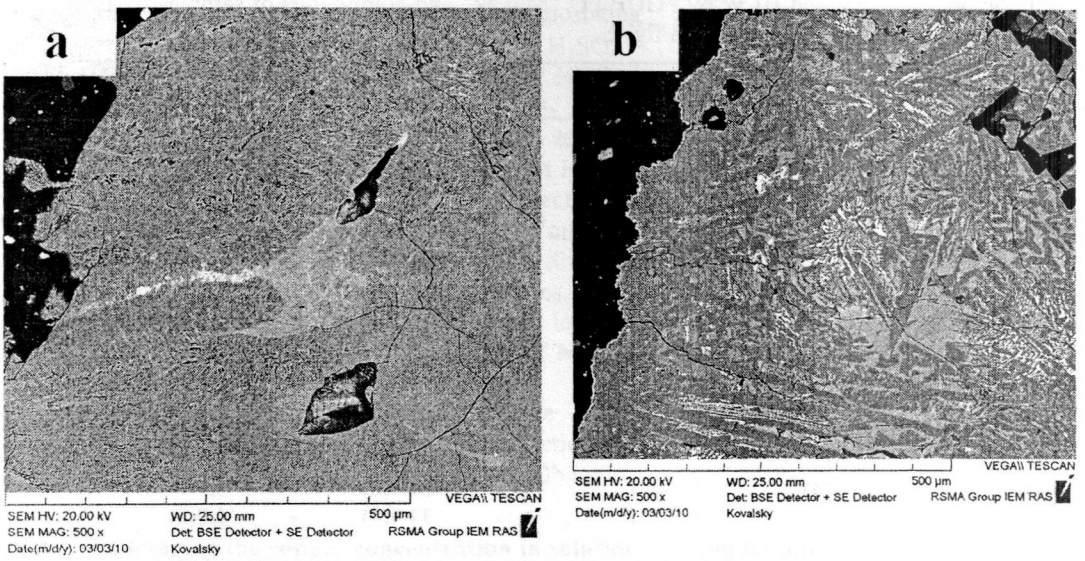

Fig.3. The polished cuts of samples C-3 (a) and C-5 (b) after heat treatment. Images are received on SEM backscatterec electron detector.

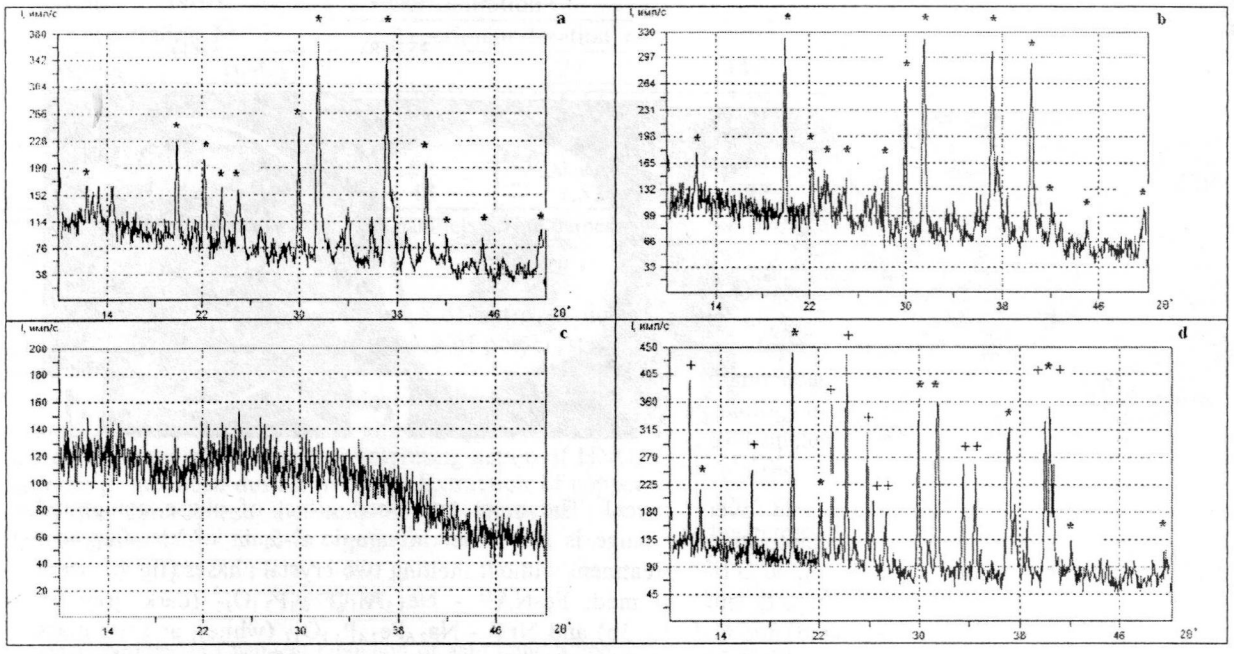

Fig.4. XRPD patterns of the samples C-0 (a), C-3 (b), C-4 (c) and C-5 (d) after heat treatment: * - NAP, + - NFP. Dron-7 diffractometer, $CoK\alpha_1$ radiation (λ = 1.78892), Fe -filter.

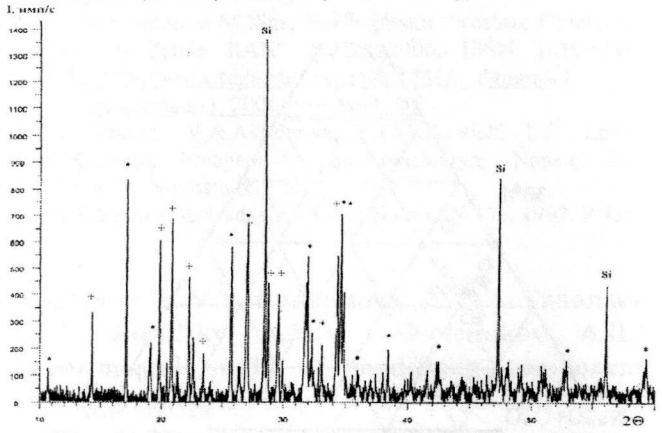

Fig.5. XRPD pattern of sample C-5 after heat treatment: * - Fe-NAP, + - NFP, Si - spectral pure silicon, a = 5.4305 Å. $CuK\alpha_1$ radiation (λ = 1.5406 Å).

XRPD pattern of the polyphase sample C-5 has been removed at 25°C on Bruker D8 ADVANCE X-ray diffractometer, using $CuK\alpha_1$ radiation (λ = 1.5406 Å) with step of 0.010°2Θ for specification of crystal phases structures (fig.5). Angular positions of reflections were corrected by the internal standard (spectral pure Si, a = 5.4305 Å). CRYSFIRE 2004 (THEOR90 procedure) and CHEKCELL computer programs have been used for definition of reflection indexes and calculation of unit cell parameters. 14 reflections for Fe-NAP and 12 ones for NFP in the angular interval of 10-60°2Θ have been involved for calculations. The decision for unit cell parameters of Fe-NAP has been found in terms of the tetragonal system: a = 9.303(1) Å, c = 18.733(2) Å, V = 1621.3(6) $Å^3$, body centered lattice is possible. The orthorhombic crystal system, PBAM space group has been offered for NFP: a = 18.114(3) Å, b = 9.251(2) Å, c = 8.533(2) Å, V = 1430.0(8) $Å^3$.

IR spectra of samples have been recorded at room temperature on Specord M80 spectrophotometer with the instrumental resolution of 4 sm^{-1} (fig. 6). Samples were dispersed in melted NaCl matrix. The quantity of the sample in a matrix made 1.5 wt.%. The IR spectra of initial glasses in the region of 1200-1050 cm^{-1} shows the intense strongly overlapping absorption bands assigned to stretching vibrations ν_{as} and ν_s of different phosphate

groups (PO_4). The bands of medium intensity in the region 1050-900 cm-1 are correspond to the antisymmetric vibrations of the bridging groups vas P-O-P and P-O-Al. Very weak bands exhibits in the spectral range 750-640 cm-1 due to stretching vibrations (AlO4) tetrahedra. The weak bands in the region 600-400 cm-1 are indicative of bending vibrations of the bridging groups (T-O-T), where T = P or Al.

The IR spectra of C-0, C-3 and C-5 glasses after heat treatment are demonstrated not only the best resolution of the absorption bands of ν(PO4) and bridging groups (P-O-P) and (P-O-Al), but also increase their intensity, which is probably associated with greater ordering of the high-temperature phase. The spectrum of melted glass C-4 differs slightly from the parent spectrum, and shows only a decrease of the intensity of deformation vibrations δ(T-O-T) at low frequencies. Thus, the original glasses undergone some structurisation already in the course of storage at room temperature, and for devitrificated samples these changes far more radical as they are connected with the formation of crystalline phases.

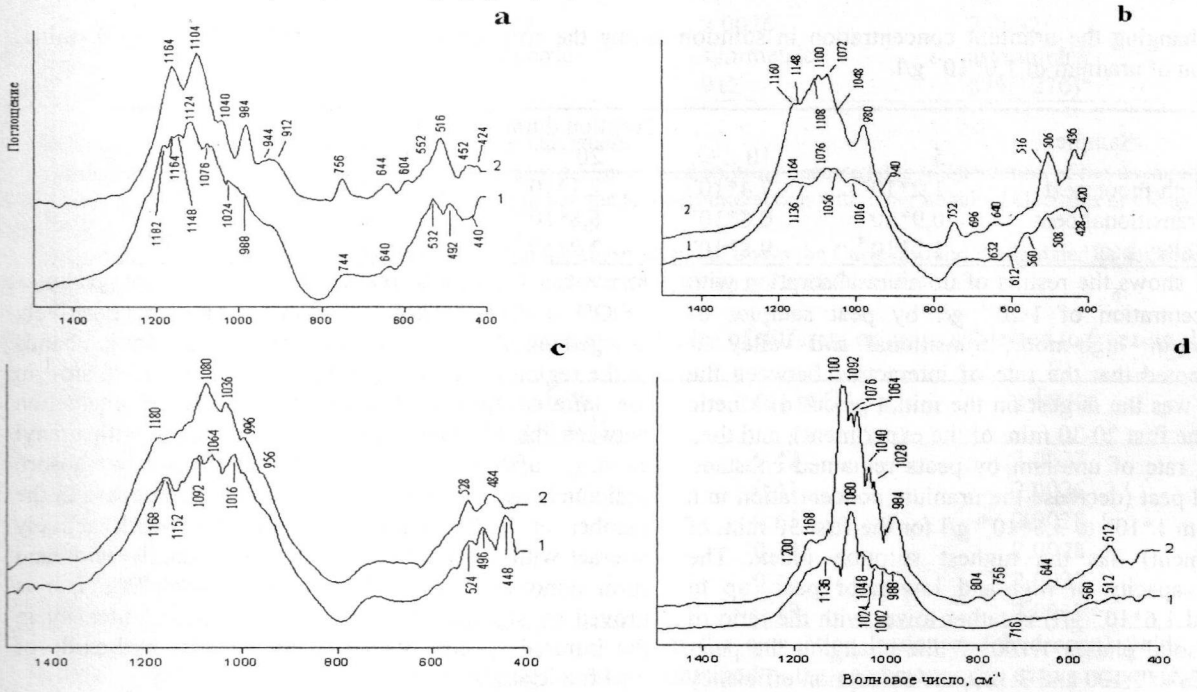

Fig.6. IR spectra of C-0 (a), C-3 (b), C-4 (c) и C-5 (d) samples before (1) и after (2) heat treatment.

Discussion of results and conclusions On radiochemical manufacture all glasses after pouring in containers cool down long enough. Our experiments simulate processes which can occur at slow cooling glassed radioactive waste. It is shown that elements-modifiers can both to brake process of glass devitrification (Si), and to make active it (Fe). Anyway all laboratory tests on mechanical and chemical stability of glasses are correct for spending not with the quenched metastable glass, and with the material after heat treatment.

This work was supported by the Presidiums of RAS program № 4, the RFBR grant № 10-05-90749-mob_st, the President of RF grant № MK-4888.2009.5

Razvorotneva L.I., Gilinskaya L.G., Markovich T.I. The influence of freeze – thaw process on the stability of natural geochemical barriers during sorpting radionuclides on them

Institute of Geology and Mineralogy SB RAS, 630090 Novosibirsk, Koptyug ave.,3 mark@igm.nsc.ru fax: (383)333-27-92 tel.: (383)333-31-12

Key words: Radionuclides, sorption, geochemical barriers, peat

Modern periodic variations in climate affect the steady-state equilibrium processes in both natural and anthropogenic systems. Reveal regularities of influence of climatic parameters changing on the natural environment in order to forecast ecological consequences is a challenge. In recent decades for the environmental protection there is a tendency to safe disposal of radioactive wastes using natural materials. The use of peats as a matrix for binding and long-term retaining of radionuclides allows one the hand to ensure reliability and durability of conservation, on the other hand to reduce the production costs, because peat is cheap to obtain.

Humic substances (HS) contained in peat form stable compounds with radionuclides and can be used as a powerful geochemical barrier. In addition, the HS show a high resistance to chemical and thermal destruction. However, in conditions of global climate fluctuation, structural parameters of the mineral matrix and their ability to absorb toxicant elements as sorption barriers have been changed.

Below there are some experimental results about the uranium absorption from solutions by the peat samples of different genesis (high-moor, transitional and valley), and also establishment of relationship between the structural changes under the influence of climate variations and their sorption capacity. We used samples of peat of different origin - high-moor, transitional and valley, obtained from different Siberian deposits.

Sample preparation included screening peat patterns and then splitting into fractions by sedimentation. For experiments on the uranium sorption the peat fractions less than 2 microns were used. Sorption capacity was determined by changes in the concentration of initial

solutions of uranyl in the liquid phase after contact with the sample of peat during the recorded time intervals. Proportion of liquid and solid phases varied in the range of 100:1 - 100:3. Phase separation (after sorption) was carried out in a centrifuge at 15 thousand rpm. Uranium concentrations in the range of 10^{-1} – 10^{-7} g/l were measured on an atomic emission spectrometer with inductively coupled plasma IRIS Advantage. The mass spectrometry method with inductively coupled plasma (ICP MS) of high-resolution ELEMENT by FINNIGAN MAT (Germany) with a magnetic sector and double focusing was used for the analysis of low concentrations of radionuclides. EPR researches were performed on radiospectrometer «Kadiopan», fmod= 100 kHz, T = 293°C. Shooting of infrared spectra were recorded on double-beam spectrometer Specord 75 IR in the range of 400-4000 cm^{-1} with a tablet of pure KBr in the parallel channel.

Table 1. Changing the uranium concentration in solution during the sorption by different types of peat (g/l). Initial concentration of uranium of $1{,}0*10^{-3}$ g/l.

Sample	Sorption duration, min				
	5	10	20	30	50
High-moor peat	$1{,}2*10^{-4}$	$7{,}4*10^{-5}$	$2{,}1*10^{-5}$	$1{,}1*10^{-5}$	$8{,}2*10^{-6}$
Transitional peat	$0{,}9*10^{-4}$	$0{,}8*10^{-5}$	$6{,}8*10^{-6}$	$3{,}6*10^{-6}$	$2{,}3*10^{-6}$
Valley peat	$1{,}2*10^{-4}$	$9{,}8*10^{-5}$	$3{,}9*10^{-5}$	$1{,}6*10^{-5}$	$1{,}0*10^{-5}$

Table 1 shows the results of uranium absorption with initial concentration of $1{\cdot}10^{-3}$ g/l by peat samples of different origin: high-moor, transitional and valley. It should be noted that the rate of interaction between the two phases was the largest on the initial pieces of kinetic curves (in the first 20-30 min. of the experiment), and then the binding rate of uranium by peats remained constant. Transitional peat (decrease the uranium concentration in a solution from $1*10^{-3}$ to $3{,}6*10^{-6}$ g/l for the first 30 min. of the experiment) has the highest sorption index. The absorptive capacity of high-and low-moor peat (up to $1{,}3*10^{-5}$ and $1{,}6*10^{-5}$ g/l) is rather lower with the ratio of liquid and solid phases 1:100. While changing the peat-solution ratio to 2:100 and 3:100, the absorption efficiency during 30 min. slightly reduced - for the transitional, high- and low-moor peats to values of $7{,}4*10^{-5}$ –$3{,}8*10^{-5}$ g/l; $5{,}4*10^{-5}$ –$8{,}9*10^{-5}$ g/l; $7{,}8*10^{-5}$ – $1{,}1*10^{-4}$ g/l, respectively. But further while the period of contact of solution with peat was prolonged, absorption coefficients increased that indicates the diffusive nature of the process. High exchange capacity of humic acids (1200-1950 mg-eq/100g) provides the formation of strong complexes with radionuclides, that plays a crucial role in their distribution and deposition in natural conditions.

Present variations in climatic conditions (temperature jump, changing the amount of water in the structure, rising the ionic strength of solutions due to increased leaching of salts from minerals) lead to alteration of the equilibrium sorption parameters. This affects the absorption and the retention of peats. It is known that the peat ion-exchange properties are associated with the ability to chemical interaction of functional groups, mainly carboxyl and amino groups of organic acids. The method of infrared spectroscopy was used to evaluate structural changes in peats and to define the role of different functional groups in a stable binding of the radionuclides molecules. Water molecules that are parties in the formation of supramolecular structures acts an important role in operation of the peat geochemical barriers. According to differential thermal analysis it is revealed that water in peats has various forms (physically and chemically bound, structurally trapped water and water of mechanical retention). We have found that depending on the amount of water in the initial structure of peats (from 41,7 to 65,9%) carboxyl groups of humic acids of peats were ionized. While the number of freezing-thawing cycles increases, the transformation into carboxylate group: -COOH → $-COO^-$ followed by interaction with a positively charged ion of uranyl. The appearance of absorption bands in the region of stretching vibrations 1580 – 1590 sm^{-1} in the infrared spectra is a direct evidence of interaction between the -COOH groups of humic acids with uranyl cations, affecting the ability of peat to absorb radionuclides. At the same time there is an increase in the number of hydroxo forms of uranium, which actively interact with other functional groups of humic acids and form donor-acceptor and hydrogen bonds. This fact is proved by significant reduction in the peaks intensity in the infrared spectra belonging to phenolic hydroxide of peat fulvic acids.

In comparison with the original samples significant changes in the region of stretching and deformation vibrations of ionized carboxyl groups, alcohol groups, were observed in the infrared spectra of uranium samples. While the cycles of thermal fluctuations with the freezing - thawing of uranium-bearing peats for the region below 950 - 980 sm^{-1} increased, the specific absorption of substituted aromatic structures of humic acids appeared. Later the bands at 600, 1100 – 1160 sm^{-1} arose that indicates the variations in peat of groups of $RCH{=}CH_2$, CH_2-O-CH_2, etc. The manifestation of these groups related to the components of humic acids showed the profound structural changes in peats. In general, the infrared-spectrometric researches of peats subjected to repeated freeze – thaw procedures revealed the presence of deformation disruptions, and also partial destruction of the initial supramolecular structures.

Along with the presence of the significant amount of functional groups in humic substances mineral matrix of peats contains all sorts of structural defects. The method of electron paramagnetic resonance (EPR) was used to fix such states and to estimate their number. The EPR recorded a free organic radical (FOR) and ion Fe^{3+} complexes in the studied peat patterns. Spectrum of FOR is represented as a single symmetric line in the samples of high-moor and transitional peats and as an asymmetrical line (due to the superposition of two points) in a sample of low-moor peat with a g-factor close to that for a free electron with an unresolved hyperfine structure. This paramagnetic center is typical of the high-molecular natural compounds to which humic acids belong. It has been established that the unpaired FOR electron is

localized on broken links in the side branches of condensed carbon rings. FOR formation in peats can be represented as a result of the breaking of the carbon-hydrogen bonds under drastic temperature fluctuations. In addition, dehydroxylation (removal of OH groups), demethylation (removal of methyl groups, break of aliphatic chains) can cause the bond breaking. Simultaneously, the size of nets (the number of rings) increase. Detachment of side groups from the ring leads to the formation of new C-C bonds, that promotes the growth of the ring system. Parameters of FOR spectra are presented in Table 2.

Table 2. Parameters of free organic radicals spectra

Peat	№ 1 high-moor	№2 transitional	№3 valley
ΔH mTl	0,4	0,4	0,6
g-factor	2,0027	2,0026	2,0032
Line shape	symmetric	symmetric	asymmetric
Int., rel. unit.	355	912	879(1270)*

*The total intensity of the two centers is shown in parentheses.

ΔH (the width of the spectrum line) is determined by the unresolved splitting occurred due to interaction of the unpaired electron with the surrounding protons (shown by the DENR), but not due to direct interaction with other unpaired electrons or the spin-lattice interaction with the rest of the molecule.

The g-factor value close to g_e (2,0023) testifies that the observed signal obeys the Curie law and is stipulated by localized centers of aromatic nature. If g > 2,0023, it can be the conduction electrons which obey Fermi-Dirac statistics.

Table 3. Parameters of the organic radicals' spectra in peat samples of different origins, subjected to freezing-thawing

Sample	Organic radical Nx spin/g X 10^{17}	ΔH mTl	g-factor
High-moor peat initial	0,61	0,42	2,0027
Transitional peat initial	1,52	0,41	2,0026
Valley peat initial	1,87	0,55	2,0028
High-moor peat (-18^{0}C)	1,43	0,38	2,0028
Transitional peat (-18^{0}C)	2,84	0,41	2,0027
Valley peat (-18^{0}C)	3,73	0,48	2,0033

Table 3 presents the results of changing in the structure parameters at fivefold freezing - thawing of peat samples of different genesis from Western Siberian deposits. It was experimentally shown that multiple freezing - thawing of peat considerably intensifies structural defects, and further leads to the destruction of the near-surface layer. In this case, the number of fine-grained debris that are carried away by surface water for significant distances increases.

Rudakov V.P., Tsyplakov V.V. Comparative analyses of the radon and hydrogen fieldes in conditions of the seismoactive and platform regions

EPI RAS rudak@mail.ru , tel.: (499)254 90 06

Key words: emanational monitoring, tidal deformations, spectral analyses

We have previously shown that, realizing requirements of technology developed for the purpose of seimoprognostic emanation measurements, allowing measurement of variations of the earth crust deformation at the level of tidal disturbances, one can monitor the processes of regional and global changes in the stress-strain state of the lithosphere during periods of anticipating and accompanying the release of seismic and volcanic energy [1].

In development of methodological aspects of assessing the reaction of the fluid dynamic systems of fault structures of the Earth's crust to the processes of preparing geodynamic events the comparative analysis of time series of the emanation (radon and hydrogen) fields variations obtained in the geodynamically active region (Kamchatka) and passive seismic conditions of the Russian Platform (Moscow syneclise) have been made. Spectral components of time series data were compared with the results of spectral analysis of laser deformometry obtained in the Caucasus [2].

Continuous monitoring of the fluid dynamic regime variations of the Moscow depression was carried out in the area of dynamic influence of faults intersecting at the center of Moscow on radon and hydrogen emanations [3] using the original technology, which provides registration geodeformation processes at the level of 10^{-8}. Similar measurements were carried out on the Kamchatka Peninsula, near the village Paratunka where the geodynamic activity of the territory permanently appears by the output on the surface of the thermal mineral waters sources [4].

Analyzed fragments of time series of simultaneous recording of these parameters (Fig. 1) represents the results of quasi-continuous records averaged at hourly intervals, a total duration of 13510 hours, i.e. more than 1.5 years.

Arrows indicate the moments of catastrophic earthquakes in the Indian Ocean.

Comparison of time series of the emanation fields obtained on the Kamchatka Peninsula and in the Russian Platform by calculating the sliding correlation function shows a certain general character of the geodeformation processes that determine the regimen of the fluid transmission in obviously different geodynamic conditions. This is indicated by correlation between the analyzed parameters (Fig. 2), which in the intervals that are multiples of the seasonal cycles lasting several months,

ranging from one hundred percent positive to one hundred percent negative.

And, for the time series of radon a wholly positive correlation is observed from December to March and negative - in April - May. At the same time, the time series of hydrogen absolutely positive correlation is noted in late February - early March and from November to December, and negative - from August to September and from January to February. At the same trend components of the strain in the Caucasus and strains defending the fluid transmission in the Moscow depression and on Kamchatka, have a pronounced seasonal (annual) character.

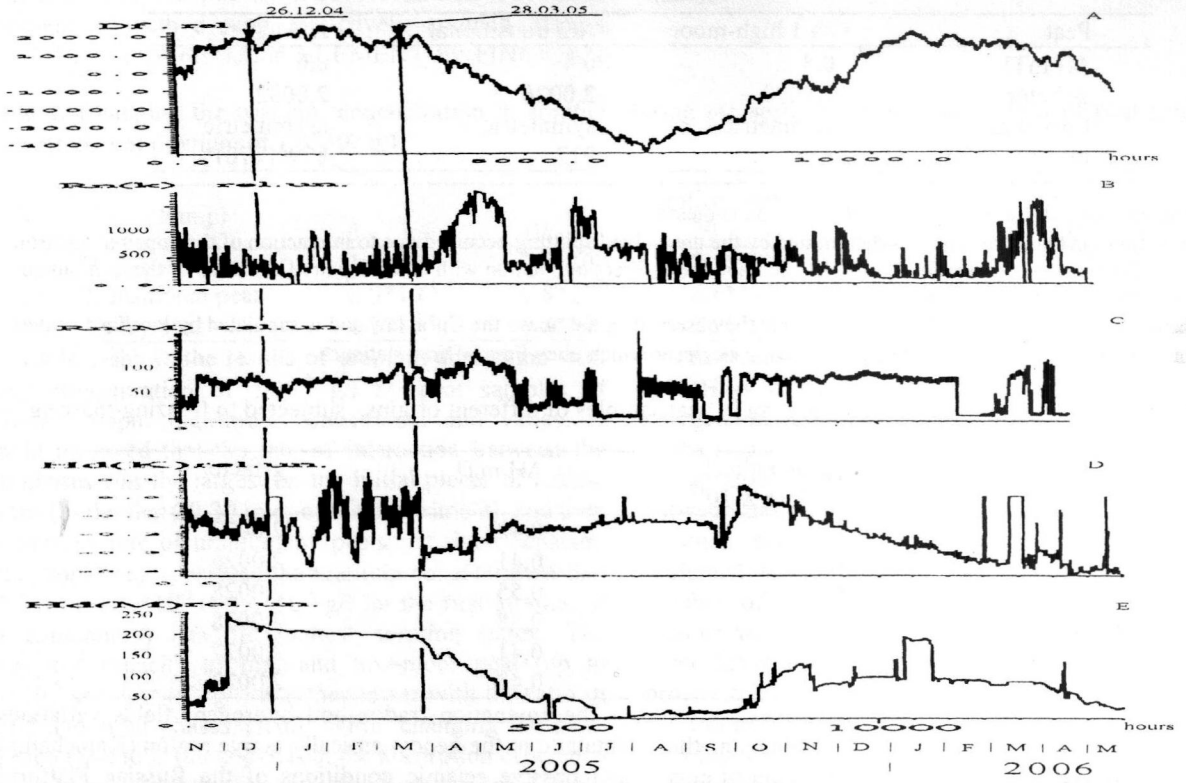

Fig.1. Time series of variations: a) deformation of rocks in the Caucasus, b) radon in Kamchatka, c) radon in Moscow, d) of hydrogen in Kamchatka, e) of hydrogen in Moscow

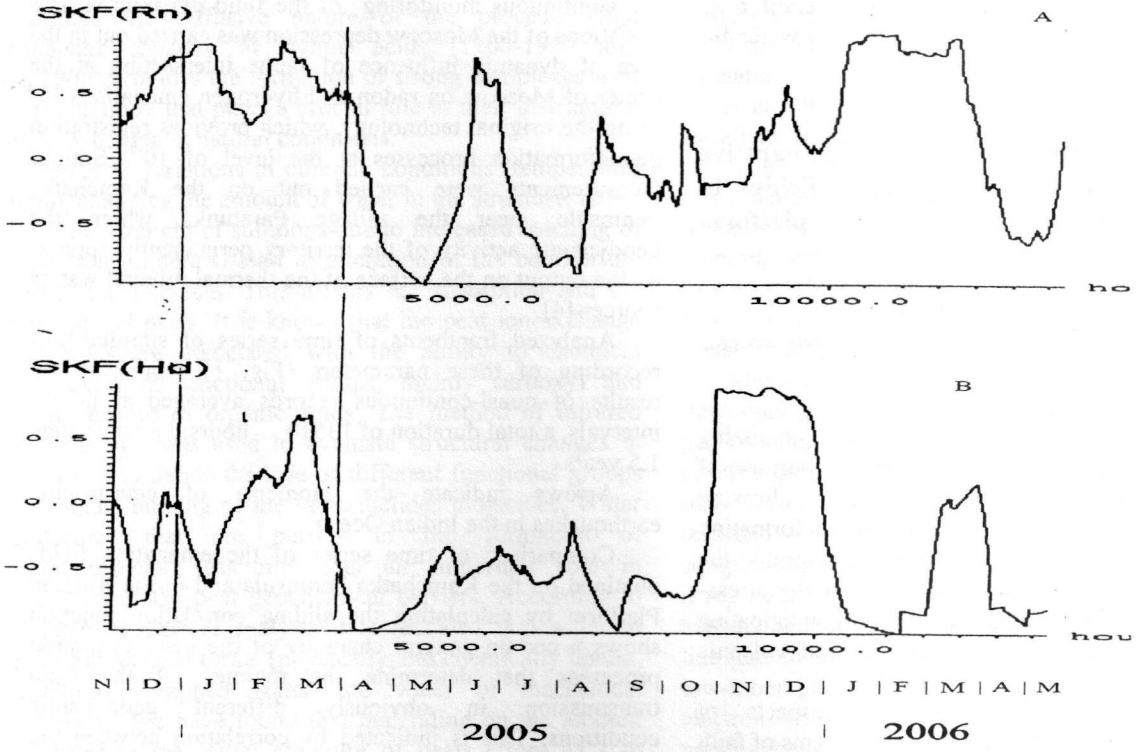

Fig.2. Graphs of the sliding correlation functions of time series: a) radon, b) hydrogen received in Kamchatka and in the Moscow depression

Table 1. Tidal components of the mutual correlation spectrum of the filtered data in the Baksan laser strainmeters and variations of radon and hydrogen in Moscow and Kamchatka, in comparison with the tidal components of the deformometry data (1stitch).

	T hour	A(rel) $*10^{-3}$	T hour	A(rel) $*10^{-3}$	T hour	A(rel) $*10^{-3}$	T hour	A(rel) $*10^{-3}$	T hour	A rel $*10^{-3}$	T hour	Arel* 10^{-3}
Def.			25.75	0.7	24.0	0.7	12.7	0.13	12.4	2.6	12.0	0.5
1rd/d.	26.9	0.08	25.75	4.9	24.0	0.35	12.7	0.1	12.4	0.6	12.0	0.17
1hd/d.	26.9	0.04	25.9	0.2	24.0	1.1	12.7	0.02	12.4	0.15	12.0	0.09
2rd/d.	26.9	0.17	25.75	0.6	24.0	1.1	12.7	0.16	12.4	0.5	12.0	0.6
2hd/d.			25.75	0.13	24.0	0.93	12.7	0.04	12.4	0.2	12.0	0.3
Km/rd			25..9	1.0	24.0	1.85	12.7	0.11	12.4	0.8	12.0	2.0
Km/hd	26.9	0.3	25.8	1.6	24.0	1.6			12.4	1.1	12.0	0.5

Legend: 1 rd, 1hd – sensors of radon and hydrogen in the first point of measurement; 2 rd, 2 hd - radon and hydrogen sensors in the second point of measurement in Moscow. Km /rd - radon in Kamchatka; Km /hd - hydrogen in Kamchatka

Table2. Spectral components of mutual-correlation spectrum of variations of the envelope of the filtered data series of laser strainmeter in Baksan and variations of radon and hydrogen in Moscow and Kamchatka.

LD, T	28.4d	14.8d	26.9h	25.8h	24.0h	22.4h		12.9h	12.4h	12.0h	8.4h	8.2h	8.0h	6.2h	6.1h
A($*10^{-3}$)	2.8	8.7	1.7	6.6	6.3	2.2		0.7	1.2	0.5	1.2	1.2	0.6	1.6	1.2
KRd, T	27.3d	14.5d		25.8h	24.0h	22.4h	16.5h		12.4h	12.0h	8.4h	8.2h	8.0h	6.2h	6.1h
A($*10^{-3}$)	13.8	8.4		11.7	9.6	4.3	1.4		0.7	1.1	0.4	0.43	0.4	0.5	0.6
1Rd, T	27.3d	14.8d	26.9h	25.8h	24.0h	22.4h	17.3h		12.4h	12.0h	8.4h	8.2h	8.0h	6.2h	6.1h
A($*10^{-3}$)	14.7	28.7	3.5	17.8	10.0	5.7	0.2		0.2	0.6	0.1	0.25	0.05	0.15	0.15
2Rd, T	27.3d	14.5d	26.9d	25.8h	24.0h	22.4h	17.2h	12.9h	12.4h	12.0h	8.4h	8.2h	8.0h	6.2h	6.1h
A($*10^{-3}$)	12.1	11.6	0.7	2.1	4.0	0.6	0.3	0.2	0.13	0.12	0.1	0.23	0.1	0.2	
KHd, T	27.3d	14.8d	13.9d	25.8d	24.0h	22.4h	16.6h		12.4h	12.0h	8.4h	8.2h	8.0h	6.2h	6.1h
A($*10^{-3}$)	17.6	19.2	10.0	2.9	1.6	0.7	0.1		0.1						
1Hd, T	28.4d	14.5d	26.9h	25.8h				12.8h	12.4h		8.4h	8.2h		6.2h	6.1h
A($*10^{-3}$)	3.0	7.6	0.13	0.6				0.05	0.05		0.06	0.05		0.03	0.04
2Hd, T	28.4d	14.5d		25.6h	24.0h	22.4h		12.8h	12.4h	12.0h	8.4h	8.2h	8.0h	6.2h	6.1h
A($*10^{-3}$)	5.6	11.4		0.4	2.4	0.2		0.07	0.06	0.06	0.05	0.04	0.05	0.06	

Legend: LD-laser deformograph; KRd-radon in Kamchatka; 1Rd (1Hd)- first radon detector (hydrogen) in Moscow

Spectral analysis of the time series of deformometric measurements, filtered in the tidal range of frequencies with periods from 30 to 5 hours and subsequent spectral analysis of time series interrelation functions fields of radon and hydrogen within the selected fragment made it possible to identify the components of the measured parameters in the variations spectrum due to lunar solar tides (Table 1). The results of this identification, indicate the adequacy of global mapping geodeformation processes, which are primarily terrestrial tides, in the measured parameters of the geosynclinal (seismically) and platform regions. In addition, as shown in the table, the nature of the response emanation fields on the tidal deformation of the earth's crust in the most characteristic components of the spectrum is almost identical to the character of deformation in the Caucasus mountain massif detected by the deformometric observations.

To mark out the low-frequency variations of the radon and hydrogen fields, similar to the corresponding components of the earth crust deformations the envelope of the filtered data of the strainmeter records was obtained, on which the spectrum envelope of the tidal deformations was calculated used for testing the mutual spectrum of the radon and hydrogen fields (Table 2).

And this testing (as shown in table) also reveal subordination of the fluid transmission in the geodynamically differing regions to influence of the planetary geodeformation processes determined primarily by the tidal influence of the moon and sun. At the same time, as can be seen, the spectral composition of the emanation field's time series is somewhat different from deformometric data that is associated with the technology of emanation measurements that can extract information about the volumetric massif deformations, whose spectrum is much richer the spectrum of linear strain. Apparently, this also explains the nature of the emanation field's reaction (Fig. 1) to global change of the stress-strain state of earth's crust, triggered the release of seismic energy near the island of Sumatra on Dec. 26, 2004 and on March 28, 2005. The level of seismic energy release during these earthquakes reached 9-ball marks on the Magnitude Scale, reflecting the extraordinary geodeformation processes involved in their preparation, and, apparently, affecting the Earth's crust as a whole.

As can be seen from figure 1, the disposition of the emanation fields reaction in Kamchatka and the Russian platform and strains in the Caucasus on the global changes of the stress-strain state of earth's crust, triggered the release of seismic energy in the Indian Ocean, are significantly different. So in the field of the hydrogen field of Moscow depression practically one month prior to tragic events there was a sharp jump, five times exceeded level of the concentration of previous months. In a field of radon this effect was on the contrary noted more than

double (on fig.1 it is not shown because of limitation of the time series) by reduction of the concentration level [3]. In Kamchatka, the field of hydrogen and radon have changed at this time is not so anomalous. However, almost one hundred percent correlation between the fields of radon before the events in December 2004 and March 2005, as well as wholly-correlation fields of hydrogen in March 2005 in the points of measurement, separated by a distance equal to nearly one third of the globe perimeter, show the global nature of the stress-strained state of the earth's crust, caused the catastrophic events in the Indian Ocean.

After the earthquake realization on 28.03.05 within 3 months there was a decrease of the hydrogen concentration up to initial, and the next months practically up to a zero level. Concentration of radon on an initial level has not returned, that, probably, is connected with descending trend in the emanation fields time series, connected with the wave geodeformation processes influence of the higher hierarchical level [1]. In addition, it confirms that the field variations of radon mediated variations of the hydrodynamic regimen of tectonic structures that are used for fluid dynamic monitoring, while the field variation of hydrogen directly reflect the regimen of earth crust deformations [3].

In the deformometric measurements the effect of global changes in the stress-strain state of the Earth's crust emerged in the results of the joint analysis of records obtained in the Caucasus and in the settlement Protvino (Moscow region) [5], in which the period of preparation and implementation of the earthquake is characterized by a monotonous change in the registered parameters.

Consequently, according to the fluid dynamic (emanation) monitoring of the geodeformation processes in the geodynamically active region - in Kamchatka and in the Russian platform, based on data deformometric observations in the Caucasus, in the preparation and realization of catastrophic geodynamic events such as, for example, earthquakes near the island Sumatra on Dec. 26, 2004 and March 28, 2005, the processes of the global change in the stress-strain state of the crust are involved. The rational use of data tracking changes in fluid dynamic regimes of the geostructural formations in the geodynamically active and platform regions allows to control these processes and predict periods of the seismotectonic areas formation of rock's massif destruction.

The authors express their gratitude to the worker of SAI, Dr. Science Miliukov VK for the provision of laser deformometry data and for his attention to the work, as well as to the worker of the Institute of Volcanology and Seismology Dr. Science Firstov P.P. for the provision of emanation monitoring data in Kamchatka and fellow-fightering in the emanation investigations.

References

1. Rudakov V.P. Emanation monitoring of the geoenvironments and processes. Moscow: Scientific World. 2009. 176p.
2. Miljukov V.K., Kopaev A.V., Lagutkina A.V., Mironov A.P., Myasnikov A.V. Observations of tidal deformations of the earth's crust in the Elbrus region. Earth physics, 2007. V.43. № 11. P.922-930.
3. Rudakov V.P., Tsyplakov V.V. Fluid dynamic effects of the fault structures of the Moscow sineclise in relation to global geodeformation processes. // Geochemistry. 2008. № 11. P.1238-1244.
4. Firstov P.P. Monitoring of the volume activity of subsurface radon (Rn-222) on Paratunka hydrothermal system in 1997-1998 to search for precursors of strong earthquakes of Kamchatka.// Volcanology and Seismology 1999, № 6. P.1-11
5. Latynina, L.A/, Miliukov V.K. Vasil'ev V.I. The strongest earthquakes and global tectonic processes. / / Science and Technology in Russia. 2006. № 1-2. P. 4-6.

Martynov K.V.[1], Safiulina A.M.[1], Tananaev I.G.[1], Kovalsky A.M.[2], Kotelnikov A.R.[2]

Experimental study of cesium sedimentation from multicomponent water solutions using sodium and ammonium tetraflouroborates at room temperature

[1]-IPCE RAS; [2]- IEM RAS mark0s@mail.ru; fax: (495) 335 20 30; ph.: (495) 335 20 30

Keywords: tetraflouroborates, sedimentation method, degree and selectivity of separation, processing of spent nuclear fuel

^{137}Cs is one of the most dangerous and, at the same time, valuable isotope of radiochemical manufacture at processing of spent nuclear fuel. Owing to low concentration of cesium in solutions, its separation usually make by an extraction method. However in certain cases, for the concentrated solutions more simple and low cost method of sedimentation can be used. We investigated cesium sedimentation from nitrate and alkali-carbonate multicomponent (Na, Mg, Al, K, Ca, Sc, Ti, Cr, Mn, Fe, Ni, Cu, Zn, Sr, Y, Zr, Nb, Mo, Pd, Ag, Cd, Sn, Cs, La, Ce, Nd, Eu, Gd, Ho, Yb, Hf, W, Hg, Pb, Th, U) water solutions at 20°C by sodium and ammonium tetraflouroborates, based on their higher (on 1-1.5 order) solubilities in water, than solubility of cesium tetraflouroborate. A subject of our research was degree and selectivity of cesium sedimentation as well as the

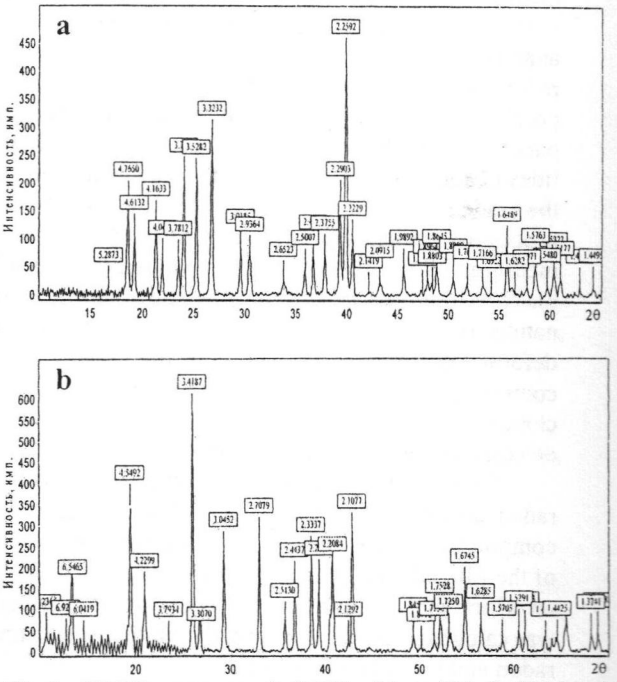

Fig.1. XRPD patterns of $CsBF_4$ (a) and $NaCs(BF_4)_2$ (b). Dron-4 diffractometer, CuKα radiation ($\lambda = 1.54018$Å).

characteristic of received sediments.

Besides cationic compound, initial solutions for experiments differed a parity of cesium and sodium concentration, and also on pH (tab.1), controlled by concentration of nitric acid or sodium carbonate in solutions. Sodium and ammonium tetraflouroborates were added to initial solutions in the form of solid substance or the sated water solutions. At addition the tetraflouroborates there was a formation heavy glassy deposits. After deposits filtration and drying white color thin crystal powders were turned out. X-ray powder diffraction (XRPD) patterns of deposits have shown presence in all of them cesium tetraflouroborate $CsBF_4$ (CBF) (fig.1a), crystallizing in orthorhombic system, space group Pnma (XRPD patterns database PCPDFWIN v.2.02, card 95828). Most crystalline single-phase deposits turned out at addition to starting solutions NH_4BF_4. Addition $NaBF_4$ led to occurrence in deposits of one more crystal phase (fig.1b) which analog in the database it was revealed not. To define chemical compound of this phase deposits have been studied by electron microprobe analysis on a scanning electron microscope (SEM) Tescan Vega II XMU combining with X-ray energy dispersive spectrometer INCAx-sight. The unknown phase has appeared double salt of sodium and cesium having chemical compound close to ideal stoichiometry: $NaCs(BF_4)_2$ (NCBF). It is characterized by higher solubility than $CsBF_4$, it is better recrystallized in water and forms joints large tabular crystals (fig.2).

To define cell parameters of $NaCs(BF_4)_2$ XRPD pattern of the single-phase sample together with the internal standard (spectral pure Si, a = 5.4305 Å) has been removed at 25°C on Bruker D8 ADVANCE X-ray diffractometer, using $CuK\alpha_1$ radiation (λ = 1.5406 Å) with step of 0.010°2Θ. CRYSFIRE 2004 (THEOR90 procedure) and CHEKCELL computer programs have been used for definition of reflection indexes and calculation of unit cell parameters. There were 37 experimental reflections in a range 13-71°2Θ which angular positions were corrected by internal standard. The decision for unit cell parameters has been found in terms of the rhombohedral system: a = 5.4575(1) Å, c = 20.1508(5) Å, V = 519.77 Å^3, Z = 3, several space groups without systematic absences are possible. It is established that $NaCs(BF_4)_2$ has higher symmetry in comparison with unicomponent salts ($NaBF_4$: orthorhombic, Cmcm; $CsBF_4$: orthorhombic, Pnma). At the same time, the size of relation V/n·Z = 86.63 Å^3 lies in an interval between its values for end-members (72.69 Å^3 and 108.73 Å^3, respectively).

Chemical compounds of solutions as initial, and after cesium sedimentation were analyzed on a mass spectrometer with inductively coupled plasma Agilent 7500ce (tab.1). From all set of cations being in starting solutions after cesium sedimentation by tetraflouroborates the maintenance of potassium, rare earth elements (TR) and thorium (the last only for sour solutions) in solutions stably decreased. On fig.4 degrees of sedimentation of these elements from solutions are presented:

$$S_i=(C_{i\ ini}- C_{i\ fin})/C_{i\ ini}\cdot 100\%,$$

where $C_{i\ ini}$ and $C_{i\ fin}$ are initial and final concentration of i-th component in a solution taking into account diluting. It is visible that in many cases sedimentation of cesium - rare earth elements - thorium fraction is close to 100 %. At the same time cesium can be taken rather selectively by ammonium tetraflouroborate from alkaline solutions. Potassium, most likely, is sedimented in a kind of tetraflouroborate, having low solubility in water; rare earth elements are sedimented presumably in the form of fluorides; the form of thorium sedimentation isn't clear. In contrast to them alkali earth elements, transition metals and uranium remain in a solution.

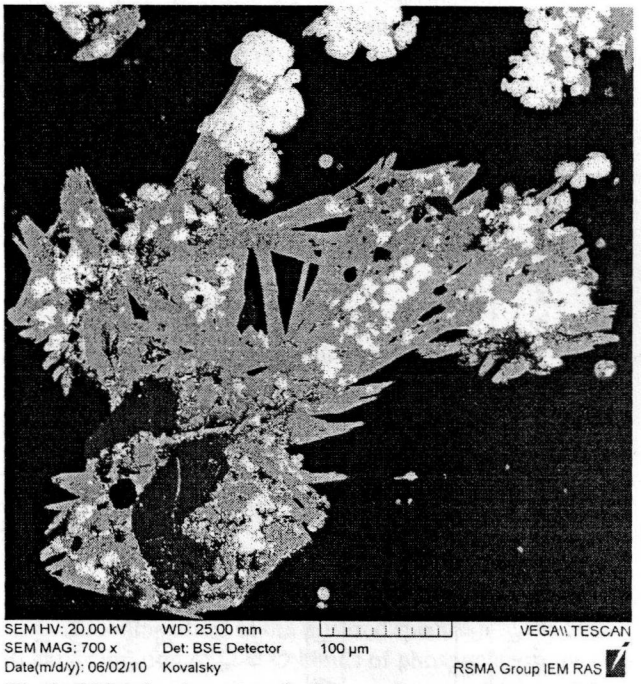

Fig.2 SEM backscattered electron detector image of the polished sample of a two-phase sediment: white - $CsBF_4$, gray - $NaCs(BF_4)_2$.

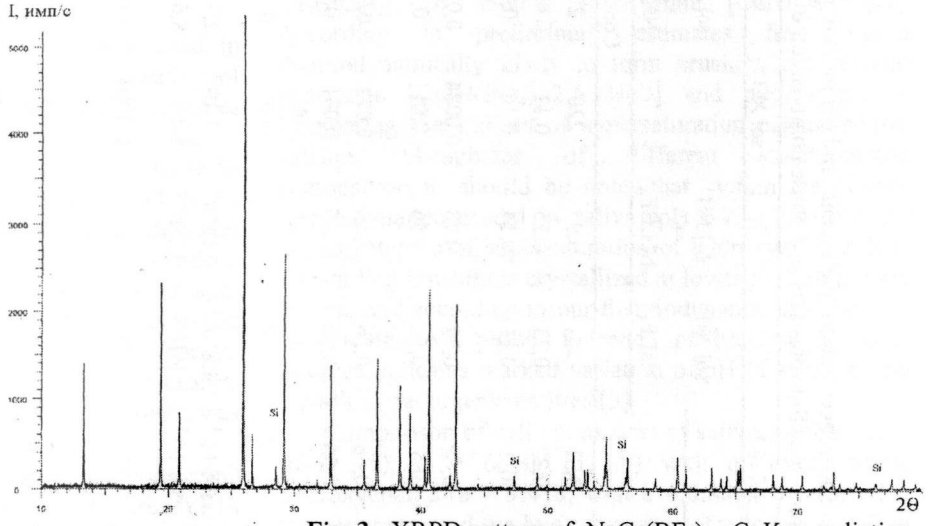

Fig. 3. XRPD pattern of $NaCs(BF_4)_2$. $CuK\alpha_1$ radiation (λ = 1.5406 Å). Si - spectral pure silicon, a = 5.4305 Å

Table 1. The concentration of elements and pH modeling solutions before and after cesium sedimentation by sodium and ammonium tetraflouroborates and phase composition of deposits: CBF - $CsBF_4$, NCBF - $NaCs(BF_4)_2$.

№ exp	sol №1	4	7	sol №3	6	8	sol №4	23	24	sol №5	26	27
Reagents		sol №1 + $NaBF_4$	sol №1 + NH_4BF_4		sol №3 + $NaBF_4$	sol №3 + NH_4BF_4		sol №4 + sol $NaBF_4$	sol №4 + sol NH_4BF_4		sol №5 + sol $NaBF_4$	sol №5 + sol NH_4BF_4
		Concentration in solution, g/l										
Na	0,31	54	0,95	220	270	170	1,7	35	0,5	99	83	47
Mg	0,22	0,23	0,25	0,11	0,0038	0,0041	0,13	0,086	0,086	0,0018	0,0079	0,0025
K	0,2	0,11	0,14	0,16	0,12	0,11	0,088	0,002	?	0,038	0,018	0,026
Cr	0,69	0,73	0,78	0,0084	0,0076	0,014	0,21	0,13	0,13	$8,5\cdot10^{-4}$	0,0016	0,0021
Fe	0,5	0,52	0,56	0,01	0,02	0,04	0,067	0,061	0,058	0,004	0,011	0,015
Ni	0,56	0,56	0,63	0,022	0,037	0,044	0,064	0,04	0,043	$4,5\cdot10^{-4}$	0,0015	$9,2\cdot10^{-4}$
Cu	0,56	0,56	0,65	0,031	0,12	0,16	0,18	0,13	0,11	0,024	0,019	0,018
Sr	0	0	0	0	0	0	4,7	2,9	2,9	0,039	0,077	$3,3\cdot10^{-4}$
Zr	0,061	0,11	0,12	0,01	0,024	0,07	0,13	0,11	0,12	0,0057	0,034	0,0086
Nb	$1,4\cdot10^{-4}$	$4,8\cdot10^{-4}$	$3,1\cdot10^{-4}$	$1,7\cdot10^{-5}$	$2,3\cdot10^{-5}$	$5\cdot10^{-5}$	$6,5\cdot10^{-4}$	0,0017	0,0019	$8,2\cdot10^{-4}$	0,0016	0,0035
Ag	$5,4\cdot10^{-4}$	$4\cdot10^{-4}$	$7,2\cdot10^{-4}$	$3,4\cdot10^{-5}$	$8,6\cdot10^{-5}$	$3,6\cdot10^{-4}$	$4,5\cdot10^{-4}$	$4,8\cdot10^{-4}$	$4,4\cdot10^{-4}$	0,0021	0,0073	0,006
Cd	1	0,98	1,2	0,0094	0,0077	0,022	0,12	0,07	0,07	$1,5\cdot10^{-4}$	$1,5\cdot10^{-4}$	0
Cs	130	16	11	98	26	17	22	0,37	1,3	29	1,6	3,8
Σ TR	0,34	0,035	0,0056	$4,5\cdot10^{-4}$	$3,3\cdot10^{-5}$	$6,3\cdot10^{-5}$	0,14	0,067	0,091	$1,4\cdot10^{-4}$	$7,2\cdot10^{-4}$	$2,2\cdot10^{-4}$
Hf	0,64	1	1,1	0,093	0,22	0,67	0,12	0,12	0,13	0,007	0,3	0,064
Pb	0,45	1	0,45	0,049	0,16	0,19	0,0037	0,11	0,11	$7,6\cdot10^{-4}$	0,0038	0,0042
Th	0,57	0,0035	$6,5\cdot10^{-4}$	0,046	0,068	0,19	0,02	$8,8\cdot10^{-4}$	0,0028	$3,8\cdot10^{-4}$	0,0076	0,0029
U	0,61	0,57	0,66	0,18	0,35	0,39	0,1	0,24	0,12	0,074	0,047	0,046
pH	1,94	2	2,81	10,8	8,78	8,5	1,29	2,33	2,24	11,99	7,51	7,9
Solid products		CBF + NCBF	CBF		CBF	CBF		CBF + NCBF	CBF		NCBF	CBF

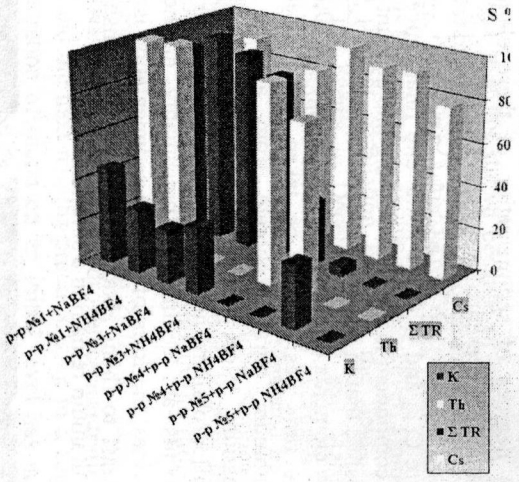

Fig.4. Degrees of K, Th, Σ TR and Cs sedimentation by $NaBF_4$ and NH_4BF_4 from solutions of various chemical compounds .

Thus, in process of sedimentation from solutions of dangerous technogenic elements by means of tetraflouroborates degrees of sedimentation Cs, Th, TR can be close to 100 %. This fact can be a basis for creation of a new technological method of allocation of the specified group of elements or selectively cesium from a high level waste at processing of spent nuclear fuel, and also their separation at processing of ores.

This work was supported by the RFBR grant № 09-03-13547_ofi-c

Biomineralogy

Belskaya L.V., Golovanova O.A. Research of mineral composition of human salivary calculi

Cchem.dep. OmSU 644077, Omsk, Pr. Mira 55a,
LudaB2005@mail.ru

Keywords: Mineral composition, XRD, IR spectroscopy, thermal analysis, pathogenic biominerals, salivary calculi, saliva

Salivary calculi - pathogenic organomineral concretions of maxillofacial areas, which are formed from the saliva more often in submandibular gland and its ducts. They are folded, usually because of rhythmically deposited layers of organic and inorganic components around a central core. Formation of salivary stones may be related to a violation of the outflow of saliva or exchange any of its elements (mostly calcium metabolism), with inflammatory processes in the salivary glands with a significant participation of microorganisms, poor nutrition, with the state of the living environment of patients, etc. [1-3]. *Objective:* to study the mineral composition of salivary calculi residents of the Omsk region.

Materials and methods Study of phase composition of salivary calculi (14 samples) was carried out by using XRD, IR spectroscopy and thermal analysis. Diffraction patterns were obtained by "the powder method" on a stationary X-ray DRON-3. During of the phase analysis used monochromatic copper (λ = 1.54178 Å), cobalt (λ = 1.79021 Å) and molybdenum radiation (λ = 0.71069 Å). Operating mode: U = 35 kV, I = 15 mA for cobalt and copper radiation; U = 38 kV, I = 10 mA for Mo radiation, the rotation speed detector 1 °/min, the velocity of the chart of 720 mm/h, operating scale grapher $1 \cdot 10^3$ pulses/sec, alignment gap: 1mm, 0.25 mm. Angles 2Θ Bragg reflections and their relative intensity were determined from the diffraction patterns. Qualitative analysis of phase composition of the sample was conducted by comparing the experimental values of interplanar distances and relative intensities of the diffraction peaks corresponding to a set of tabular values for each of the proposed phases. Sensitivity of the XRD data of the measurements was 3%.

The method of infrared spectroscopy was used in order to obtain more information on the composition of salivary calculi (spectrophotometer "FT-801"). Samples were prepared by pressing pellets with KBr: 0.5 mg of salivary calculus, pounded into powder, mixed with the 50 mg of KBr, and then the mixture was transferred into a mold and pressed into disk-shaped tablet with a diameter of 3 mm at room temperature. Record the spectrum of the samples was carried out in 4000 to 500 cm^{-1} with the total number of scans is 32. The program «ZaIR 3.5» was used for receiving, processing and retrieval of infrared spectra in the databases, which contain more than 130000 spectra. Sensitivity of infrared spectroscopy for measurements was 5%.

Thermal studies were carried out on derivatograph firm Perkin Elmer SII Diamond-TG-DTA software PYRIS 7.0; investigated temperature range was 25-1000°C; heating rate - 5-20 °C/min, were used samples weighing 25-30 mg, the sensitivity of weight measurement was 0.2 mg (the error in deter mining the weight loss ~ 0.1 %), sensitivity of the measurement thermal effects (peak position at DTA) 0.06 mV. Obtained by thermo gravimetric (TG), differential thermal (DTG) curves were determined massive changes upon heating, the differential-gravimetric curve (DTA) was used for the characteristics of the observed thermal effects. The results are presented in digital form and processed statistically using the software Statistic Soft 2006.

A detailed study of the structural features was performed semi-quantitative analysis of the spectra using the software package PeakFit_v 4.11 [4]. The degree of crystallinity of the sample was estimated by the parameter of the infrared splitting of the antisymmetric bending vibration ν_4 of O-P-O (spectral range 500 - 650 cm^{-1}), defined as the ratio of the intensities of the two peaks to the intensity of "depression" among them: IRSF = (I (564 cm^{-1}) + I (604 cm^{-1})) / I (584 cm^{-1}). By reducing the crystallinity bands with maxima 564 and 604 cm^{-1} broadened, and resolution between them becomes smaller. This reduces the value of the splitting of the infrared (K) (Fig. 1).

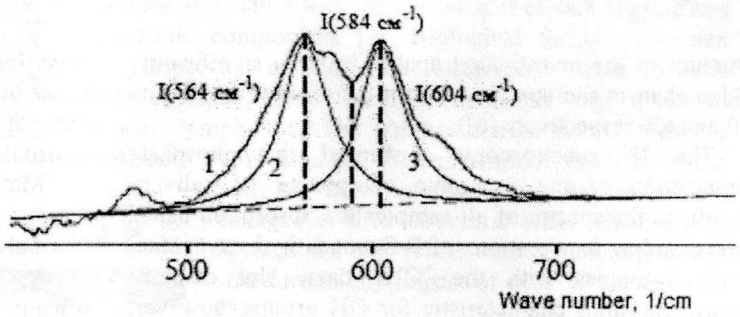

Fig. 1. Decomposition of the infrared spectrum in the 500-650 cm^{-1} vibration of O-P-O bonds of phosphate groups at two elementary absorption bands

Results and discussion Established that the mineral component of salivary calculi inhabitants of Omsk presented hydroxyapatite [$Ca_{10}(PO_4)_6(OH)_2$], in one sample with hydroxyapatite present whitlokite [β-$Ca_3(PO_4)_2$], in another - brushite [$CaHPO_4 \cdot 2H_2O$]. According to preliminary estimates from saliva thermodynamically likely to form brushite, octacalcium phosphate [$Ca_4H(PO_4)_3 \cdot 2.5\ H_2O$] and hydroxyapatite. Comparing the indices of supersaturation calculated for calcium phosphates of different stoichiometric composition, it should be noted that within the c hosen thermodynamic model in saliva (pH 5.2 – 8.0) has the greatest degree of supersaturation of hydroxyapatite. It is known that brushite is crystallized at lower pH values than apatite, and according to our thermodynamic calculations, is a metastable phase. Presence of brushite in some samples indicates marked variation of pH of saliva in the growth of pathogenic entities [5].

Comparison of cell parameters of salivary calculi (a = 9.449 (5), c = 6.883 (3) Å) with a stoichiometric hydroxyapatite (a = 9.418, with a = 6.884 Å) shows that the parameter and the hydroxyapatite of salivary calculi at 0.33% more than at stoichiometric, and the value of virtually the same. These lattice parameters are characteristic of non stoichiometric calcium-deficient

hydroxyapatite, including carbonate. Parameter and investigated hydroxyapatite close to the upper limit of this parameter variation in apatite of tooth enamel. Earlier [6] a formula for hydroxyapatite of salivary calculi:
$[Ca_{8.09-8.19}Mg_{0.13}Na_{0.21}K_{0.02}\square_{1.55-1.45}](PO_4)_{4.22-4.39}(HPO_4)_{0.97-0.87}(CO_3)_{0.75-0.76}(SO_4)_{0.06-0.00}[OH_{0.12-0.21}F_{0.10}Cl_{0.02}(CO_3)_{0.11}(\square,H_2O)_{(1.66-1.56)}]$. According to this formula, the vacancy in the positions of calcium in the

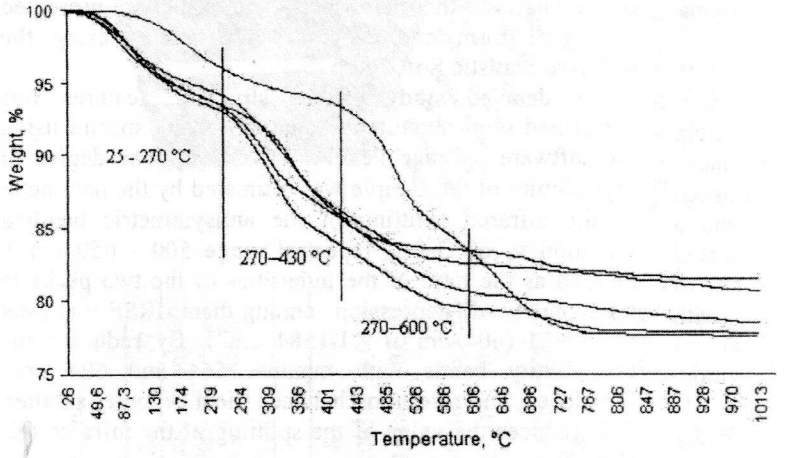

Fig. 2. Weight losses of samples of salivary calculi

structure of the investigated apatite is 15%, significantly higher than in the apatite structure of enamel and dentin (10 and 6% respectively [6]).

The IR spectroscopy confirmed the phosphate composition of the inorganic component of salivary calculi. In the spectra of all samples the absorption bands corresponding to vibrations of P-O bonds hydroxyapatite, which coincides with the XRD data. Not detected absorption bands characteristic for OH groups, however, all examined samples contain carbonate ions. The presence of bands of vibration C-O bond (1420, 1460 cm^{-1}) indicates substitution of RO_4^{3-}-tetrahedral carbonate ions (the so-called substitution of B-type). The band 1550 cm^{-1} indicates the substitution of OH - groups of carbonate ions in the channels of the structure of hydroxyapatite, which

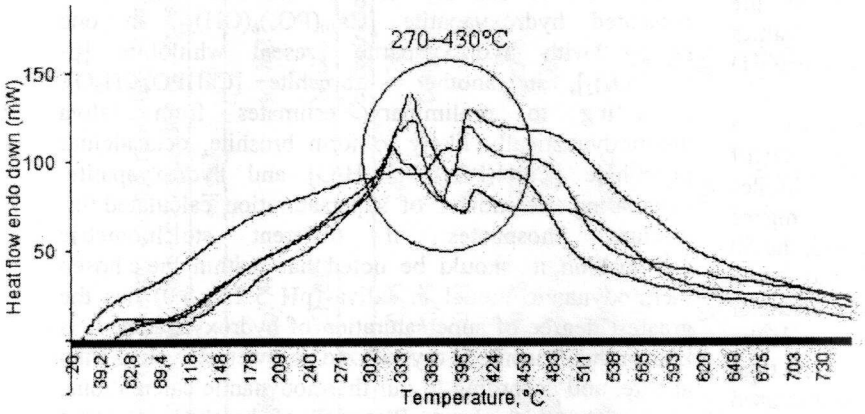

corresponds to the replacement of A-type. Ratio of carbonate ions, corresponding to the two types of replacements for all the samples is 2:1. In addition, on most of the IR spectra present a broad band of stretching vibrations of water molecules at 3440 cm^{-1}, indicating the presence of water molecules in structural channels of hydroxyapatite and a band of deformation vibrations of water at 1650 cm^{-1}.

The calculated values of crystallinity of the samples (IRSF = 4.85) show that salivary calculi is typical of apatite formation of less ordered structures characterized by less than the value of splitting the infrared peak of the antisymmetric bending vibration of the O-P-O than in the control sample (stoichiometric hydroxyapatite, IRSF = 5.35).

The results of the thermal studies on all derivatogram observed mass loss in the four main temperature ranges (Fig. 2): 25-270 °C (corresponds to the loss of adsorbed water); 270-430 °C (evaporation of structural water a nd the re moval of lo w molecular weight organic substances - amino acids, proteins of low molecular weight, glucose, etc.); 430-600 ° (conversion of macromolecular organic compounds, including glycoprotein's such as mucin) and 700-900 °C (corresponds to the transition stoichiometric carbonate hydroxyapatite, forming a crystalline substance of salivary calculi in stoichiometric due to the removal of volatile components, mainly carbon dioxide).

It was established that the maximum mass loss observed in the decomposition of the organic phase of calculi in the temperature range 270-600 °C, with most of the energy effect is observed for the loss of low molecular weight organic matter (Fig. 3).

Mathematical treatment of the consideration of the thermal characteristics showed that the mass loss during thermal decomposition of salivary stones is 42.15 ± 4.97 wt.% (Table 1) mainly due to the decomposition of organic components, namely, low molecular weight substances, the loss of volatile components and adsorption of water.

When heated in the temperature range of 50-580 °C the samples of salivary calculi are two-stage dehydration (Fig. 4). About 600-700 °C due to chemical interaction of components, are a partial decarbonization and the crystallization of products.

Fig. 3. Energy effect of the thermal decomposition of samples of salivary calculi

According to [7], the selection of gaseous water, carbon and nitrogen oxides occurs synchronously with the burning of organic matrix (230-600 °C); with the mass spectra of CO_2 and NO, in general, repeated profiles of the different curve of mass loss (two-stage combustion of organic matter) in while the peak water output corresponding to the decomposition of organic matter in the second phase is not observed (at temperatures above 350 °C separation of gaseous H_2O decreases monotonically with no defined maximum), this indirectly confirms the presence of less ordered, low molecular weight fractions of organic matter, weak hydrogen bonds which are broken at lower temperatures, and hydrogen to

form water is allocated. Authors [8] attempted to link the thermal desorption of water in synthetic hydroxyapatite with its crystal-state: the first thermo desorption peak at 100-300 °C was correlated with the strongly chemisorbed water on the porous surface of hydroxyapatite, and the second in the 350 °C - with a crystalline hydrate with water, a division of hydroxyapatite the reaction: $Ca_{10}(PO_4)_6(OH)_2 \cdot nH_2O \rightarrow Ca_{10}(PO_4)_6(OH)_2 + nH_2O$. Weak maximum at about 700 ° C, apparently due to the release of CO_2 from the structure of non-stoichiometric low-crystalline carbonate hydroxyapatite by the reaction: $Ca_{10}(PO_4,CO_3)_6(OH)_2 \rightarrow Ca_{10}(PO_4)_6(OH)_2 + 6CO_2\uparrow$.

Thus, it is shown that the mineral component of salivary stones represented carbonate containing hydroxyapatite, which was confirmed by X-ray diffraction and thermal analysis and infrared spectroscopy.

Table 1. Thermal characteristics of samples of human salivary calculi

№ sample	Total mass loss	The temperature range		
		25 – 270°C	270 – 600°C	600 – 900°C
3	40.74	6.8	32.51	1.43
8	42.96	7.4	33.59	1.97
9	36.27	6.5	28.71	1.06
10	44.21	6.4	35.43	2.38
14	40.49	7.5	30.65	2.34
average	42.15±4.97	6.9	32.18	1.84

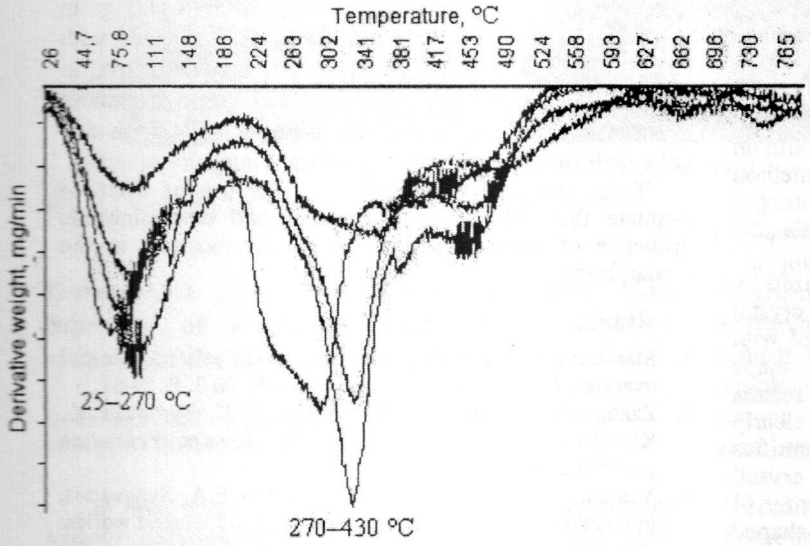

Fig. 4. Differential curves of mass loss of samples of salivary calculi

References

1. Denisov A.B. Salivary glands. Saliva. Moscow, 2003. 132 pp.
2. Coragh A.A. Introduction to biomineralogy. St. Petersburg: Nedra. 1992. 280 pp.
3. Thumb N.A., Moroz T.N., Leonova I.V. and other. Mineral and trace element composition of salivary stones // Journal of Inorganic Chemistry, 2004. № 8. P.1353-1361.
4. Shi J., Klocke A., Zhang M., Bismayer U. Thermally-induced structural modification of dental enamel apatite: Decomposition and transformation of carbonate groups // Eur. J. Mineral. 2005. V.17. P. 769-775.
5. Belskaya L.V., Golovanova O.A. Numerical simulation of dental and salivary calculi in human mouth // Izv. Vyssh. Uchebn. Zaved., Khim. Khim. Tekhnol., 2008. T.51. № 10. P.105-108.
6. Yelnikov V., Frank-Kamenetskyay O.V., Golovanova O.A., Zorina M.L. Structure, mineral and chemical composition of human salivary calculi. Educational issues // Mineralogy technogenesis, 2005. P.156-164.
7. Votyakov S.L., Sadykov N.O., Smirnov N.G. Thermal properties of fossil bone remains of small mammals as a basis to assess their relative age // Yearbook-2008, Tr. IGG UB RAS, 2009. Vol. 156. P.290-295.
8. Nedoseko V.B., Gorbunova I.L., Drozdov V.A. Mass spectral analysis of the water intact dental enamel in persons with different levels of resistance to caries // Dentistry, 2004. № 4. P.13-16.

Belskaya L.V.[1], Golovanova O.A.[1], Shukailo E.S.[1], Turmanidze V.G.[2] Experimental study of crystallization of biological liquids

[1] *Chem. Dep. OmSU,* [2] *OmSU* 644077, Omsk, Pr. Mira 55a, e-mail: LudaB2005@mail.ru

Keywords: Saliva, crystallization, crystallographic method of research, diagnosis, physical activity

Crystallization of biological fluids - genetically based process associated with the presence of certain organic and inorganic components [1]. Biological fluids - complex polydisperse non-cellular structures with fragile relationships within them components: saliva, blood serum, lymph, etc. The composition of body fluids are lyotropic liquid crystals, the most minor changes in the body's vital functions are manifested in changes in their structural order. Elements in biological fluids reacts immediately change its structure to any impact of external and internal [2].

The most simple, yet informative way to assess the physical and chemical properties of biomaterials and biological fluids are in particular crystallographic methods based on qualitative and quantitative description and interpretation crystallization of biosubstrates. They allow you to consider the integrative information content of nutrient liquid. It is important t hat the cr ystallization - a process that brings together objects like a living, and the mineral world [3], in connection with which it may be a universal method for storing and transmitting information. Currently, the crystallographic method of research used to establish the correct diagnosis for different kinds of diseases as a complement to other diagnostic methods. Its essence is to analyze the shapes of crystallization, resulting in drying of various biological fluids [4].

Oral liquid forms a crystalline structure, as in the native state, a nd by adding crystal-compounds. The morphology of these structures is due to the chemical composition of saliva [5]. When you view the resulting crystal structures under low magnification of microscope, it was found [6] that the crystal pattern is uneven and varies in different areas (zones) of dried droplets (Fig. 1).

The preparation can distinguish three zones: central zone of crystalline structures, intermediate (zone protein-salt structures) and peripheral (zone of protein structures) [7]. Most "favorable" growth in the center of the drop: it

formed typical dendrite crystals in the form of a fern, which grows not only on the plane, but also in volume. The site with the structures of ferns can be considered as a zone free of growth. Therefore, assessment of crystalline morphology can only be in the center of crystallization [8].

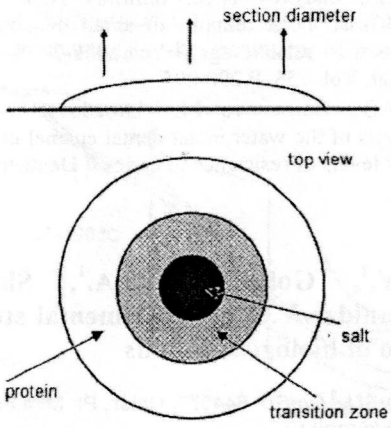

Fig. 1. A drop of body fluid on the plane [7]

Data type of microcrystallization of saliva (MCS) can be used as a method of assessing the overall condition of the human body. *Objective:* To study the structural features MCS athletes playing sports, to determine the state of sportsmen before and after exercise.

Materials and methods The experiment involved three groups of sports: volleyball (13), basketball (10), and badminton (18), one age category from 18 to 22 years. Samples of oral fluid were collected three times: before the load after load in the early morning after sleep (off load). Before the fence, the sample surveyed athlete rinsing your mouth with boiled (or distilled) water. Collection of saliva is produced in chemically clean test tubes in an amount of 3-4 ml. Experiment with volleyball players and badminton players was repeated twice with an interval of 1 week. In the process we used the method open the drop [5], subsequent analysis of obtained images was performed in accordance with the existing scale and criteria for evaluating the type of MCS (Fig. 2).

The results of MCS in the "norm" is characterized by a clear pattern of large elongated prismatic crystal structures coming from the center of the drop, fused with each other and having a tree or pteridophytes shape (picture corresponds to 5 points). In assessing the results of MCS when exposed to various adverse factors clearly states the destruction of crystal structure (Fig. 2). Identifies the following types: drawing large prismatic crystal elongated structures, fused together in a random order (4 points) in the center of the drop shows some star-shaped crystals form on the periphery of the enlarged dendrite crystals stored (3 points), the individual crystals in the form of rods or twigs arranged across the field (2 points) over the entire area of the drop a large number of crystal structures is isometrically arranged, stellate, round or irregular shape (1 point); complete absence of crystals in the field of view (0 points).

Mathematical data processing was done using the statistical package STATISTICA 6.0 (StatSoft Inc. USA). Data were analyzed using discriminate and cluster analysis using the statistical package STATGRAPHICS Plus 5.0.

Results and discussion An analysis of 72 oral fluid samples showed that none of crystals does not correspond to the maximum number of points. Only 4 samples were evaluated at 4 points (5.6%), 29 samples - 3 points (40.3%), 25 samples - 2 points (34.7%), 8 samples - 1 point (11.1%) and 6 samples - on the 0 points (8.3%). Thus, it can be noted that for the studied samples of oral fluid athletes from different sports are most common types of MCS corresponding to 2-3 points, which characterizes the violation of the structural properties of saliva.

In the study of MCS athletes chosen sport revealed a similar pattern. It was found that after training the crystallization of oral fluid as a whole is deteriorating (Table 1).

Table 1. Changing the type of MSC athletes playing sports in the workout.

Sport	Wed point before the load	Wed point after load	Wed point off load
Basketball	3 (61%)	2 (54%)	3 (49%)
Volleyball	3 (50%)	2 (44%)	3 (71%)
Badminton	3 (50%)	2 (60%)	3 (63%)

After loading in most cases, the decay of the crystals of saliva, whereas the recovery occurs after the daily improvement in her MCS. The disintegration of crystals characterized by high levels of stress and tension in the body, thus there is a violation of electrolyte composition of saliva and, above all, changing the Ca/P ratio, which is responsible for the type of the MCS. Improved crystallization shows recovery of the body after exercise (Fig. 3).

In assessing the shapes of crystallization using the methods of mathematical statistics are also observed significant differences in performance in different periods of training, which was confirmed by discriminate analysis.

It should be noted that when comparing the ISS athletes selected by sports, the best results prior to training were observed in badminton, and after training in volleyball, which in our opinion, may be associated with differences in the training process. But, as noted above, in general, the changes have the same character. Differences between the indices of the two training badminton and volleyball can be explained by different intensity of stress.

Thus, studies have shown that the use of MCS to evaluate the state of the organism and determine the influence of various factors on the homeostasis in the human body.

References

1. Martusevich A.K. Crystallographic analysis: a general overview // Vyatka Medical Journal, 2002. № 3. P. 59-61.
2. Zakharova G.P., Shabalin V.V., Yanov Yu.K., Tyrnova E.V., Klyachko L.L., Shabalina O.N. The Russian Federation patent №2293324
3. Yushkin N.P., Gavrilyuk M.V., Golubev E.A. Syngenesis, interaction and co evolution of the living and mineral worlds: abiogenic hydrocarbon and crystals as a model protobiological system. The concept of the crystallization of life // Newsletter RFBR. 1996. T. 4. P. 393.
4. Selifanova E.I. Dental status and features of the crystallization of saliva in patients with diabetes: Dis., Moscow, 2005. 132 pp.
5. Belskaya L.V. Dental and salivary stones - the chemical composition, and genetic features: Dis., Omsk, 2009. 158 pp.
6. Denisov A.B. Salivary glands. Saliva. Moscow, 2003. 132 pp.
7. Tarasevich Yu.Yu., Ayupova A.K. Effect of diffusion on the separation of components of biological fluid with wedge dehydration // Journal of Technical Physics, 2003. V.73. № 5. P.13-18.
8. Barer G.M., Denisov A.B., Sturova T.M. Variability of oral liquid crystalline aggregates in the norm // Russian Journal of Dentistry, 2003. № 1. P. 33-35

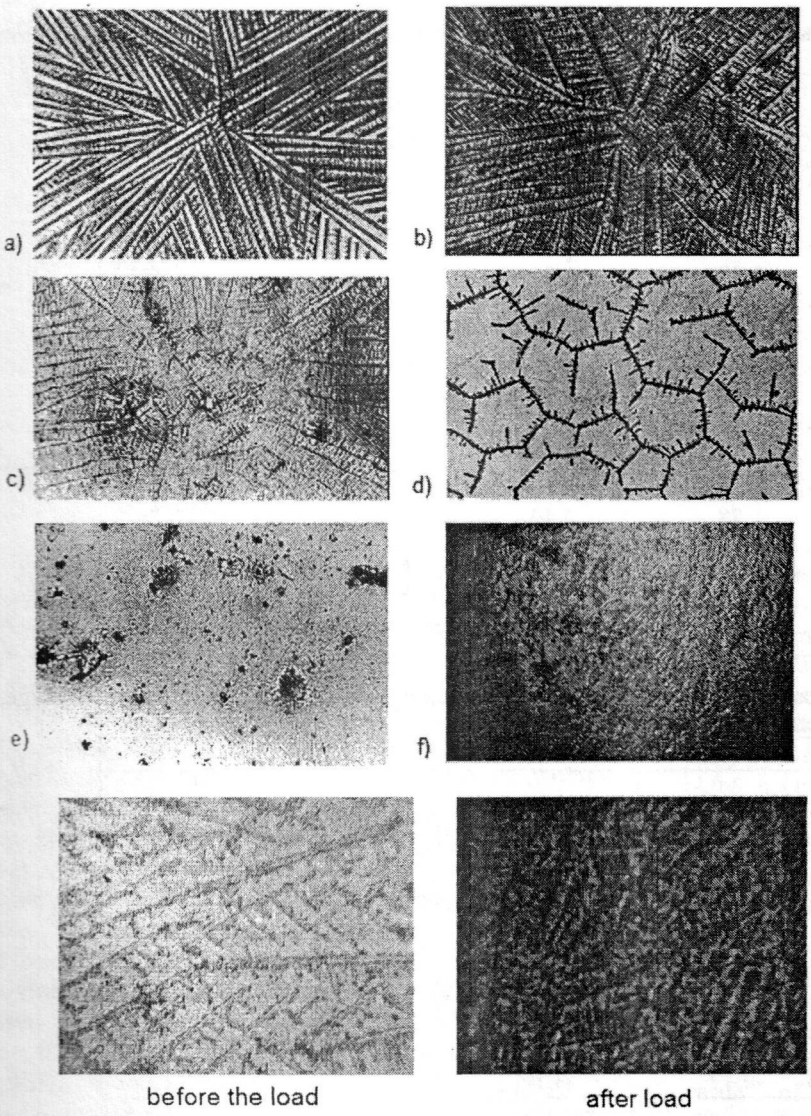

Fig. 2. Types of MCS (a – 5, b - 4, c - 3, d - 2, e - 1, f - 0 points, respectively)

Fig. 3. Change the MCS badminton during exercise

Golovanova O.A., Gerk S.A., Izmailov R.R. Studying of crystallization with participation synovial of the liquid of the person

Chem.dep. OmSU golovanoa2000@mail.ru
phaxc:(3812)642410 ph.:(3812) 26 81 99

In live organisms of biological liquids are formed various органоминеральные units (a bone and tooth fabric, nephritic, salivary and scales in a human body etc.). It is known that the major property of any liquid is its viscosity. Viscosity renders a great influence for speed of movement of a liquid, resistance which it renders to particles at their moving, thereby defines a direction and intensity of many biochemical reactions, including processes of formation of mineral phases in vivo. Change is viscous – elastic properties influences a number of physical and chemical parametres of biological system, affects speed of the chemical reactions proceeding in bioliquids. Such bioliquid is synovial a liquid (SL, synovial) the person, it is one of the basic components of a joint and substantially defines its morfo-functional condition, carries out the important role in realisation of functions of a joint and maintenance of its communication with other fabrics. The key characteristic of the given bioliquid is its viscosity which provides normal mobility of a joint, reduces a friction and provides functional congruence. Viscosity синовии considerably fluctuates depending on pH, concentration of salts, temperatures. In comparison with other bioliquids viscosity synovial liquids is high enough [Veresov A.G., etc., 2004,], in communication, with what the purpose given work is the establishment of influence of viscosity of modelling solution synovial on processes of a bone mineralization. According to earlier spent thermodynamic calculation [Lemeshev, 2010], it is shown that within the limits of the chosen thermodynamic model in an investigated range pH in solutions probably formation of following substances (tab. 1): $Ca_{10}(PO_4)_6(IT)_2$, β-$Ca_3(PO_4)_2$, $MgHPO_4 \cdot 3H_2O$, $Ca_4H(PO_4)_3 \cdot 2.5H_2O$, $CaHPO_4 \cdot 2H_2O$, $CaCO_3$-kaltsit, $CaCO_3$-aragonite, α-$Ca_3(PO_4)_2$. Thus for each system of value pH the sedimentation beginnings slightly soluble connections are various.

By comparison of values of their indexes supersaturate and energy Gibbsa of crystallisation for three values pH=7,4; pH=7,6; pH=7,8 it is revealed that the greatest thermodynamic probability of formation in modelling conditions is characteristic for hydroxyapatite. So, sizes of thermodynamic parametres (SI and ΔG) given slightly soluble phases differ from others in 1,6 and more times (fig. 1) that is in a greater degree shown at big value pH=7,8.

Table 1. Ranges of values pH, indexes пересыщения, energy of Gibbsa of crystallisation (kDg/mol) formations of firm phases in modelling solutions

№	Connection	Minimum concentration			Average concentration			Average concentration		
		pH	IS	-ΔG	pH	IS	-ΔG	pH	IS	-ΔG
1	$Ca_{10}(PO_4)_6(OH)_2$	7,00-8,00	0,80-1,36	4,17-7,11	7,00-8,00	0,89-1,45	4,66-7,60	7,00-8,00	0,95-1,51	4,93-7,90
2	β-$Ca_3(PO_4)_2$	7,00-8,00	0,21-0,75	1,07-3,90	7,00-8,00	0,32-0,86	1,65-4,48	7,00-8,00	0,39-0,93	2,01-4,84
3	$Ca_4H(PO_4)_3 \cdot 2.5H_2O$	7,10-8,00	0,01-0,34	0,02-1,8	7,00-8,00	0,06-0,45	0,33-2,33	7,00-8,00	0,13-0,51	0,65-2,65
4	$MgHPO_4 \cdot 3H_2O$	7,00-8,00	0,07-0,24	0,36-1,28	7,00-8,00	0,18-0,36	0,95-1,88	7,00-8,00	0,25-0,42	1,3-2,22
5	$CaHPO_4 \cdot 2H_2O$	7,15-8,00	0,01-0,14	0,01-7,10	7,00-8,00	0,10-0,28	0,52-1,44	7,00-8,00	0,19-0,36	0,97-1,90
6	$CaCO_3$ (kaltsit)	7,33-8,00	0,01-0,36	0,02-1,88	7,26-8,00	0,01-0,40	0,006-2,07	7,21-8,00	0,01-0,43	0,02-2,23
7	$CaCO_3$ (aragonite)	7,45-8,00	7,45-0,30	0,02-1,53	7,38-8,00	0,01-0,33	0,01-1,73	7,33-8,00	0,01-0,36	0,02-1,89
8	α-$Ca_3(PO_4)_2$	-	-	-	7,89-8,00	0,01-0,06	0,01-0,30	7,75-8,00	0,01-0,13	0,02-6,60

Table 2 of Value of indexes supersaturate almost insoluble connections of modelling solutions at the minimum, average, maximum values of an interval pH and concentration of inorganic ions

№	pH	7,4			7,6			7,8		
	Concentration*	1	2	3	1	2	3	1	2	3
1	$Ca_{10}(PO_4)_6(OH)_2$	1,04	1,14	1,2	1,15	1,25	1,31	1,26	1,35	1,41
2	β-$Ca_3(PO_4)_2$	0,45	0,56	0,63	0,55	0,66	0,73	0,65	0,76	0,83
3	$Ca_4H(PO_4)_3 \cdot 2,5\ H_2O$	0,14	0,24	0,3	0,21	0,31	0,38	0,28	0,38	0,44
4	$MgHPO_4 \cdot 3H_2O$	0,17	0,28	0,35	0,2	0,32	0,38	0,23	0,34	0,41
5	$CaHPO_4 \cdot 2H_2O$	0,06	0,2	0,29	0,09	0,23	0,32	0,12	0,26	0,35
6	$CaCO_3$ (kaltsit)	0,05	0,08	0,11	0,15	0,19	0,22	0,26	0,29	0,32
7	$CaCO_3$ (aragonite)	-0,02	0,02	0,05	0,09	0,12	0,16	0,19	0,23	0,26
8	α-$Ca_3(PO_4)_2$	-0,35	-0,24	-0,17	-0,25	-0,14	-0,07	-0,15	-0,04	0,03

*Note** 1 – minimum; 2 averages; 3 - the maximum values of concentration.

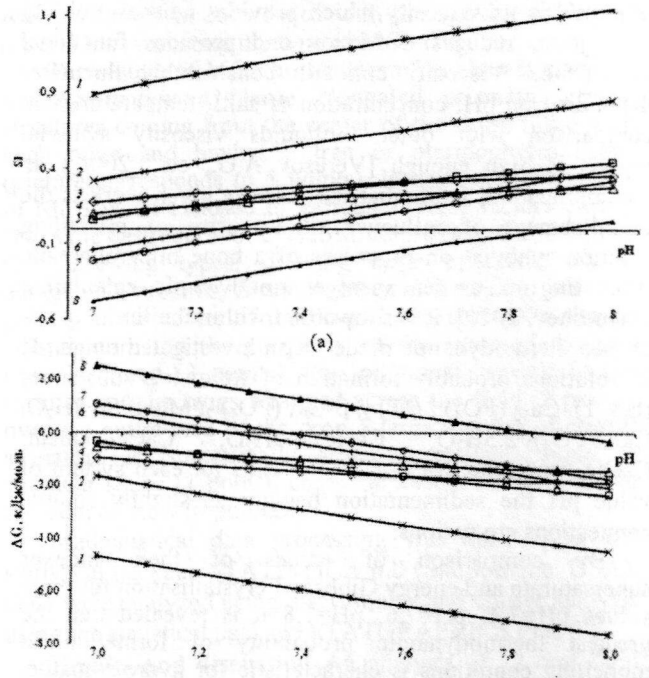

Fig. 1 Dependence of an index supersaturate (a) and energy of Gibbsa of crystallisation (b) from pH a solution for average values of a range of concentration synovial liquids for slightly soluble connections: : $Ca_{10}(PO_4)_6(OH)_2$ (1); β-$Ca_3(PO_4)_2$ (2); $MgHPO_4 \cdot 3H_2O$ (3); $CaHPO_4 \cdot 2H_2O$ (4); $Ca_4H(PO_4)_3 \cdot 2.5\ H_2O$ (5); $CaCO_3$ – kaltsit (6); $CaCO_3$ aragonite (7); α-$Ca_3(PO_4)_2$ (8)

Besides, in modelling conditions a steady phase is β-$Ca_3(PO_4)_2$. It is known, what exactly this phosphate acts initial amorphous компонентой of which as a result of recrystallization crystals гидроксилапатита bones are formed. For G (exception are marked, pHΔ7,8 negative values SI and positive >α-$Ca_3(PO_4)_2$ at pH =7,75 at the maximum concentration of ions in a modelling solution), therefore within the limits of the given model its formation

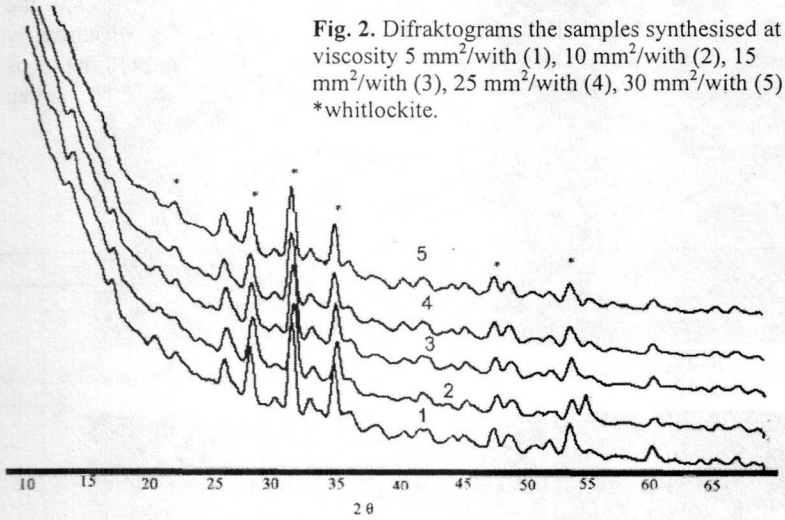

Fig. 2. Difraktograms the samples synthesised at viscosity 5 mm^2/with (1), 10 mm^2/with (2), 15 mm^2/with (3), 25 mm^2/with (4), 30 mm^2/with (5) *whitlockite.

is improbable. Other connections possess intermediate stability (tab. 2), and, hence, their participation in formation of a bone fabric depends on concentration sedimentormation ions, ionic force, acidity of the modelled environment.

So, at pH=7,40±0,05 a modelling solution the thermodynamic probability of formation decreases among $MgHPO_4 \cdot 3H_2O$ > $Ca_4H(PO_4)_3 \cdot 2{,}5\ H_2O$ > $CaHPO_4 \cdot 2H_2O$ > $CaCO_3$-kaltsit> $CaCO_3$- arag onite and is similar for all considered range of concentration. It specifies, that at the given value pH environments can be neglected influence of ionic force. With increase pH solutions the greatest thermodynamic stability is got by phases, in anions which are absent or there are at smaller quantities hydrogen ions. So, at the minimum concentration of ions pH=7,60±0,05 a phase previous sedimentation newberyite is octacalcium phosphate, and brushite – kaltsit: $Ca_4H(PO_4)_3 \cdot 2.5\ H_2O$ > $MgHPO_4 \cdot 3H_2O$ > $CaCO_3$ (кальцит) > $CaHPO_4 \cdot 2H_2O$ > $CaCO_3$ (aragonite).

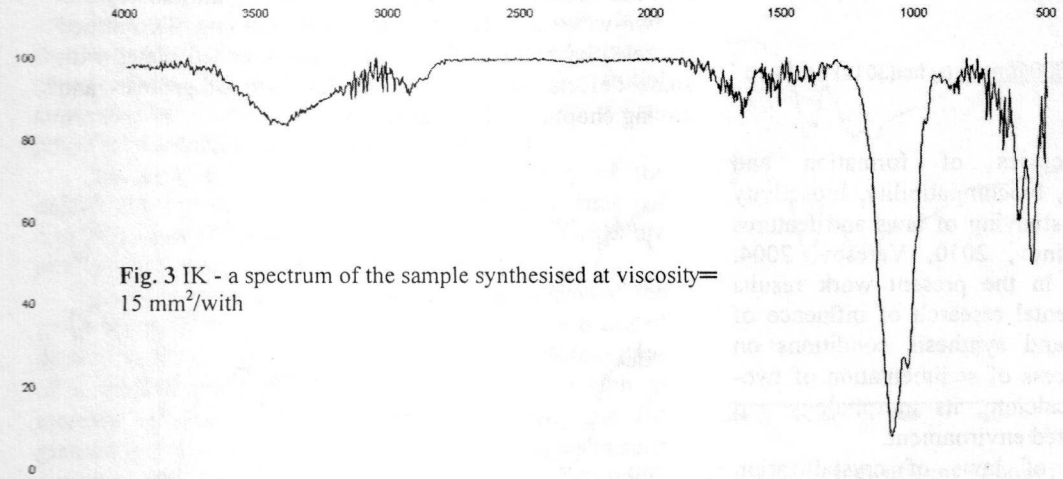

Fig. 3 IK - a spectrum of the sample synthesised at viscosity= 15 mm^2/with

At pH=7,80±0,05 the given law is traced more accurately. With increase in concentration of ions in both cases, forces of interionic pushing away that leads to reduction of factors activitts and to increase of probability of formation of the most soluble and thermodynamic an unstable phase increase. So, after sedimentation $Ca_4H(PO_4)_3 \cdot 2.5\ H_2O$ consecutive formation of the connections which solubility decreases among is marked: $MgHPO_4 \cdot 3H_2O$ > $Ca_4H(PO_4)_3 \cdot 2{,}5\ H_2O$ > $CaHPO_4 \cdot 2H_2O$ > $CaCO_3$ (kaltsit)> $CaCO_3$ (aragonite). Thus, the received results specify that optimum conditions of reception hydroxyapatite in modelling solutions synovial liquids is pH=7,8 (average, maximum concentration) where the basic dashy acts as a phase β-Ca3 (PO4) 2 and sedimentation of other almost insoluble connections thermodynamic is improbable. Sedimentormation synthesis reaction it is possible to present the basic as follows:

$10\ M_1X_2 + 6\ M_2HPO_4 + MOH \rightarrow Ca_{10}(PO_4)_6(OH)_2\downarrow + 20\ MX + 6\ H_2O$, where $M = Na^+, K^+$; $M_1 = Ca^{2+}, Mg^{2+}$; $X = Cl^-$.

For statement of modelling experiment in vitro, was the solution with the close mineral maintenance of the basic components to articulate synovial a liquid of the healthy adult average person (tab. 3) is taken. The structure of a modelling water solution was set on the basis of the minimum, average and maximum concentration of ions, the account of its ionic force, pH (7,0-8,0), temperature and viscosity which lies in an interval 26,3±3,13 mm2/with was spent. Thus in experiment viscosity equal 5,10,15,25,30 was created mm^2/with. Modelling synovial liquids created viscosity by means of a gelatin solution in water.

After necessary viscosity in a flask has been created added calcium and magnesium ions, lead up pH a solution to 7.4, tightly closed and left for 1 month for crystallisation of a firm phase from a solution. On the expiration it is specified term, a deposit strain and analyzed with the help X-ray photography the analysis (fig. 2). On the basis of data РФА in all range of the created viscosity the basic mineral phase is magnesium containing β-$Ca_3(PO_4)_2$ (whitlockite), and as it is known this mineral is initial amorphous multiplier from which as a result of recrystallization is formed crystals hydroxyapatite. On Ik-spectra of investigated tests (fig. 3) there are the strips of absorption corresponding to valency fluctuations of molecular water νH_2O - 3440 – 3400 sm^{-1} and to deformation fluctuations N-O-N in H_2O - 1680-1610 sm^{-1}; to asymmetric valency fluctuations $\upsilon 3$ P–O in PO_4^{3-} - 1090-1030 sm^{-1} and to deformation fluctuations υ_4 O-P-O the given group - 604 sm^{-1} and 546 sm^{-1}. Background signals in the field of frequencies can specify of 1560-1410 sm^{-1}, and also 900-600 sm^{-1} in impurity presence carbonate substitute hydroxyapatite. In our opinion, a limiting stage of sedimentation whitlockite is mass transfer particles in the viscous environment. Therefore in the absence of bone diseases of the further crystallisation hydroxyapatite with participation synovial liquids it is not observed and синовия together with the blood brought by blood capillaries from outside of a bone provide a food and

functioning of an articulate cartilage, and, hence, mobility of the joint. Obviously, on character of a current of processes mineralformation besides viscosity of environment synovial liquids, influence value pH and change of the maintenance of some organic substances. This fact confirms earlier spent thermodynamic and experimental modelling without viscosity in which the basic formed mineral is hydroxyapatite, with impurity whitlockite, brushite, octacalcium phosphate. On the basis of the spent thermodynamic calculation the given connection is thermodynamic the steadiest.

Table 3. Mineral structure synovial liquids of the person [Matveeva, etc., 1999], mmol/l

Connection	Minimum concentration	Average concentration	Average concentration
Calcium	2,25	2,80	2,53
Sodium	130,00	150,00	140,00
Magnesium	0,70	1,50	1,10
Kaly	3,80	5,40	4,60
Chlorides	95,00	111,00	103,00
Carbonates	24,00	30,00	27,00
Phosphates	2,42	6,34	4,38
Sulfates	9,90	12,90	11,40

Thus, it is possible to notice that in synovial liquids can be formed two basic minerals one of which is thermodynamic a steady product – hydroxyapatite, and another kinetic teady - magnesium containing β-Ca_3 (PO_4) $_2$ (whitlockite). Probably, it is formed at early stages diseases of oporno-impellent system of the person, then in hydroxyapatite which formation leads to infringement of many characteristics in a joint, first of all pH [Larionov V. P, 2003] eventually passes, and it in the the turn influences viscosity synovial liquids, it decreases. It promotes abrasion hyaline a cartilage and to contact of a bone fabric of the person with synovial a liquid that leads to disease progressing.

Work is executed with partial financial support of the Russian fund of basic researches (the grant №10-05-00881-a)

Solonenko A.P., Golovanova O.A. Definition of parameters of crystallization at formation brushite

Chem.dep. OmSU golovanoa2000@mail.ru fax(3812) 64 24 10 ph.:(3812) 26 81 99

Participation in processes of formation and degradation of firm fabrics, biocompatibility, bioactivity brushite cause necessity of studying of laws and features of its crystallization [Barinov, 2010, Veresov, 2004, Danilchenko S.N., 2007]. In the present work results theoretical and an experimental research of influence of parameters crystallization and synthesis conditions on possibility and laws of process of sedimentation of two-water hydrophosphate of calcium, its morphology and disperse structure are presented environment.

For an establishment of laws of crystallization brushite synthesis in which basis reaction lies has been carried out:

$$Ca(NO_3)_2 + (NH_4)_2HPO_4\,2H_2O \rightarrow CaHRO_4 \cdot 2H_2O + 2NH_4NO_3$$

System studying is spent at equimolar concentration of solutions Ca (NO_3) $_2$ and (NH_4) $_2HPO_4$ at room temperature.

By results of experiment by Ik-spectroscopy methods (fig. 1) and optical microscopy of the deposits received at synthesis from solutions with concentration of 10 and 25 mmol/l, it is established that at sedimentation during the initial moment of time are formed small crystals brushite (fig. 2) which at deposit maturing are mainly transformed in hydroxyapatite (fig. 2).

In a material which has been selected from system after phase maturing in a solution within two days, not numerous extended large rhombic crystals brushite in a matrix small crystals hydroxyapatite are found out.

In case of higher initial concentration of ions of calcium and phosphates-ions (With ≥ 50 mmol/l) formed deposits are presented brushite that is confirmed by methods of IK-spectroscopy and X-ray photography the analysis. Maturing of the besieged firm phase was reduced to growth of originally formed germinal crystals of two-water hydrophosphate of calcium (fig. 3). Formed particles have the form of the large extended plates with some defects on a surface in the form of grooves and having chopped off on edges (fig. 3)

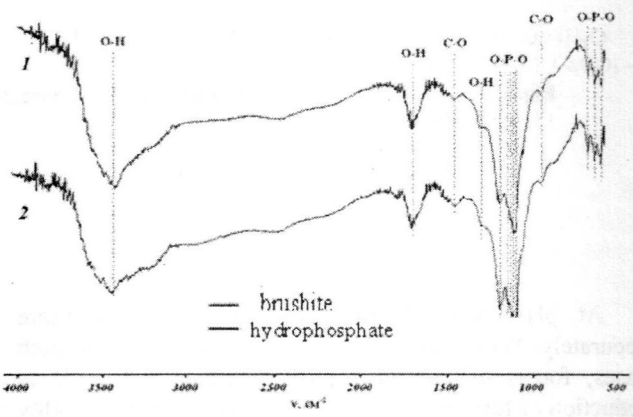

Fig. 1. IK-spectra of the samples received by sedimentation from systems: 1 - With (Ca^2, HPO_4^{2-}) = 25 mmol/l; 2 - With (Ca^2, HPO_4^{2-}) = 10 mmol/l

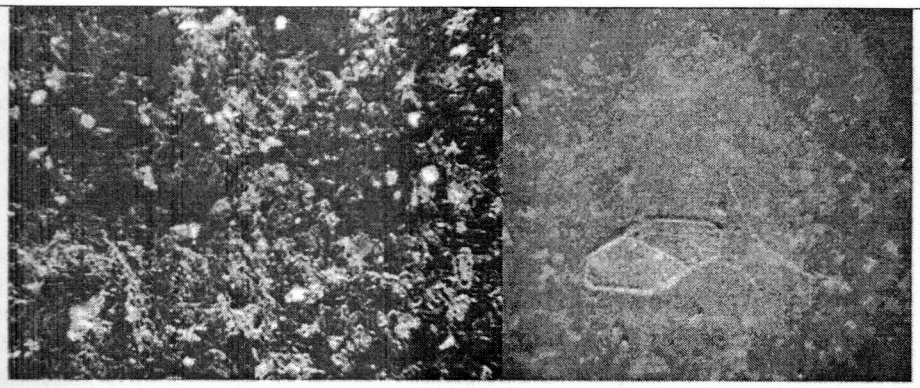

Fig. of 2 Photos of particles brushite, received from a solution with Cish=10 mmol/l:A - at the moment of draining, - after 2 days of maturing.

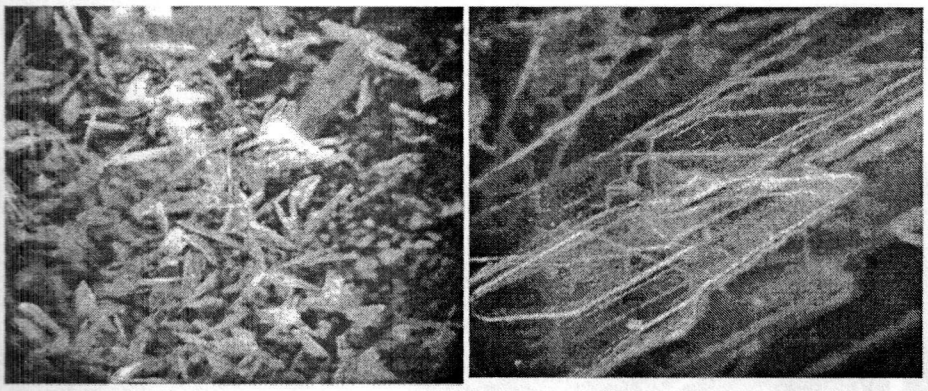

Fig. of 3 Photos of particles brushite, received from a solution with Cish=50 of mmol/l: And - at the moment of draining; – after 2 days of maturing

By methods of the chemical analysis of liquid phases it is established that the residual maintenance Ca^2 in a solution changes in limits from 2,6 to 6,7 mmol/l, and concentration of ions HPO_4^{2-}, makes 4,5–7,3 mmol/l. The maintenance of Ca and P in a deposit linearly increases depending on initial concentration. Dependence of weight of a deposit on initial concentration of reagents is linear in an investigated range that testifies to absence of phase transitions in studied conditions. Also it is found out that at increase initial concentration of degree of transformation of Ca^2 and HPO_4^{2-} aspire to unit. It is established that the parity of Ca/P in the received samples changes from 1,36 to 1,00 depending on the taken initial concentration. The parity equal 1,00, confirms that a firm phase is two-water hydrophosphate of calcium.

The analysis a method of IK-spectroscopy of the deposits received as a result of change of time of crystallization in an interval has shown that samples are monophase and are presented brushite (fig. 4).

Research by a method of optical microscopy of the given samples, has allowed to establish that as a result of deposit keeping under a uterine solution within one days of a particle small lamellar crystals brushite which at increase in time of maturing grow represent, and the greatest growth occurs in a direction of one of axes in such a manner that the parity of length of a crystal to its width makes approximately 10:1.

At the analysis of dependence of weight of a deposit from crystallization time, it is possible to tell that the exit brushite in the given conditions doesn't change at deposit keeping under a uterine solution more than two days. The carried out chemical analysis supernatant liquids has shown that the residual maintenance of ions of Sa^2 and HPO_4^{2-} in a solution very slightly decreases eventually.

Almost not changing after two days of crystallization residual concentration of Ca^2 and HPO_4^{2-} and the calculated degrees of transformation allow to draw a conclusion that the keeping time, exceeding two days, slightly influences crystallization process, i.e. balance between a liquid phase and a deposit is established in this time. The calculated parities of Ca/P changing from 1,08 to 1,06, confirm that a firm phase is brushite.

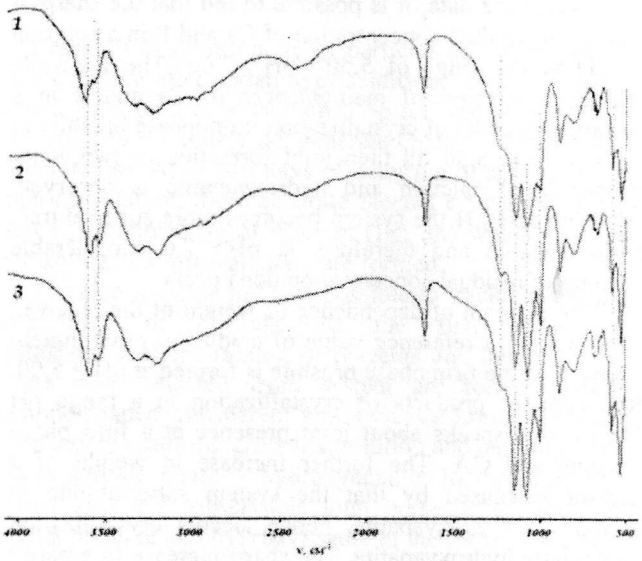

Fig. 4 IK -spectra of samples brushite, received through: 1 – 1 days; 2 – 3 days; 3 – 9 days

At a following stage of work influence researches pH on phase structure of deposits are conducted environments.

According to the IK-spectroscopy data (fig. 5), sedimentation brushite occurs enough in a narrow interval, namely from pH from 5.00 till. At shift pH in more alkaline area there is a joint loss of two-water hydrophosphate of calcium and hydroxyapatite [Ca_{10} (PO_4) $_6$ (OH) $_2$] up to pH=7,00. At the further increase pH crystallizes monophase hydroxyapatite.

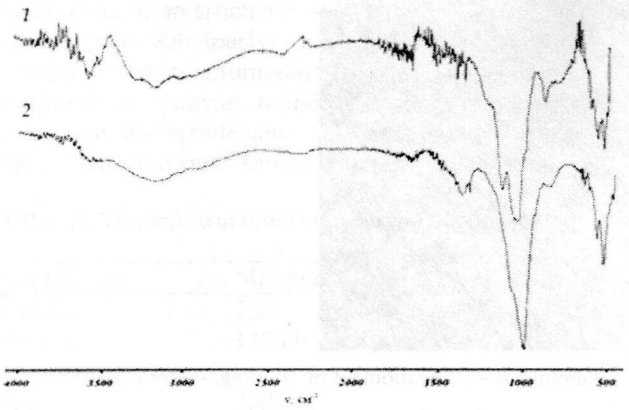

Fig. 5 IK -spectra of the samples received by sedimentation from systems with $(Ca^2, HPO_4^2)_{исх}$=50 mm at: 1 - pH = 6.50, 2 - pH = 8.00

Research by a method of optical microscopy of the samples who have been selected at the moment of draining of reagents and after two days of crystallization at $pH_{исх}$=5,0 and 6,0 has shown that during the initial moment of time are formed small crystals brushite which at deposit maturing grew and turned to the thin extended plates (fig. 6).

In a range pH from 6,50 to 7,00 after maturing the phase is presented by crystals брушита in a matrix small crystals hydroxyapatite (fig. 6). In case of higher reference values pH (≥ 8,0) the GA crystallizes in the form of a continuous opaque film with the whitish shade, fissuring at drying.

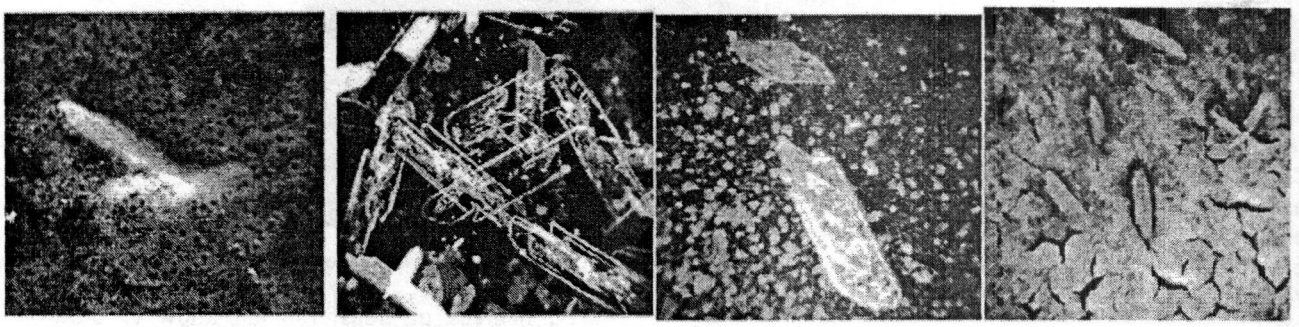

Fig. of 6 Photos of particles pH=6.0: And – at the moment of draining; – after 2 days of maturing pH=7.0: In – at the moment of draining; Г – after 2 days of maturing.

Data of the chemical analysis testifies to changes of phase structure of deposits supernatant liquids also. Analyzing the data, it is possible to tell that the sharpest change of residual concentration of Ca and P in a solution occurs in the range of 5.50> pH> 7.00. The Plausible reason of increase of maintenances of Ca and P in a deposit is process of crystallization monophase brushite in a range from 5.50 till then joint formation of two-water phosphate of calcium and hydroxyapatite is observed. With increase pH the system becomes more supersaturate hydroxyapatite and therefore, at pH> 7.0 considerable changes of residual concentration don't occur.

The diagram of dependence of weight of the received deposit from a reference value of acidity of environment shows that the firm phase brushite is formed at pH ≥ 5.00. Reduction of products of crystallization in a range pH from 6 to 7 speaks about joint presence at a firm phase brushite and GA. The further increase in weight of a deposit is caused by that the system supersaturate in relation to hydroxyapatite, hence, occurs crystallization monophase hydroxyapatite. The sharp increase in a parity of Ca/R at pH> 6 says that the firm phase in the given interval isn't brushite

Further influence of an order of draining of solutions has been studied.

It is established that that the deposits received by a way addition of solution Ca $(NO_3)_2$ to solution $(NH_4)_2HPO_4$ are presented brushite whereas at a return order of draining of reagents, as a part of firm phases crystallizing in studied conditions in common are present brushite and hydroxyapatite.

The method of optical microscopy has allowed to establish that crystals brushite in both cases have the form of the thin extended plates, with some defects on a surface in the form of furrows and having chopped off on edges. However as a part of the samples which formation occurred at addition a solution of hydrophosphate of ammonium to a solution of nitrate of calcium, besides lamellar crystals brushite there are the various form units hydroxyapatite.

Settlement sizes of degree of course on calcium and hydrophosphates-ions of reaction of sedimentation in cases of a different order of draining of reagents have close values. Possibly, incomplete course of process formation is caused by solubility of a firm phase. The parity of Ca/P in the received samples close by 1.00 that corresponds stoichiomete brushite. Also influence of speed of draining of reagents on characteristics of crystallizing substance of process of sedimentation is studied. The analysis spent by a method of Ik-spectroscopy, has shown that the samples received as by fast addition of solution Ca $(NO_3)_2$ to solution $(NH_4)_2HPO_4$, and slow draining of reagents (on drops), are formed brushite.

Research of samples by a method of optical microscopy has allowed to establish that, in comparison with besieged at fast draining of reagents, small crystals, received by a way addition solutions on drops, have the smaller sizes. Particles brushite in the form of thin needles and plates form units of the various sizes. Possibly, it is connected with a high supersaturation in system, and as consequence, formation of set of germinal skeletal crystals brushite which, incorporating in large units, drop out in a deposit.

By the received results it is possible to draw a conclusion that at reception brushite a way addition reagents on drops degree of course of reaction more than

in the samples synthesized by draining of solutions, and the received parity of Ca/R in a deposit makes 1,02 that is closer to theoretical stoichiomete for brushite 1,00.

Conclusions

1. Crystallization possibilities brushite by $CaHRO_4 \cdot 2H_2O$ from system $Ca(NO_3)_2 - (NH_4)_2HPO_4 - H_2O$, containing equivalent quantities of ions of Ca^2 and HPO_4^{2-} are experimentally defined.
2. Influence on phase structure of a deposit and the characteristic of process of sedimentation of experimental conditions (concentration of initial components are investigated; crystallization time; pH crystallization environments; an order of draining of solutions; speed of draining of reagents).

Optimum conditions for reception of crystals brushite are picked up: crystallization time - 2 days; concentration of initial reagents $Ca(NO_3)_2$ and $(NH_4)_2HPO_4$ - 50 mmol/l; an order of draining of initial solutions: $Ca(NO_3)_2$ to a solution $(NH_4)_2HPO_4$; pH = 5,0 – 6,0.

Filchenko M.B., Golovanova O.A., Solonenko A.P. Features of crystallisation in system $Ca(NO_3)_2 - (NH_4)_2HPO_4 - NH_4OH - H_2O$

Chem.dep. OmSU filchenkomarija @rambler.ru

For today considerable progress will reach at use of biologically active materials on the basis of the substances initially close on chemical and phase structure to a bone fabric, - calcium orthophosphates [Veresov 2004, Ezhova Z.A., 2000].

Phosphates of calcium widespread in the nature. They meet in the form of minerals, such as apatites, брушит, etc., and also are important building components of firm fabrics of the person. Synthetic analogues of biogene minerals possess property of biocompatibility, therefore studying of crystallisation of phosphates of calcium, in particular hydroxyapatite, in various conditions Kibalchits V. L, V.F.Komarov, 2000 gives the chance in the long term workings out of materials and composites with the set properties for fabric engineering and orthopedy [to Barinov S.M., Komlev V. S, 2005, to Danilchenko S.N., 2007].

The purpose of the given work - research of influence of acidity of environment on phase education in system $Ca(NO_3)_2 - (NH_4)_2HPO_4 - H_2O$. Following problems were thus solved: 1) to receive a series of samples hydroxyapatite at a variation pH the reactionary environment and 2) to study influence pH on phase structure of deposits, crystallinity, morphology, solubility and some other characteristics.

During experiments sedimentation hydroxyapatite spent by slow draining of solutions of nitrate of calcium and disubstituted phosphate of the ammonium, taken in the ratio $n_{starting} = Ca/HPO_4 = 1.70/1$. pH the received solution corrected to a preset value from an interval from 4.00 till (solutions HNO_3 (1:1) or NaOH (20 %)). The received deposit analyzed Ik-spectroscopy methods, Rentgeno-phase analysis , optical microscopy. In supernatant liquids methods of the chemical analysis defined residual concentration of phosphates-ions and calcium ions. pH systems defined size potentiometric.

Under the received data it is established that deposit formation in studied system is observed at pH ≥ 5.50. In these conditions, it agree to data Rentgeno-phase analysis (fig. 1) and IK-spectroscopy, there is a sedimentation brushite $CaHPO_4 \cdot 2H_2O$ (fig. 2).

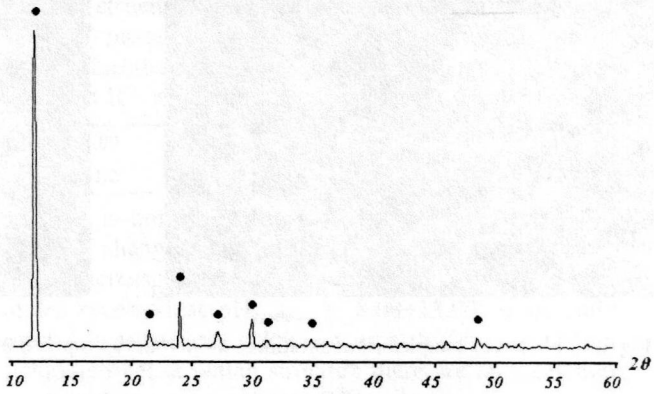

Fig. of 1 Difraktogram of the sample received at pH=5.50

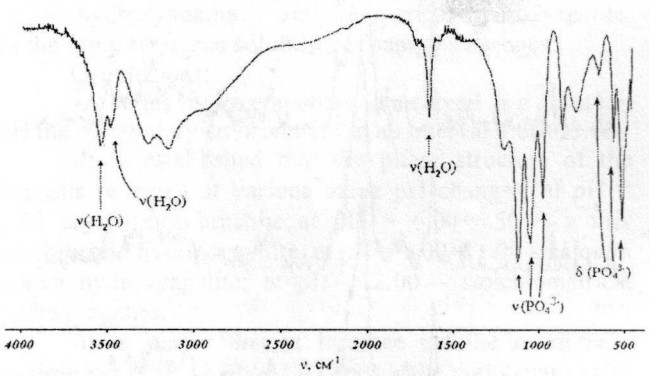

Fig. 2. IK-spectrum of the sample received at pH=5.50

Research of morphology of particles of a firm phase has shown that after updating of acidity of environment to value 5.50 ± 0.05 in a solution drop on subject glass the thin extended accurately not generated plates brushite (fig. 3a) crystallise. After two days of maturing of substance in a uterine solution, more accurate faceted crystals of two-water hydrophosphate of calcium (fig. 3b) which remain after drying of a mineral phase are formed.

At value increase pH it is possible to track change of morphology of crystals. At the first stage of crystallisation after draining of reagents and updating pH in the drop selected from system are formed small diamond-shaped transparent кристаллики brushite which in process of maturing grow in a solution and partially turn to less soluble phase – hydroxyapatite. In the dried up deposit also it is observable joint presence of lamellar crystals brushite and hydroxyapatite in the form of units of the smallest crystalline particles of the various form.

By results of РФА the firm phases received during experiment at pH > 7.00, are presented only hydroxyapatite. And improvement of the permission of peaks in the field of 30 - 35 bragg reflexion corners on difractogram synthetic samples hydroxyapatite, and accordingly and increase of their degree of crystallinity at growth pH synthesis from 7.00 till (fig. 4) is observed.

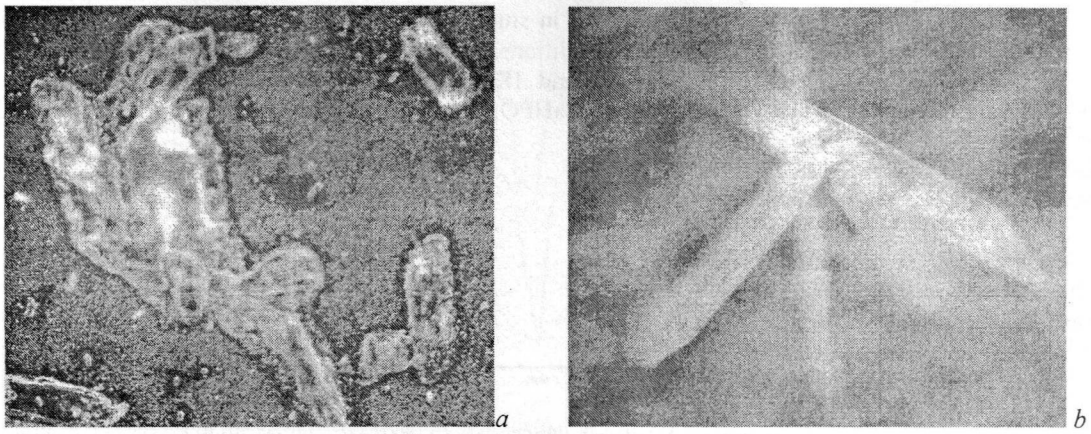

Fig. of 3 Photos of samples from solutions: a - pH=5.50,b - pH=6.00

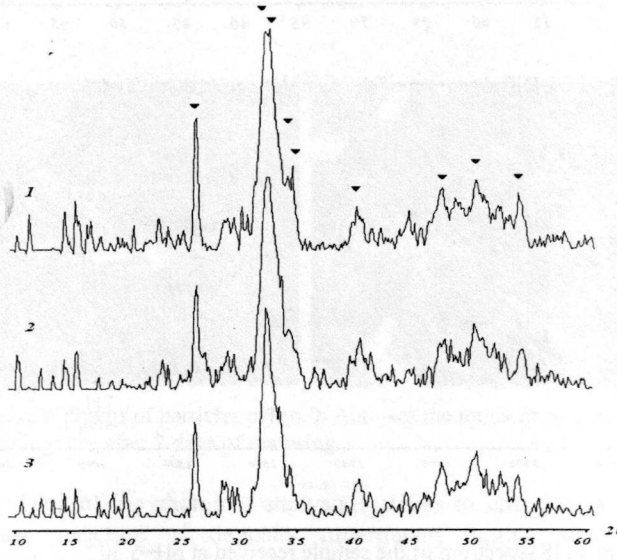

Fig. of 4 Difraktograms of samples of the deposit received at various values pH:1 - pH=6.50, 2 - pH=7.00, 3 - pH=11.00 (a phase - hydroxyapatite)

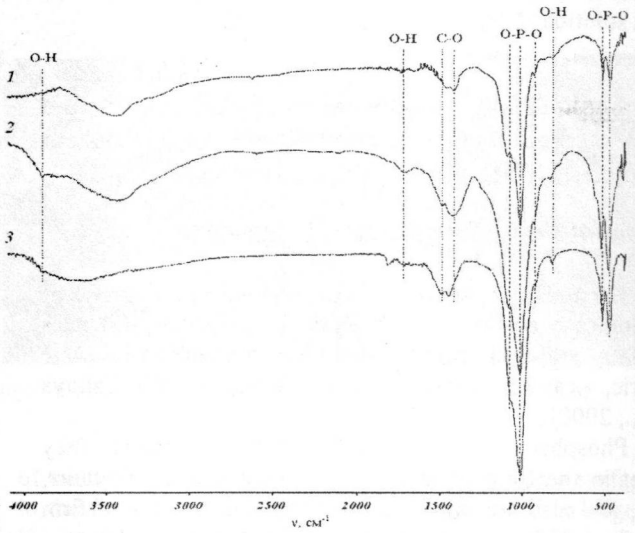

Fig. of 5 IK-spectrum of the samples received by sedimentation: 1 - at pH=6.50, 2 - at pH=9.00, 3 - at pH=13.00 (a phase - hydroxyapatite)

According to Rentgeno-phase analysis by means of the formula of Seljakova-Sherrera the sizes of crystalline particles (tab. 1) are calculated.

Under the received data, it is established that with growth pH synthesis the size of crystalline particles decreases. It, possibly, is connected with growth of a supersaturation of system rather hydroxyapatite at increase pH and formations at the initial stage of crystallisation of a great number of small germs.

Results of IK-spectroscopy are in the consent with data Rentgeno-phase analysis. On spectra of samples absorption strips only hydroxyapatite are shown, phosphatic groups in which structure are partially replaced by carbonates-ions to what presence on spectra of strips with minima in the field of 1400-1450 sm^{-1} (fig. 5).

Thus, all samples received at pH $\geq$ 7.00, are presented carbonate substitute hydroxyapatite the V-type which particles in a deposit look like units of the various size and consist of the smallest crystalline particles.

For data acquisition about a parity of Ca/P in the received samples, spent quantitative definition of structure supernatant liquids.

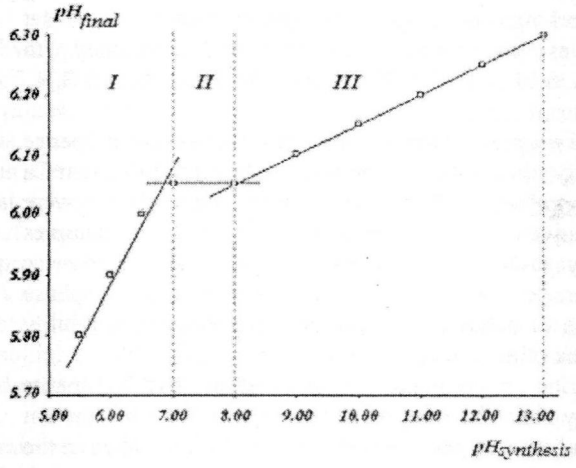

Fig. of 6 Diagram of dependence pH final from pH synthesis (t=60 minutes)

It is established that at increase pH residual concentration of Ca and phosphate of ions in supernatant liquids decrease. The strongest change of concentration is observed in an interval pH from 5.50 till since in these conditions there is a phase transition brushite in hydroxyapatite. At the further increase pH synthesis insignificant reduction of residual concentration sediment

ions that is connected with growth of degree of sedimentation of apatite and hobby sediment ions in the firm phase which weight accrues at increase alcalinity environments is observed.

Table 1. Dependence of the sizes of crystalline particles hydroxyapatite from value pH synthesis

pH	6,50	7,00	8,00	9,00	10,00	11,00	12,00	13,00
D, Å	226.8	226.8	226.8	181.4	181.4	181.4	151.2	151.2

Observable laws are caused by increase of a supersaturation of system on the basic phosphate of calcium at increase pH a solution.

On the basis of the data of the analysis of a liquid phase, it is established that at pH = 5.50 the phase with a parity of Ca/P ≈ 1.00 is formed that corresponds stoichiometry brushite. At values pH = 6.00÷11.00 calcium-scarce hydroxyapatite with a parity of Ca/P <1.67 crystallizes. At pH = 12.00 the increase pH till 13.00, possibly is formed stoichiometrical hydroxyapatite with a parity of Ca/P = 1.67, and, calcium-superfluous of hydroxyapatite leads to formation, the parity of Ca/P in which is equal 1.70. Hence, optimum conditions of reception hydroxyapatite correspond to a range pH = 12.00÷13.00.

The important characteristic of phosphates of calcium is their ability to dissolution in solutions of various acidity. For studying of solubility of images hydroxyapatite, received at various pH environments, spent their dissolution in a solution 0.01 moth/l HCl within 60 minutes.

It is established that all samples received in experiments, have the similar curves of dissolution differing with values maximum pH which is reached in the course of dissolution. It testifies to differences in structure of the synthesized samples. So, pH systems from pH synthesis hydroxyapatite it is possible to allocate 3 areas for dependences of final value (fig. 6).

I. In an interval $pH_{synthesis}$ = 5.50÷6.50 increase of final value pH systems is observed. It can be connected with change of structure of dissolved substance: brushite (sour phosphate) passes in calcium-scarce hydroxyapatite; in its structure, besides phosphate - and hydrophosphates-ions, are present It - which pass in a solution at dissolution and cause increase pH;

II. In a range $pH_{synthesis}$ = 7.00÷8.00 changes final pH systems it is not noticed that, in our opinion, testifies to absence of changes in apatite structure;

III. Increase final pH systems at dissolution of the samples received at $pH_{synthesis}$ = 8.00÷13.00, is possibly caused by transition calcium-scarce hydroxyapatite in stoichiometrical at which structure there are only calcium ions, phosphates-ions and ions OH^-.

Thus, in process of increase pH synthesis the structure of a firm phase changes as follows: брушит> calcium-scarce hydroxyapatite > stoichiometrical hydroxyapatite. In the same sequence solubility of samples changes.

Conclusions:

-A series hydroxyapatites is received at a variation pH the reactionary environment in an interval 4.00÷13.00.

-It is established that the phase structure of the deposits received at various value pH changes: at pH = 5.50 crystallizes brushite; at pH = 6.00÷6.50 – a mix brushite and hydroxyapatite; at pH = 7.00÷11.00 – calcium scarce hydroxyapatite; at pH> 12.00 – stoichiometrical hydroxyapatite.

-It is shown that at increase pH the reactionary environment the weight of a deposit, the maintenance Ca^2 and PO_4^{3-}, and also a parity of Ca/P in it increases.

-It is revealed that in process of increase pH synthesis the structure of a firm phase changes as follows: brushite > calcium-scarce hydroxyapatite > stoichiometrical hydroxyapatite. In the same sequence solubility of samples changes.

Methodological and applied research

Shchekina T.B., Batanova A.M., Gramenitskiy E.N., Grigoriev B.N., Kurbyko T.A., Guseva E.V., Korotaeva N.N. **Experimental study of stability chromite-periclase and periclase-carbon refractories**

Geol.dep.MSU, OOO OgneuporTreidGrupp t-shchekina@mail.ru FAX: (495)9398889 ph.:(495)9392040

The comparative study of stability of chromite-periclase (Cr-Per) refractory (HPTU mark) and periclase-carbon (MgO-C) refractory (PU-9 mark) were carried out under laboratory conditions. These refractories applied in furnaces RNB 5500 of nickel plant ZF OAO "Norilsk Nickel" in the manufacture of non-ferrous metals. Slag, crushed with metal (nickel), were placed to crucibles made from the respective refractories. The samples were heated to a temperature of 1500 or 1600 ° C, maintained for 12 hours and were quenched. After the experiments, samples were examined under optical and electron microscopes. The chemical composition of all phases was studied by electron-probe energy dispersive microanalyzer based on scanning electron microscope Jeol JSM-6480LV (spectrometer INCA-Energy 350) of Department of Petrology, Moscow State University.

The start composition of chromite-periclase (Cr-Per) refractory consists of 64% of the periclase (Per), from 25% chrome spinel (Spl), from 7% monticellit (Mont) and 4% olivine (Ol). Periclase-carbon (MgO-C) refractory consists of ~ 80-85% of the periclase, 5% monticellit and dicalcium silicate and 10-15% carbon (data Mol.%). Studies under the electron microscope showed that both types of refractory material as a result of the experiments assume a zonal structure. There is a sharp contrast to the resulting zoning in Cr-Per and MgO-C refractories at the border with molten slag and metal, expressed as a width of reaction zones, their structure, phase and chemical composition. In chromite-periclase refractory width of macroscopically visible reaction zone is about 5 - 6 mm, in periclase-carbon - less than 1 mm. Column interaction of Cr-Per refractory with the molten slag and nickel allocated 5 zones with a total width of 30 mm. The boundary of the first two zones established by the detection of Ni in the refractory in the amount of the 0,1-0,2 per cent. Throughout I and II zones in the refractory the content of

SiO_2 (5 wt.%) and FeO (7%) increases and MgO (17%) and Cr_2O_3 (6%) decreases. In this case, Per and chrome Spl corrode, the content of monticellit decreases and the number of olivine increases (from 4 to 12%). Ni enters into the composition of periclase first in small and then in significant quantities (up to 0,25 form. unit), and Fe - up to 0.13 form.unit. Chrome spinel grains are surrounded by rims of more aluminous and ferrous spinels, emerging and re-formed crystals of Spl. Periclase formed intergrowths with Spl, containing in addition to Cr - Al, Fe and Ni. The boundary between zones II and III clearly break off by changing the paragenesis phases: periclase disappears, the association Per + Spl + Mont + Ol is replaced by a Spl + Ol + Glass, in which spinel greatly predominates. Glass is present in an amount of about 10% and is formed in the space between the crystals of spinel. Among the newly-formed spinels of zone III crystals with a high content of Al $[(Mg_{0,95}Ni_{0,09}Co_{0,02})_{1,06}(Al_{1,20}Fe_{0,18}Cr_{0,63})_{2,01}O4]$ with rims of more ferrous spinels, containing Ni and Co $[(Mg_{0,83}Ni_{0,19}Co_{0,04})_{1,06}(Al_{0,50}Fe_{0,97}Cr_{0,37})_{1,84}O4]$, are dominated. Ni appears also in the olivine, and the ratio of Ni / (Mg + Ni) from 0,03 to 0,22 increases in zone III. Phases paragenesis in IV zone differs from one in zone III: decrease in the number of Ol (7%) and glass (up to 5%), even greater predominance of spinel and a change of its composition. The ratio of Ni/(Mg + Ni) in olivine increases to 0,36. Spinels form zonal crystals of two types: the first type, the center of the grains make up chrome-alumina spinel, the border - less than alumina, but more of nickel spinel, in the second type of reverse situation is observed. Crystals of both spinel types overgrow with phase corresponding bunsenit NiO with small amount of Mg (up to 0.1 fu) and the impurities Al, Fe, Cr and Co. The composition of the glass which is formed in the refractory conform to phonolites (SiO_2-56,2%, Al_2O_3-19, 5%, MgO-1, 0%, CaO-1,8%, Na_2O-4, and 7%, K_2O-11, 8% Cr_2O_3-0, 3%, NiO-1,0%, CoO-0, 3%). Fine crystals of clinopyroxene are contained in the glass. There are fundamental changes of the phase composition in the V zone. It consists of bunsenit with a small amount (about 10 mol.%) of spinels. There is bunsenit solid solution with other components, which consist of 86-90 wt. % NiO, 4-8% Mg0, 2-3% FeO and Cr_2O_3. Thus, at the interaction of metallurgical melts with chromite-periclase refractory intense interdiffusion of components is observed leading to the removal of Mg and Cr from it, and introduction of Al, Fe, Ni and Co from melts. This process causes the corrosion in the refractories, leading to its destruction.

Zone of the active interaction between periclase-carbon (MgO-C) refractory and the molten slag and metal are very small and amounts to 0.5 -1 mm unlike chromite-periclase. Throughout the column (from the bottom of the crucible to melt), the chemical composition of the refractory remains practically unchanged for all components. Neither of silica from the slag nor nickel from molten metal are introduced. The phase composition of refractories varies significantly only in the immediate vicinity (1-0,5 mm) to the molten slag: along with monticellit and calcium silicates- olivine and MgAl-spinel appears. Both these phases have also crystallized in the slag. None of the studied phase does contain Ni. It is obvious that such indifference in periclase-carbon (MgO-C) refractory to aggressive metallurgical melts associated with the presence of carbon in its composition. Carbon prevents the diffusion of the components of slag and nickel melt in the refractory, acting as an antioxidant. It is likely that it forms a graphite film on the boundary of the periclase grains of refractory and the melt, preventing the passage of the mutual diffusion of components.

According to the studying result of the composition and structure of refractories should be concluded that periclase-carbon (MgO-C) refractories are much more resistant to slag and nickel melts at high-temperature conditions of experiment compared with chromite-periclase refractories. Hence MgO-C refractories are more efficient at their use in commercial production of nickel.

AUTHORS INDEX

AUTHORS INDEX